LAWRENCE
LIVERMORE
NATIONAL
LABORATORY

LLNL-TR-792469

Shell Element Material Model Verification Problems for DYNA3D

Brian D. Giffin

September 30, 2019

This work was performed under the auspices of the U.S. Department of Energy by Lawrence Livermore National Laboratory under Contract DE-AC52-07NA27344.

Abstract

A suite of shell element material model verification tests were developed for the explicit finite element program DYNA3D. Each test consists of a single quadrilateral shell element, whose nodal displacements and rotations have been prescribed such that the deformation of the material is fully controlled throughout the analysis. At one of the element's integration points, the numerically computed stress, through-thickness strain, and equivalent plastic strain are compared against closed-form reference solutions that are derived to be consistent with the theory of finite deformation elasto-plasticity. A collection of 31 feature-specific verification tests are proposed, each of which may be used to verify all models which share in common the tested feature of interest. For each material model, a subset of these tests are selected and used to verify the correct behavior of all features of the model. The collective suite of tests cover 26 of the 27 currently available material models in DYNA3D. In the course of developing the proposed test suite, 18 implementation bugs were identified and have subsequently been resolved.

Contents

Shell Element Material Model Verification Problems for DYNA3D

Brian Giffin
Methods Development Group
Defense Technologies Engineering Division
Engineering Directorate

September 30, 2019

1 Introduction

The DYNA3D finite element code was developed at Lawrence Livermore National Laboratory to model transient dynamics for solids and structures undergoing large deformations (e.g. high-velocity impact problems). A variety of material models which account for the effects of material anisotropy, plasticity, rate-dependence, temperature-dependence, and damage have been introduced to provide more advanced modeling capabilities for the aforementioned problems of interest. Given the variety and complexity of the models currently available in DYNA3D, it is necessary to verify that these models are correctly implemented and yield accurate results.

DYNA3D provides users with a number of material models which are intended for use in conjunction with both solid and shell element formulations, alike. The available models are referred to generically by their model number, but the implementation of a given model is different for each element type. For this reason, element type-specific verification tests must be developed for each material model. This report presents a suite of shell element-specific material model verification tests.

Section 2 of this report presents a brief overview of the existing shell element formulations and material models currently available in DYNA3D, and a high-level perspective of the available "features" provided by each model (e.g. orthotropic elasticity, isotropic hardening plasticity, etc.). The resulting catalog of features forms the basis for the proposed test suite, with each test focusing on the verification of a specific model feature of interest.

Section 3 establishes the generic problem setup used by every verification test, consisting of a single shell element whose kinematics are fully prescribed according to one of a handful of parameterized motions – termed "load cases." A given test problem is defined in terms of its assigned load case, and its corresponding "material parameterization:" an enumeration of all of the relevant material properties, and their assigned values.

Section 4 describes the general methodology used to numerically verify the results of each test, entailing a comparison of the numerical results obtained for a given model against the corresponding exact (mathematically derived) reference solution. To this end, suitable error metrics and bounded error estimates are established for general finite deformation elasto-plasticity problems. The proposed approach facilitates a compact representation – and precise quantification – of solution errors and their corresponding rates of convergence under temporal refinement.

Section 5 summarizes the newly proposed suite of verification tests, consisting of: a description of each model feature being verified; the definition of all problems designed to test a given feature; the derivation of corresponding reference solutions; and the presentation/comparison of the numerical results obtained for each test applied to every model which shares the indicated feature in common.

Section 6 concludes with a tabulated presentation of the verification status of all tested model features, and a catalog of all implementation bugs that were discovered (and resolved) in the course of this work.

2 Overview of DYNA3D's Shell Element Material Models

Table 1: Index of shell element-specific material models.

Model	Name
1	Elastic
2	Orthotropic Elastic
3	Kinematic/Isotropic Elastic-Plastic
4	Thermo-Elastic-Plastic
12	Isotropic-Elastic-Plastic
15	Johnson/Cook Elastic-Plastic
18	Power Law Isotropic Elastic-Plastic
19	Strain Rate Dependent Isotropic Elastic-Plastic
21	Thermal Orthotropic Elastic
22	Fiber Composite with Damage
23	Thermal Orthotropic Elastic with Variable Properties
24	Rate-Dependent Isotropic Elastic-Plastic
28	Resultant Plasticity
30	Closed-Form Update Elastic-Plastic for Shells
33	General Anisotropic Elastic-Plastic
34	Normal Anisotropic Elastic-Plastic for Shells
35	Elasto-Plastic with Forming Limit Diagram
38	Bammann Plasticity Model
39	Sandia Damage Model
41	Fabric with Damage
42	Multi-Material Shell Element Model
46	Anisotropic Elastic (calls subroutine for model 2)
50	Braided Composite Model with Damage
52	Rate-Dependent Tabular Elastic-Plastic with Fracture
54	Zerilli-Armstrong Elasto-Plasticity with Fracture
71	General Elasto-Plastic with Optional Rate & Temperature Dependence
74	Laminated Composite with Damage

DYNA3D supports a broad range of different shell element formulations and material models. Currently, a total of 27 different material models are available for use with shell elements, enumerated in table 1. Henceforth, all material models will be referred to by their corresponding model number. For the complete enumeration of all input parameters – and a detailed description of the formulation for each model, the reader is referred to the DYNA3D manual [12].

It is emphasized that the primary goal of the proposed tests is to verify the correct implementation of each material model – not the individual shell element formulations, nor their kinematics. To this end, a number of simple single-element test problems are devised in section 3 for the sake of comparing the computed stress state in the element to exact reference solutions, given known kinematic inputs. Nonetheless, a brief overview of the available shell formulations in DYNA3D is presented in section 2.2.

2.1 Available Material Model Features for Shell Elements

Many of the available shell models share a number of similar features in common with one another. For this reason, a collection of general tests are created which may each be used to verify all models that implement the same feature. This further allows for the results obtained from different models to be directly compared against one another, providing an additional level of verification.

Table 2 provides a high-level overview of the available features for each model, and an indication of which features are shared across multiple models. Model features for which tests have been created are indicated with a ✓ symbol. Presently untested features are denoted by a ✗ symbol.

Table 2: Tested features for shell element material models in DYNA3D

Model	Isotropic Elasticity	Orthotropic Elasticity	Isotropic Thermal Expansion	Orthotropic Thermal Expansion	Linear Hardening	Piecewise Hardening	Power-Law Hardening	Exponential Hardening	Hill Yield Criterion	Linear Rate-Hardening	Logarithmic Rate-Hardening	Drucker-Prager Yield Criterion	Kinematic Hardening	Temperature-Sensitive Properties	Strain Rate-Sensitive Properties	Variable Properties	Damage and Failure
1	✓	-	-	-	-	-	-	-	-	-	-	-	-	-	-	-	-
2	✓	✓	-	-	-	-	-	-	-	-	-	-	-	-	-	-	-
3	✓	-	-	-	✓	-	-	-	-	-	-	-	✗	-	-	-	-
4	✓	-	✓	-	✓	-	-	-	-	-	-	-	-	✗	-	-	-
12	✓	-	-	-	✓	-	-	-	-	-	-	-	-	-	-	-	-
15	✓	-	-	-	✓	-	✓	-	-	-	-	✓	-	✗	✗	✗	✗
18	✓	-	-	-	-	-	✓	-	-	-	-	-	-	✗	-	✗	-
19	✓	-	-	-	✓	-	-	-	-	-	-	-	-	-	✗	-	-
21	✓	✓	✓	✓	-	-	-	-	-	-	-	-	-	✗	-	-	-
22	✓	✓	-	-	-	-	-	-	-	-	-	-	-	-	-	-	✗
23	✓	✓	✓	✓	-	-	-	-	-	-	-	-	-	✗	-	-	-
24	✓	-	-	-	✓	✓	✓	-	-	✓	-	✓	-	-	✗	-	-
28	✓	-	-	-	✓	-	-	-	-	-	-	-	-	-	-	-	-
30	✓	-	-	-	✓	-	-	-	-	-	-	-	✗	-	-	-	-
33	✓	✓	-	-	✓	-	-	-	✓	-	-	-	-	-	-	-	-
34	✓	-	-	-	✓	-	-	-	✓	-	-	-	-	-	-	-	-
35	✓	-	-	-	✓	✓	-	-	-	-	-	-	-	-	-	-	✗
38	✓	-	-	-	✓	-	-	-	-	-	-	-	✗	-	-	-	-
39	✓	-	-	-	✓	-	-	-	-	-	-	-	✗	-	-	-	-
41	✓	✓	-	-	-	-	-	-	-	-	-	-	-	-	-	-	✗
42	-	-	-	-	-	-	-	-	-	-	-	-	-	-	-	-	-
46	✓	✓	-	-	-	-	-	-	-	-	-	-	-	-	-	-	-
50	✓	✓	-	-	-	-	✗	-	✗	-	-	-	-	-	-	-	✗
52	✓	-	-	-	✓	✓	-	-	-	-	-	-	-	-	✗	-	✗
54	✓	-	-	-	✓	-	✓	-	-	✓	-	-	-	✗	✗	-	✗
71	✓	-	✓	-	✓	-	✓	✓	-	✓	✓	✓	-	✗	✗	-	✗
74	✓	✓	-	-	-	-	-	-	-	-	-	-	-	-	-	-	✗

✓: Verification tests have been created for this model feature.
✗: Model feature currently remains untested.

2.2 Shell Element Formulations in DYNA3D

DYNA3D currently supports a variety of different shell/membrane element formulations, including: the 8-node thick shell; the Hughes-Liu (HL) shell; the modified Belytschko-Wong-Chiang (MBWC) shell; the Belytschko-Lin-Tsay (BLT) shell; the C^0 triangular shell; the Bazeley-Cheung-Irons-Zienkiewicz (BCIZ) triangular shell; the 4-node membrane element; and the 4-node resultant shell with BLT hourglass control. All of the aforementioned elements support variable through-thickness integration, and 1-point in-plane integration with appropriate stabilization. The HL, MBWC, and BLT shell formulations also provide a 4-point in-plane integration option.

Irrespective of the specific formulation, all shell elements in DYNA3D ultimately call the same underlying subroutine (`shl#s`) for a given material model. However, the corotational formulation used to update the the kinematics at a given material point may differ between element types. Specifically, the HL and thick shell formulations utilize the Jaumann rate to update the stress and state variables. For all other shell formulations, the stresses/strains are computed and updated in the element's co-rotational/lamina coordinate system.

To clarify the terminology employed herein, a "material model" refers exclusively to the underlying subroutine (`shl#s`) which updates the state of stress in the material, and therefore does not encompass the particular choice of corotational formulation. According to this definition, the ideal verification testing strategy would be to create "unit tests" for the individual `shl#s` subroutines, these being the atomic units of code whose implementations we seek to verify. Unfortunately, the current architecture of DYNA3D does not easily allow for these subroutines to be tested in a modular fashion. In the absence of such a testing framework, it suffices to select and utilize a single shell element formulation (ideally the simplest one) for all tests. Unless otherwise noted, the BLT shell is utilized for all of the proposed shell element material model verification problems.

3 Generic Test Problem Setup

In what follows, a generic test problem is proposed which consists of a single quadrilateral shell element whose displacements and rotations have been fully specified. The intent is to create a general test capable of isolating and testing all features of each material model, without introducing potential sources of error due to transient dynamic effects or the particular choice of element formulation.

The generic test setup is constructed in such a fashion as to be sufficiently flexible in its ability to fully prescribe the entire history of deformation at a single material point. This allows for the possibility of additional tests to be created more easily in the future.

Particular specializations of the generic test are devised to establish a finite number of parameterized motions, herein termed "load cases." Each of the verification tests proposed in this report is identified by an assigned load case, and a material parameterization. While multiple tests may share the same load case, the results of each test may differ depending on the choice of material parameterization.

3.1 Single-Element Test Setup

A square, planar quadrilateral element is henceforth considered for all test problems, as depicted in Figure 1. For convenience, let $L = 1.0$ such that the element's isoparametric parent coordinates $\boldsymbol{\xi}$ coincide with the physical coordinates $\mathbf{X}$ of the element in its (undeformed) reference configuration. Furthermore, the element is prescribed to have unit thickness, and the time interval $t \in [0, 1]$ over which each test problem takes place is also assumed to have unit duration.

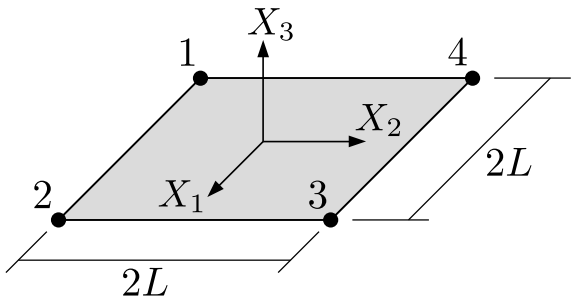

Figure 1: Single quadrilateral shell element used in all verification tests.

With the exception of model 28 which must be used with the resultant shell element formulation, all test problems for the remaining shell models employ the Belytschko-Lin-Tsay (BLT) shell element described in [1], [2], [3]. Unless otherwise specified, the element is defined to possess a single through-thickness integration point located at the center of the element, effectively rendering it a membrane element.

According to the presentation given in [1], the components of the corotational rate of deformation tensor $\hat{\mathbf{D}} = \frac{1}{2}(\hat{\mathbf{L}} + \hat{\mathbf{L}}^T)$ at the element's center ($\mathbf{X} = \mathbf{0}$) are given by:

$$\begin{Bmatrix} \hat{D}_{11} \\ \hat{D}_{22} \\ 2\hat{D}_{12} \\ 2\hat{D}_{23} \\ 2\hat{D}_{13} \end{Bmatrix} = \sum_{a=1}^{4} \begin{bmatrix} N_{a,1} & 0 & 0 & 0 & +\hat{x}_3 N_{a,1} \\ 0 & N_{a,2} & 0 & -\hat{x}_3 N_{a,2} & 0 \\ N_{a,2} & N_{a,1} & 0 & -\hat{x}_3 N_{a,1} & +\hat{x}_3 N_{a,2} \\ 0 & 0 & N_{a,1} & -N_a & 0 \\ 0 & 0 & N_{a,2} & 0 & +N_a \end{bmatrix} \begin{Bmatrix} \hat{v}_{1a} \\ \hat{v}_{2a} \\ \hat{v}_{3a} \\ \hat{\omega}_{1a} \\ \hat{\omega}_{2a} \end{Bmatrix}, \tag{1}$$

where $N_a(\boldsymbol{\xi}) \, \forall a \in 1, \ldots, 4$ represent the element's nodal shape functions, and $N_{a,i} \equiv \partial N_a / \partial \hat{x}_i$ for $i = 1, 2$ are the first partial derivatives of the shape functions with respect to the element's lamina coordinates. Hatted quantities indicate that the variable in question has been defined within the element's corotational (lamina) coordinate frame, distinct from the global coordinate frame. If one assumes that all nodal rates of rotation are the same (i.e. $\hat{\omega}_{1a} = \hat{\omega}_1$ and $\hat{\omega}_{2a} = \hat{\omega}_2 \, \forall a \in 1, \ldots, 4$), and if the element experiences zero transverse displacement (i.e. $\hat{v}_{3a} = 0, \; \forall a \in 1, \ldots, 4$), then the kinematics governing the in-plane stretching and the

transverse shears may be decoupled, as follows:

$$\left\{ \begin{array}{c} \hat{D}_{11} \\ \hat{D}_{22} \\ 2\hat{D}_{12} \end{array} \right\} = \sum_{a=1}^{4} \left[\begin{array}{cc} N_{a,1} & 0 \\ 0 & N_{a,2} \\ N_{a,2} & N_{a,1} \end{array} \right] \left\{ \begin{array}{c} \hat{v}_{1a} \\ \hat{v}_{2a} \end{array} \right\}, \qquad 2\hat{D}_{23} = -\hat{\omega}_1, \qquad 2\hat{D}_{13} = \hat{\omega}_2, \tag{2}$$

i.e. the in-plane strain rate components may be written exclusively in terms of the in-plane nodal velocities, whereas the transverse shear strain rates may be written independently in terms of the nodal rates of rotation.

For most of the shell elements in DYNA3D (including the BLT shell), a local lamina coordinate system is constructed via the method presented by Hughes in [6], section 6.2.2. Considering the construction of the lamina system, it can be shown that the following patterns of deformation will preserve the orientation of the lamina system, such that the local and global coordinate systems are identical (i.e. $\hat{v}_i = v_i$, $\hat{\omega}_i = \omega_i$, and therefore $\mathbf{D} = \hat{\mathbf{D}}$), for all time:

$$\mathbf{u}(\mathbf{X}, t) = (\mathbf{F}_u(t) - \mathbf{1}) \cdot \mathbf{X}, \qquad \mathbf{v}(\mathbf{X}, t) = \dot{\mathbf{F}}_u(t) \cdot \mathbf{X}, \tag{3}$$

$$\mathbf{F}_u(t) = \exp\left(\boldsymbol{\varepsilon}_u(t)\right), \qquad \dot{\mathbf{F}}_u(t) = \dot{\boldsymbol{\varepsilon}}_u(t) \cdot \mathbf{F}_u(t), \tag{4}$$

$$\boldsymbol{\varepsilon}_u(t) = \left[\epsilon(t) + \gamma(t)\right] \mathbf{q}_1 \otimes \mathbf{q}_1 + \left[\epsilon(t) - \gamma(t)\right] \mathbf{q}_2 \otimes \mathbf{q}_2, \tag{5}$$

$$\dot{\boldsymbol{\varepsilon}}_u(t) = \left[\dot{\epsilon}(t) + \dot{\gamma}(t)\right] \mathbf{q}_1 \otimes \mathbf{q}_1 + \left[\dot{\epsilon}(t) - \dot{\gamma}(t)\right] \mathbf{q}_2 \otimes \mathbf{q}_2, \tag{6}$$

$$\mathbf{Q} = \left[\begin{array}{ccc} \mathbf{q}_1 & \mathbf{q}_2 & \mathbf{q}_3 \end{array} \right] = \left[\begin{array}{ccc} \cos\alpha & -\sin\alpha & 0 \\ \sin\alpha & \cos\alpha & 0 \\ 0 & 0 & 1 \end{array} \right] \quad \forall \alpha \in \left\{ \alpha \in \mathbb{R} \,:\, \alpha = \frac{n\pi}{4} \, \forall n \in \mathbb{Z} \right\}, \tag{7}$$

$$\epsilon(t),\, \gamma(t) \in \mathcal{V} = \left\{ f(t) \in C^0([0,1]) \,:\, f(0) = 0 \right\}, \quad \forall t \in [0,1]\,. \tag{8}$$

In the preceding expressions, $\boldsymbol{\varepsilon}_u$ denotes the in-plane Hencky (or logarithmic) strain tensor, absent of any transverse shear or thickness strains.

In addition to the in-plane displacements, any arbitrary and spatially constant in-plane rotation field may be applied simultaneously, without altering the orientation of the lamina system, such that:

$$\theta_i(t) \in \mathcal{V} \quad \forall i = 1, 2, \quad \forall t \in [0,1], \qquad \omega_i(t) \equiv \dot{\theta}_i(t). \tag{9}$$

This yields

$$\boldsymbol{\varepsilon}_\theta(t) = -\frac{1}{2}\theta_1(t) \left(\mathbf{e}_2 \otimes \mathbf{e}_3 + \mathbf{e}_3 \otimes \mathbf{e}_2\right) + \frac{1}{2}\theta_2(t) \left(\mathbf{e}_1 \otimes \mathbf{e}_3 + \mathbf{e}_3 \otimes \mathbf{e}_1\right), \tag{10}$$

$$\dot{\boldsymbol{\varepsilon}}_\theta(t) = -\frac{1}{2}\dot{\theta}_1(t) \left(\mathbf{e}_2 \otimes \mathbf{e}_3 + \mathbf{e}_3 \otimes \mathbf{e}_2\right) + \frac{1}{2}\dot{\theta}_2(t) \left(\mathbf{e}_1 \otimes \mathbf{e}_3 + \mathbf{e}_3 \otimes \mathbf{e}_1\right), \tag{11}$$

where $\boldsymbol{\varepsilon}_\theta$ denotes the small strain tensor containing only the transverse shear terms.

For hypoelastic – rate-formulated constitutive models, the rate of deformation under consideration is the superposition of the in-plane and transverse strain rates:

$$\mathbf{D}(t) - D_{33}(t)\, \mathbf{e}_3 \otimes \mathbf{e}_3 = \dot{\boldsymbol{\varepsilon}}_u(t) + \dot{\boldsymbol{\varepsilon}}_\theta(t). \tag{12}$$

The above serves as the kinematic input to the constitutive model, where $D_{33}(t)$ is solved for internally as a Lagrange multiplier to enforce the plane stress constraint $\dot{\sigma}_{33}(t) = 0$.

3.1.1 Application of Kinematic Boundary Conditions

Owing to the generality of the expressions established for the prescribed translational and rotational velocity fields in equations (3) and (9) respectively, careful attention must be paid to the application of kinematic boundary conditions such that the desired material motion is reproduced. To this end, parameterized load curves are used to precisely assign the correct nodal velocities and rotations at each time step. It should be noted that the parameterized load curve types presently in DYNA3D (described in greater detail in [4]) are a new set of features that were added specifically for the purpose of developing the verification problems described in this report.

The prescribed translational and rotational nodal velocities for the generic test setup may respectively be written as:

$$\mathbf{v}_a(t) = (\mathbf{q}_1 \cdot \mathbf{X}_a)\,(\dot{\epsilon}(t) + \dot{\gamma}(t))\,e^{\epsilon(t)+\gamma(t)}\mathbf{q}_1 + (\mathbf{q}_2 \cdot \mathbf{X}_a)\,(\dot{\epsilon}(t) - \dot{\gamma}(t))\,e^{\epsilon(t)-\gamma(t)}\mathbf{q}_2 \quad \forall a = 1, \ldots, 4, \tag{13}$$

$$\omega_{ia}(t) = \dot{\theta}_i(t) \quad \forall a = 1, \ldots, 4. \tag{14}$$

This prescription is facilitated by virtue of the displacement/velocity field being a purely linear function of the reference configuration coordinates $\mathbf{X}$, and because the rotation field is spatially constant.

For all test problems considered herein, it is assumed that the loading parameters $\epsilon(t)$, $\gamma(t)$, $\theta_1(t)$, and $\theta_2(t)$ are chosen as linear functions of time. Consequently, the in-plane principal strains $\varepsilon_1(t)$ and $\varepsilon_2(t)$ may also be expressed as linear functions of time of the form:

$$\varepsilon_1(t) = \epsilon(t) + \gamma(t) = \dot{\varepsilon}_1 t, \qquad \varepsilon_2(t) = \epsilon(t) - \gamma(t) = \dot{\varepsilon}_2 t, \qquad \dot{\varepsilon}_1,\, \dot{\varepsilon}_2 \in \mathbb{R}. \tag{15}$$

Moreover, if the in-plane orientation parameter $\alpha = 0$:

$$v_{1a}(t) = X_{1a}\,\dot{\varepsilon}_1\,e^{\dot{\varepsilon}_1 t}, \quad v_{2a}(t) = X_{2a}\,\dot{\varepsilon}_2\,e^{\dot{\varepsilon}_2 t} \quad \forall a = 1, \ldots, 4, \tag{16}$$

Otherwise, if $\alpha = \pi/4$:

$$v_{1a}(t) = \frac{X_{1a} + X_{2a}}{2}\,\dot{\varepsilon}_1\,e^{\dot{\varepsilon}_1 t}, \quad v_{2a}(t) = \frac{X_{1a} + X_{2a}}{2}\,\dot{\varepsilon}_1\,e^{\dot{\varepsilon}_1 t} \quad \forall a = 1, 3, \tag{17}$$

$$v_{1a}(t) = \frac{X_{1a} - X_{2a}}{2}\,\dot{\varepsilon}_2\,e^{\dot{\varepsilon}_2 t}, \quad v_{2a}(t) = \frac{X_{2a} - X_{1a}}{2}\,\dot{\varepsilon}_2\,e^{\dot{\varepsilon}_2 t} \quad \forall a = 2, 4. \tag{18}$$

The above representation ultimately permits the direct specification of each independent nodal velocity component via individual load curves, defined via the exponential parameterized load curve type.

To achieve sufficient accuracy and to eliminate errors in the time-integration of the (logarithmic) strain and stress rate equations, a large number of time steps should ideally be used. However, excessive temporal refinement introduces a prohibitive computational expensive for each test. For this reason, a maximum number of 10 time steps are utilized by all problems in the finalized test suite. Nonetheless, the results presented in this report explore the convergence of various error measures under time step refinement.

3.2 Definition of Load Cases

The prescribed motion characterized by equation (12) provides a general parameterization of the complete space of tests which can be created for the single-element test setup. Nonetheless, it proves convenient to devise a finite set of "load cases" which can be modulated by one or two scalar parameters. All such parameterized load cases of current interest are presented in table 3, and depicted graphically in figure 2.

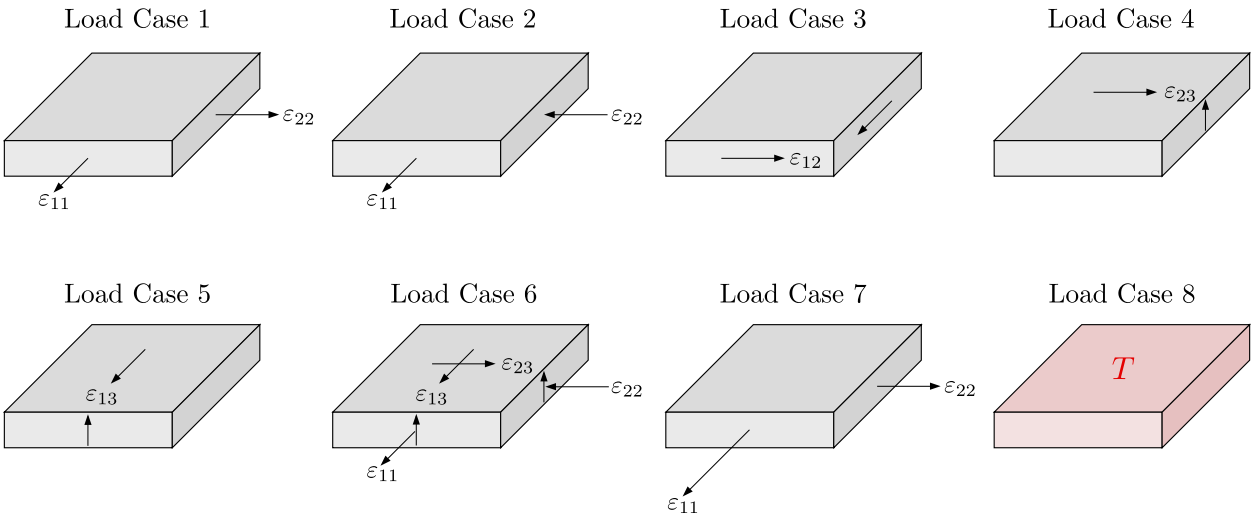

Figure 2: Depiction of all load cases for the generic single-element test setup.

Table 3: Summary of all load cases for the generic single-element test setup

Load Case	$\epsilon(t)$	$\gamma(t)$	$\theta_1(t)$	$\theta_2(t)$	α	$T(t)$	Description
1	$\bar{\gamma}\,t$	0	0	0	0	T_0	Isotropic in-plane expansion ($\dot{\varepsilon}_{11} = \dot{\varepsilon}_{22} = \bar{\gamma}$)
2	0	$\bar{\gamma}\,t$	0	0	0	T_0	Isochoric in-plane extension ($\dot{\varepsilon}_{11} = -\dot{\varepsilon}_{22} = \bar{\gamma}$)
3	0	$\bar{\gamma}\,t$	0	0	$\pi/4$	T_0	Pure in-plane shear ($\dot{\varepsilon}_{12} = \bar{\gamma}$)
4	0	0	$-2\bar{\gamma}t$	0	0	T_0	Pure transverse shear ($\dot{\varepsilon}_{23} = \bar{\gamma}$)
5	0	0	0	$2\bar{\gamma}t$	0	T_0	Pure transverse shear ($\dot{\varepsilon}_{13} = \bar{\gamma}$)
6	0	$\bar{\gamma}t$	$-2\bar{\gamma}t$	$2\bar{\gamma}t$	0	T_0	Combined shear ($\dot{\varepsilon}_{11} = -\dot{\varepsilon}_{22} = \dot{\varepsilon}_{23} = \dot{\varepsilon}_{13} = \bar{\gamma}$)
7	$3\bar{\gamma}t$	$\bar{\gamma}t$	0	0	0	T_0	Biaxial stretching ($\dot{\varepsilon}_{11} = 2\dot{\varepsilon}_{22} = 4\bar{\gamma}$)
8	0	0	0	0	0	$T_0 + \bar{T}t$	Static heating ($\dot{T} = \bar{T}$)

For the majority of load cases described in table 3, the parameter $\bar{\gamma}$ denotes the constant strain rate (as well as the final value of total strain at $t = 1$) of one or more strain components, whereas the parameters T_0 and $\bar{T}$ denote the initial temperature and constant rate of temperature increase, respectively.

Load cases 1 and 7 are volume-changing deformations which produce a hydrostatic component within the overall state of stress. Load case 1 is used by the pressure-dependent plasticity test, and by the isotropic and orthotropic elasticity tests to verify the hydrostatic response of each model. Load case 7 is used by one of the anisotropic plasticity tests, resulting in proportional loading of the chosen anisotropic yield surface.

Load cases 2, 3, 4, 5, and 6 produce volume-preserving deformations, which for isotropic materials result in a purely deviatoric state of stress, and proportional loading conditions for von Mises plasticity models. Load case 6 in particular is used extensively by the various hardening plasticity tests because it engages most of the components of the stress tensor in the computation of the effective stress.

Load case 8 is used by all thermal expansion tests, inducing changes in the normal strain and in-plane stress components due to heating.

3.3 Material Parameterizations

While the load case assigned to a given problem fully defines the geometry and boundary conditions of the single-element test setup, the complete description of a specific test must also appropriately define all relevant material properties. To this end, each test is also assigned a particular material parameterization: a specification of all relevant material parameters and their corresponding values, presented in a tabular format resembling table 4.

Table 4: Example material parameterization

Parameter	Value
Parameter name 1, *Parameter symbol 1*	*Parameter value 1*
⋮	⋮
Parameter name N, *Parameter symbol N*	*Parameter value N*

A given material parameter is deemed to be "relevant" to a specific test problem if:

1.) The parameter is necessary for the sake of testing the specific model feature of interest.

2.) The parameter cannot be uniquely determined/surmised from the other defined parameters.

All other other parameters are regarded as either irrelevant or redundant, and are not defined explicitly.

Because each test is designed to be fairly general and therefore applicable to a variety of similar material models, the corresponding material parameterization for each test constitutes a subset of the parameters which may be defined for a specific model. Moreover, not all material models share the same input parameters. For example, models with isotropic elastic properties may only require the definition of two parameters (e.g. E and ν), whereas models which orthotropic elastic properties require as many as nine parameters to be defined (e.g. E_a, E_b, E_c, ν_{ba}, ν_{ca}, ν_{cb}, G_{ab}, G_{bc}, and G_{ca}). In such cases, the auxiliary parameters are implicitly determined and prescribed to render consistency with the assumptions set forth by the associated test problem. In the previous example, if a given material parameterization only specifies the isotropic elastic properties E and ν, an orthotropic material model would retain this assumption such that $E_a = E_b = E_c = E$, $\nu_{ba} = \nu_{ca} = \nu_{cb} = \nu$, and $G_{ab} = G_{bc} = G_{ca} = \frac{E}{2(1+\nu)}$.

For some of the generic test collections proposed in this report, similar tests within a grouped collection are defined to share a core set of "default" parameter values, but each test may perturb the value of an individual parameter being tested. To avoid repetition, a "default parameterization" and a corresponding set of "overriding parameters" for each test are defined in lieu of specifying a complete material parameterization for each test individually. In such cases, all material parameters assume their default values, unless they have been overridden for a given test.

Because the purpose of the tests proposed in this report is to verify the implementation of each material model, the chosen material parameterizations for each test are selected primarily for the sake of procedurally testing and verifying individual model features. Consequently, all specified parameters are dimensionless, purely fictitious in their construction, and not intended to validate the physical properties of real materials. Any resemblance to actual material datasets is purely coincidental.

4 Numerical Analysis of the Test Results

To verify the implementation of each material model, verification tests are created by first postulating a relatively simple problem designed to isolate and independently verify a single model feature (e.g. isotropic linear hardening plasticity). The generality of such tests permits them to be used to verify the implementation of multiple models which share the same or similar features. This has the added benefit of facilitating cross-verification between different models with shared functionality.

For each test, an exact mathematical solution is derived to be consistent with the theoretical formulation of the model feature of interest. For some problems, this entails the solution to an ordinary differential equation. The exact mathematical representation of such solutions permits a high degree accuracy in their corresponding numerical representation, and further allows for such solutions to be easily modulated by individual problem or model parameters, thereby establishing an extensible family of verification problems.

With an exact solution in hand for a given test problem, the numerical solution computed by a specific material model in DYNA3D can be directly compared to the exact solution and verified through the evaluation of several appropriately chosen error metrics, defined in the following sub-section.

4.1 Definition of Error Measures

The entrywise p-norm (distinct from the operator p-norm) for a tensor-valued quantity $\mathbf{A} \in \mathbb{R}^{3\times 3}$ is herein defined as

$$||\mathbf{A}||_p \equiv \left[\sum_{i=1}^{3} \sum_{j=1}^{3} |A_{ij}|^p \right]^{\frac{1}{p}}. \tag{19}$$

For the special case of $p = 2$, the Frobenius norm is obtained:

$$||\mathbf{A}||_2 = \sqrt{\mathbf{A} : \mathbf{A}}, \tag{20}$$

corresponding to the "averaged" root-mean-square (RMS) value of all components of $\mathbf{A}$.

Additionally, consider the L^p-norm defined for scalar-valued functions of time $f(t) \in C^0([0,1])$:

$$||f(t)||_{L^p} \equiv \left[\int_0^1 |f(t)|^p \, dt \right]^{\frac{1}{p}}. \tag{21}$$

For the special case of $p = 2$, the L^2 norm is obtained:

$$||f(t)||_{L^2} = \sqrt{\int_0^1 [f(t)]^2 \, dt}, \tag{22}$$

corresponding to the root-mean-square of $f(t)$ over all times $t \in [0,1]$.

By extension, given some tensor-valued function of time $\mathbf{A}(t) \in \left[C^0([0,1])\right]^{3\times 3}$, the L^p-norm is defined as

$$||\mathbf{A}(t)||_{L^p} \equiv \left[\int_0^1 ||\mathbf{A}(t)||_p^p \, dt \right]^{\frac{1}{p}}, \tag{23}$$

and for $p = 2$:

$$||\mathbf{A}(t)||_{L^2} = \sqrt{\int_0^1 \mathbf{A}(t) : \mathbf{A}(t) \, dt}, \tag{24}$$

corresponding to the RMS averaged value of all components of $\mathbf{A}(t)$ over all times $t \in [0,1]$.

In practice, $||f(t)||_{L^2}$ and $||\mathbf{A}(t)||_{L^2}$ are evaluated numerically as:

$$||f(t)||_{L^2} \approx \sqrt{\sum_{k=1}^{N_{\Delta t}} [f(t_k)]^2 \, \Delta t_k}, \qquad ||\mathbf{A}(t)||_{L^2} \approx \sqrt{\sum_{k=1}^{N_{\Delta t}} \mathbf{A}(t_k) : \mathbf{A}(t_k) \, \Delta t_k}, \tag{25}$$

where $\Delta t_k \in \{\Delta t_k : k = 1, \ldots, N_{\Delta t}\}$ denotes the chosen time-discretization used to obtain a given model's numerically computed solution values at all discrete analysis times t_k.

Making use of the numerically evaluated norms defined in equation (25), the primary scalar- and tensor-valued relative (and absolute) error metrics of interest for all verification problems are established:

$$e^{\text{rel}}_{L^2}(f) \equiv \frac{e^{\text{abs}}_{L^2}(f)}{||f^{\text{model}}(t)||_{L^2}} \qquad e^{\text{abs}}_{L^2}(f) \equiv ||f^{\text{model}}(t) - f^{\text{exact}}(t)||_{L^2}, \qquad \forall f(t) \in C^0([0,1]), \tag{26}$$

$$e^{\text{rel}}_{L^2}(\mathbf{A}) \equiv \frac{e^{\text{abs}}_{L^2}(\mathbf{A})}{||\mathbf{A}^{\text{model}}(t)||_{L^2}} \qquad e^{\text{abs}}_{L^2}(\mathbf{A}) \equiv ||\mathbf{A}^{\text{model}}(t) - \mathbf{A}^{\text{exact}}(t)||_{L^2}, \qquad \forall \mathbf{A}(t) \in \left[C^0([0,1])\right]^{3\times 3}, \tag{27}$$

where superscripted text is used to distinguish between the "exact" solutions for a given quantity of interest and the approximate values computed numerically by a given material "model," and between the "absolute" and "relative" (normalized) measures of solution error. The above metrics are positive-definite (i.e. $e^{\text{rel/abs}}_{L^2}(\cdot) \geq 0$), and satisfy the equivalence condition:

$$e^{\text{rel/abs}}_{L^2}(f) = 0 \iff f^{\text{model}}(t) = f^{\text{exact}}(t)\, \forall t \in [0,1]. \tag{28}$$

Intuitively, $e^{\text{rel/abs}}_{L^2}(f)$ captures the time-averaged relative/absolute error in $f(t)$, and $e^{\text{rel/abs}}_{L^2}(\mathbf{A})$ captures the time-averaged relative/absolute error in all components of $\mathbf{A}(t)$. For example, $e^{\text{rel}}_{L^2}(\bar{\varepsilon}^p)$ measures the time-averaged relative error in the equivalent plastic strain, and $e^{\text{abs}}_{L^2}(\boldsymbol{\sigma})$ measures the time-averaged absolute error in all components of the stress tensor. The tensor-valued error metric $e^{\text{rel/abs}}_{L^2}(\mathbf{A})$ is particularly useful for the sake of collectively evaluating the measured error in all tensor components of $\mathbf{A}$. Otherwise, one would need to examine the error measured for each tensor component individually, producing an excessive volume of data whose results would be cumbersome to present.

For all tests, the accuracy of a given material model is determined by examining the errors in the complete time-history for the stress $\boldsymbol{\sigma}(t)$, the normal strain $\varepsilon_{33}(t)$, and the equivalent plastic strain $\bar{\varepsilon}^p(t)$ variables. For a given problem, if the exact solution for a particular quantity is identically zero for all time (e.g. if $\bar{\varepsilon}^p(t) = 0\, \forall t \iff ||\bar{\varepsilon}^p(t)||_{L^2} = 0$), the absolute error metric is used. Otherwise, the relative error metric is examined. For sufficiently refined time discretizations, it is expected that – when used in the aforementioned contexts – both metrics should produce errors on the order of machine precision (i.e. $e^{\text{rel/abs}}_{L^2}(\cdot) \approx 10^{-16}$).

4.2 Error Estimation and Convergence Analysis

Several distinct sources of error which contribute to the overall error observed between the exact and numerical solutions of a particular problem can be estimated or directly quantified. These include:

1.) Errors due to finite-precision floating point arithmetic.

2.) Errors in the time-integration of the equations of motion.

3.) Errors in the time-integration of the stress rate equations.

4.) Errors in the time-integration of the equations of plastic flow.

Item 1 constitutes an inherrent source of error that ultimately establishes a lower bound on the minimum error that can ever be achieved (roughly on the order of machine precision), regardless of the chosen time discretization. In contrast, items 2, 3, and 4 collectively contribute to the "temporal discretization error" for a given problem, whose magnitude can be diminished under temporal refinement – by decreasing Δt.

To distinguish between the aforementioned sources of temporal discretization error and potential inconsistencies in the implementation of a given model, it is of interest to investigate the rate of convergence in a given error metric under temporal refinement – to examine whether the model errors are successively diminished if an increasing number of time steps are taken. An implementation error may be indicated either by a reduced rate of convergence compared to the theoretical rate for the dominant source of discretization error, or by a sudden loss of convergence below a certain threshold for Δt.

To this end, bounded error estimates are derived for the various temporal discretization error sources, measured in the L^2-norm:

$$e_{L^2}^{\text{rel/abs}}(\cdot) < C\,\Delta t^r, \tag{29}$$

for some $C > 0$, and where r denotes the corresponding "rate of convergence" in $e_{L^2}^{\text{rel/abs}}(\cdot)$ with respect to the (assumed uniform) time step size Δt.

Henceforth, big O notation is employed to characterize the rate of convergence in the L^2-error measure for a given quantity as $O(\Delta t^r)$, where the rate of convergence r can been estimated mathematically, and computationally verified through a corresponding temporal convergence study.

4.2.1 Error Estimates for Incremental Kinematic Algorithms

For all rate-formulated material models implemented in DYNA3D, the constitutive state (consisting of the stress and any other state variables) is updated from time t_k to t_{k+1} by an increment in the total strain, denoted $\Delta\boldsymbol{\varepsilon}$. For the special case of zero material spin ($\mathbf{W} = \mathbf{0}$), the strain increment may be computed exactly as

$$\Delta\boldsymbol{\varepsilon} = \boldsymbol{\varepsilon}(t_{k+1}) - \boldsymbol{\varepsilon}(t_k) = \int_{t_k}^{t_{k+1}} \mathbf{D}(t)\,dt. \tag{30}$$

In practice, the strain increment is approximated numerically via a mid-point time-integration formula, as proposed by Hughes and Winget [7]:

$$\int_{t_k}^{t_{k+1}} \mathbf{D}(t)\,dt \approx \mathbf{D}_{k+\frac{1}{2}}\,\Delta t, \qquad \Delta t = t_{k+1} - t_k, \tag{31}$$

where the mid-point rate of deformation $\mathbf{D}_{k+\frac{1}{2}} = \mathbf{D}(t_{k+\frac{1}{2}})$ is evaluated directly via

$$\mathbf{D}_{k+\frac{1}{2}} = \frac{1}{2}\left(\mathbf{L}_{k+\frac{1}{2}} + \mathbf{L}_{k+\frac{1}{2}}^T\right), \qquad \mathbf{L}_{k+\frac{1}{2}} = \frac{\partial \mathbf{v}_{k+\frac{1}{2}}}{\partial \boldsymbol{\xi}}\left(\frac{\partial \mathbf{x}_{k+\frac{1}{2}}}{\partial \boldsymbol{\xi}}\right)^{-1}. \tag{32}$$

The second-order approximation given by equation (31) is exact if $\mathbf{D}(t)$ is at most a linear function of time.

However, as discussed in [7], the material motion that takes place over any given analysis time interval Δt is assumed to belong to a 1-parameter family of deformation states, specifically:

$$\mathbf{x}(t) = \mathbf{x}_k + \mathbf{v}_{k+\frac{1}{2}}\,(t - t_k) \quad \forall t \in [t_k, t_{k+1}], \tag{33}$$

where $\mathbf{v}_{k+\frac{1}{2}}$ denotes the mid-step velocity, assumed to remain constant over the time step $t \in [t_k, t_{k+1}]$ but which may vary spatially. The resulting time-varying expression for the rate of deformation is therefore:

$$\mathbf{D}(t) = \dot{\mathbf{J}}_{k+\frac{1}{2}}\left(\mathbf{J}_k + (t - t_k)\,\dot{\mathbf{J}}_{k+\frac{1}{2}}\right)^{-1} \quad \forall t \in [t_k, t_{k+1}], \tag{34}$$

where the (constant) element Jacobian $\mathbf{J}_k$ and its time-rate $\dot{\mathbf{J}}_{k+\frac{1}{2}}$ at times t_k and $t_{k+\frac{1}{2}}$, respectively are:

$$\mathbf{J}_k = \sum_{a=1}^{4} \mathbf{x}_{a;k} \otimes \frac{\partial N_a}{\partial \boldsymbol{\xi}}, \qquad \dot{\mathbf{J}}_{k+\frac{1}{2}} = \sum_{a=1}^{4} \mathbf{v}_{a;k+\frac{1}{2}} \otimes \frac{\partial N_a}{\partial \boldsymbol{\xi}}. \tag{35}$$

Clearly, the expression for $\mathbf{D}(t)$ in equation (34) is a non-linear function time, and the strain increment therefore cannot be exactly integrated by the mid-point rule given by equation (31). Because the chosen time-integration formula in equation (31) is (locally) second-order accurate in time, it may be shown that the corresponding (global) approximation errors in the strain rate $e_{L^2}^{\text{rel/abs}}(\mathbf{D})$ are likewise of order $O(\Delta t^2)$.

Moreover, the application of velocity boundary conditions at discrete analysis times introduces additional errors of order $O(\Delta t^2)$ into the computation of the updated nodal positions using the Newmark time-integration formula. This ultimately precludes an exact representation of the time-history of deformation over a single time step. Consequently, the strain (increments) which ultimately enter the constitutive model

are not consistent with their derived reference solutions, and thus incur an error proportional to the chosen time discretization.

Assuming that the approximation errors in the computation of the strain increment constitute the dominant source of error for a particular verification problem, it suffices to verify that the rate of convergence in a given L^2 error measure (e.g. $e_{L^2}^{\text{rel/abs}}(\boldsymbol{\sigma})$) is of order $r = 2.0$.

The indicated rate of $r = 2.0$ uniformly bounds the kinematic discretization error for all possible input motions. However, it is still possible to observe faster rates of convergence. Notably, only the in-plane strain components are consistent with the logarithmic strain measure, whereas the transverse shear strains are consistent with the corresponding components of the small strain tensor. As such, the anticipated kinematic discretization errors for tests which employ either load case 4 or 5 should be on the order of machine precision.

4.2.2 Error Estimates for Return-Mapping Plasticity Algorithms

As discussed in [9], classical (radial) return-mapping algorithms employed by the vast majority of plasticity models in DYNA3D are predicated upon a backward – or in some cases, a forward – Euler approximation of the rate equations of plasticity. Such methods have been shown to be only first-order accurate with respect to the strain increment over a given time step. Consequently, they yield only first-order accuracy in time, potentially introducing errors of order $O(\Delta t)$ in the computation of both the stress and the plastic strain variables.

For this reason, verification problems designed to test a given plasticity feature should be expected to yield rates of convergence on the order of $r = 1.0$ (at worst) in the various L^2 error measures.

However, as noted by Krieg and Krieg in [8], it may nonetheless be possible to achieve superlinear convergence in the time-integration of the plastic flow for certain loading configurations and hardening rules (e.g. linear hardening under proportional loading conditions). In such cases, the dominant sources of discretization error arise from the computation of the strain increment, and one may recover convergence of order $O(\Delta t^2)$.

4.3 Limited Numerical Precision of Material Input Parameters

A subtle issue that was identified as a substantial challenge in the reproduction of accurate test results regards the currently limited precision for material input parameters to DYNA3D. The fixed format input structure for the material definition cards allows up to 10 characters to be used to define any single material parameter. When specifying input parameters with a sufficiently large number of decimal digits (e.g. $\frac{1}{3} = 0.333\ldots$), this ultimately limits the relative precision of the corresponding input values to 1.0×10^{-10} at best (assuming no decimal, sign, or exponent characters are used), and 1.0×10^{-4} at worst (e.g. `-2.456e-90`). Because not all material models share the same input parameterization, this presented a significant obstacle to creating generic tests that could be used by multiple models. For example, some models require E and ν to define the elastic properties, while others require $\mu = \frac{E}{2(1+\nu)}$ and $\kappa = \frac{E}{3(1-2\nu)}$, which for arbitrary finite-decimal precision values of E and ν does not yield correspondingly finite-decimal precision values for μ and κ.

To overcome this limitation, careful attention was paid to the selection of material parameterizations which guaranteed that any alternative parameterizations employed by other models could be represented exactly by up to four decimal digits. For example, if $E = 7.5$ and $\nu = 0.25$, then $\mu = 3.0$ and $\kappa = 5.0$. Doing so allowed for cross-verification to be conducted between different models run using the same test, even if these models accepted differing input parameters.

5 Summary of Newly Proposed Verification Tests

This section of the report provides a comprehensive summary of all tests comprising the newly proposed verification suite for shell element material models in DYNA3D. The presentation of the test suite is organized into collections of tests designed to verify a generic model feature shared by multiple material models. Each subsection provides a brief theoretical overview of a specific model feature of interest (e.g. isotropic hardening plasticity), along with a summary of the tests that were developed to verify the implementation of all material models which share this feature in common.

Each individual test is defined by its assigned load case (described in section 3.2), and its corresponding material parameterization (described in section 3.3). For brevity, collections of tests which share the same load case and/or material parameterization are noted as such up front.

For each test, closed-form reference solutions are derived to be consistent with the underlying mathematical theory for each model feature. The numerical results for each test are compared between all material models which implement the tested feature of interest, and against the mathematically derived reference solution. Solution errors in the $e^{\text{rel}}_{L^2}(\cdot)$ metric (or in the $e^{\text{abs}}_{L^2}(\cdot)$ metric when $e^{\text{rel}}_{L^2}(\cdot)$ is undefined) for the stress $\boldsymbol{\sigma}(t)$, the normal strain $\varepsilon_{33}(t)$, and the equivalent plastic strain $\bar{\varepsilon}^p(t)$ are examined for a highly refined time discretization of the problem, i.e. $\Delta t = 10^{-4}$.

The convergence of each error metric under temporal refinement is also examined across four different time discretizations, namely: $\Delta t \in \left\{10^{-1}, 10^{-2}, 10^{-3}, 10^{-4}\right\}$. Error convergence plots and the measured rates of convergence are presented for the sake of comparison between different models, and against the estimated theoretical convergence rate. In certain cases, the error across all refinement levels is either identically zero or is on the order of machine precision for double precision arithmetic ($e^{\text{abs/rel}}_{L^2}(\cdot) \approx 10^{-16}$), and no further convergence can be obtained through temporal refinement. In such cases, the computed rate of convergence is not displayed in the tabulated results for the corresponding test.

In the course of creating the proposed suite of verification tests, a number of bugs were discovered and fixed. The complete list of resolved issues is presented at the end of the report, in section 6.1. Despite these efforts, a few discrepancies remain which are recognized (and in some cases quantified) to be the result of model-specific assumptions that are inconsistent with the theory employed by most other models in DYNA3D. In such cases, comparatively large errors or slow convergence rates in the tabulated results for each test are highlighted in red. A cautionary note is provided, and a recommendation is given regarding the scope of work required to properly address the observed inconsistencies.

Along with the tabulated results for each test, the verification "status" of each model is indicated symbolically using one of the following characters:

- ✓: The indicated model feature has been verified and is functioning properly.
- ⚠: The indicated model feature is functioning as intended, but makes an assumption that is inconsistent with most other models in DYNA3D.
- ✗: The indicated model feature is not functioning properly.

5.1 Hypoelasticity

All shell models in DYNA3D employ a hypoelastic constitutive law which expresses the (usually linear) relationship between the co-rotational rate of deformation $\hat{\mathbf{D}}$ and the time-rate of the co-rotational stress $\hat{\boldsymbol{\sigma}}$:

$$\dot{\hat{\boldsymbol{\sigma}}} = \mathbb{C} : \hat{\mathbf{D}}, \tag{36}$$

subject to the plane stress constraint:

$$\dot{\hat{\sigma}}_{33} = 0. \tag{37}$$

It is worth noting that the above relation in equation (36) is *not* consistent with the Jaumann rate of the Cauchy stress which is used by most of the rate-formulated material models for solid elements. Nonetheless, under the conditions of zero material spin, the particular choice of co-rotational rate becomes arbitrary, and all stress rates yield identical expressions for the time rate of the Cauchy stress. Namely, if the lamina and global coordinate systems coincide (as they do for all of the proposed load cases), then $\hat{\mathbf{D}} = \mathbf{D}$ and $\hat{\boldsymbol{\sigma}} = \boldsymbol{\sigma}$. Thus, it is equivalent to henceforth assume that:

$$\dot{\boldsymbol{\sigma}} = \mathbb{C} : \mathbf{D} \quad \text{s.t.} \quad \dot{\sigma}_{33} = 0. \tag{38}$$

"Grade zero" hypoelasticity refers to the special case where the rank 4 elastic modulus tensor $\mathbb{C}$ remains constant, irrespective of the history of deformation. Grade zero models are also rate-independent, and it therefore suffices to integrate the stress rate directly to obtain an expression for the stress $\boldsymbol{\sigma}(t)$ at a given time t:

$$\boldsymbol{\sigma}(t) = \int_0^t \dot{\boldsymbol{\sigma}}\, d\tau = \mathbb{C} : \int_0^t \mathbf{D}\, d\tau. \tag{39}$$

Xiao et al. demonstrated in [11] that $\dot{\boldsymbol{\varepsilon}} = \mathbf{D}$ if $\boldsymbol{\varepsilon}$ corresponds to the logarithmic (Hencky) strain measure. Given the previously derived expression for $\mathbf{D}$ in equation (12), the strain rate may be integrated in time to obtain an expression for the total strain $\boldsymbol{\varepsilon}(t)$ (though it is not properly logarithmic in the transverse shear components):

$$\boldsymbol{\varepsilon}(t) = \int_0^t \mathbf{D}\, d\tau = \int_0^t \dot{\boldsymbol{\varepsilon}}_u\, d\tau + \int_0^t \dot{\boldsymbol{\varepsilon}}_\theta\, d\tau + \int_0^t D_{33}\, \mathbf{e}_3 \otimes \mathbf{e}_3\, d\tau = \boldsymbol{\varepsilon}_u(t) + \boldsymbol{\varepsilon}_\theta(t) + \varepsilon_{33}(t)\, \mathbf{e}_3 \otimes \mathbf{e}_3. \tag{40}$$

Therefore:

$$\boldsymbol{\sigma}(t) = \mathbb{C} : \boldsymbol{\varepsilon}(t), \tag{41}$$

and

$$\sigma_{33}(t) = C_{33ij}\, \varepsilon_{ij}(t) = 0 \quad \Rightarrow \quad \varepsilon_{33}(t) = -\frac{C_{33ij}}{C_{3333}} \left[\varepsilon_{u;ij}(t) + \varepsilon_{\theta;ij}(t)\right] \quad \forall t. \tag{42}$$

The above serves as the basis for the vast majority of tests described henceforth for isotropic and anisotropic elasticity and plasticity.

5.1.1 Isotropic Elasticity

For isotropic elastic models with constant Lamé parameters $\lambda = \frac{E\nu}{(1+\nu)(1-2\nu)}$ and $\mu = \frac{E}{2(1+\nu)}$, the general expressions for the Cauchy stress and normal strain in equations (41) and (42), respectively reduce to:

$$\boldsymbol{\sigma}(t) = \lambda \operatorname{tr}[\boldsymbol{\varepsilon}(t)]\,\mathbf{1} + 2\mu\,\boldsymbol{\varepsilon}(t), \qquad \varepsilon_{33}(t) = -\frac{\lambda}{\lambda+2\mu}\left[\varepsilon_{11}(t) + \varepsilon_{22}(t)\right]. \tag{43}$$

For each isotropic elasticity test considered herein, the assigned load cases and exact solutions for the individual stress and normal strain components as functions of time are provided in table 5. For all tests, the equivalent plastic strain $\bar{\varepsilon}^p(t)$ is identically zero. These tests are applicable to all shell element material models in DYNA3D.

Table 5: Assigned load cases and corresponding exact solutions for isotropic elasticity tests 1-5

Test	Load Case	Non-zero stress components (all other $\sigma_{ij} = 0\,\forall t$)	$\varepsilon_{33}(t)$
1	1 ($\bar{\gamma} = 0.01$)	$\sigma_{11}(t) = \sigma_{22}(t) = 2\mu\left[\bar{\gamma}\,t - \varepsilon_{33}(t)\right]$	$-\frac{2\lambda}{\lambda+2\mu}\bar{\gamma}\,t$
2	2 ($\bar{\gamma} = 0.01$)	$\sigma_{11}(t) = -\sigma_{22}(t) = 2\mu\bar{\gamma}\,t$	0
3	3 ($\bar{\gamma} = 0.01$)	$\sigma_{12}(t) = 2\mu\bar{\gamma}\,t$	0
4	4 ($\bar{\gamma} = 0.01$)	$\sigma_{23}(t) = 2\mu\bar{\gamma}\,t$	0
5	5 ($\bar{\gamma} = 0.01$)	$\sigma_{13}(t) = 2\mu\bar{\gamma}\,t$	0

The generic material parameterization for all isotropic elasticity tests is presented in table 6. The results

Table 6: Material parameterization for isotropic elasticity tests 1-5

Parameter	Value
Elastic modulus, E	7.5
Poisson's ratio, ν	0.25

of each test are presented individually in tables 7 through 11, and figures 3 through 7.

With the exception of model 28 for test 1, all other models yield sufficiently small errors in all metrics. The measured convergence rates are consistent with the theoretical rate of $r = 2$ for tests 1, 2, and 3. The errors for tests 4 and 5 are on the order of machine precision across all time discretizations, as expected.

Regarding model 28: because this model is predicated on a resultant stress formulation, it does not directly compute a normal strain rate. Instead, the resultant shell element formulation imposes the assumption of incompressibility, such that the normal strain is computed as $\varepsilon_{33} = -(\varepsilon_{11} + \varepsilon_{22})$. This is tantamount to assuming that the plastic strains are significantly larger than the elastic strains, such that one may reasonably approximate the total strain as $\boldsymbol{\varepsilon} \approx \boldsymbol{\varepsilon}^p$, and where the usual assumption of plastic incompressibility yields $\operatorname{tr}(\boldsymbol{\varepsilon}) \approx \operatorname{tr}(\boldsymbol{\varepsilon}^p) = 0$. This accounts for the observed error in the computed value for the normal strain for model 28 (shown in red in table 7). It may be worthwhile to revisit this assumption at a later time.

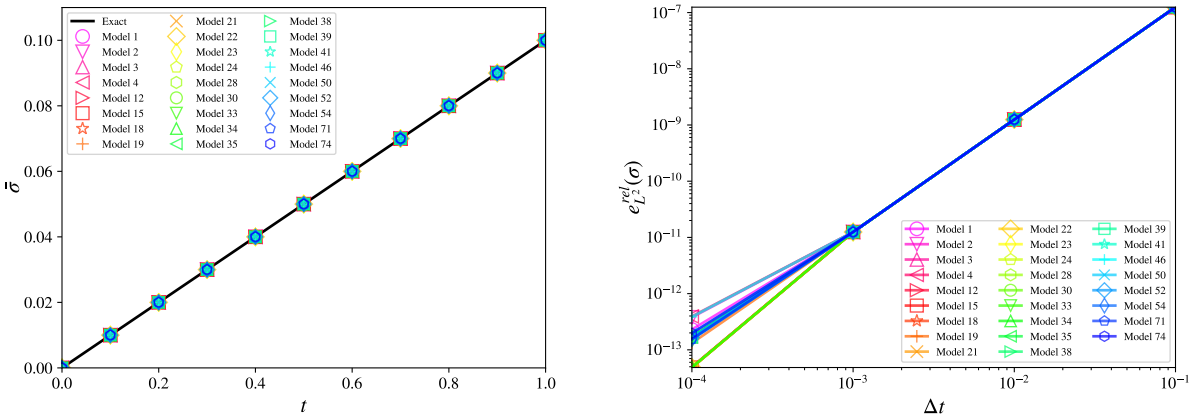

(a) Time-history plot of $\bar{\sigma}$ vs. t using $\Delta t = 0.1$.

(b) Convergence plot for $e^{\text{rel}}_{L^2}(\boldsymbol{\sigma})$ errors vs. Δt.

Figure 3: Isotropic elasticity test 1.

Table 7: Computed errors for isotropic elasticity test 1.

Model	$e^{\text{rel}}_{L^2}(\boldsymbol{\sigma})$	r	$e^{\text{rel}}_{L^2}(\varepsilon_{33})$	r	$e^{\text{abs}}_{L^2}(\bar{\varepsilon}^p)$	r	Status
1	2.299e-13	1.73	1.822e-13	1.84	0.000e+00	-	✓
2	3.789e-13	1.52	1.822e-13	1.84	0.000e+00	-	✓
3	4.949e-14	2.00	2.082e-13	1.78	0.000e+00	-	✓
4	3.931e-13	1.50	2.200e-13	1.75	0.000e+00	-	✓
12	4.939e-14	2.00	1.822e-13	1.84	0.000e+00	-	✓
15	4.867e-14	2.00	1.686e-13	1.87	0.000e+00	-	✓
18	4.867e-14	2.00	1.686e-13	1.87	0.000e+00	-	✓
19	1.319e-13	1.98	1.686e-13	1.87	0.000e+00	-	✓
21	4.846e-14	2.00	1.677e-13	1.87	0.000e+00	-	✓
22	4.875e-14	2.00	1.684e-13	1.87	0.000e+00	-	✓
23	1.602e-13	1.89	1.684e-13	1.87	0.000e+00	-	✓
24	4.875e-14	2.00	1.684e-13	1.87	0.000e+00	-	✓
28	1.703e-13	1.86	2.000e+00	-0.00	0.000e+00	-	⚠
30	1.703e-13	1.86	1.698e-13	1.87	0.000e+00	-	✓
33	1.703e-13	1.86	1.684e-13	1.87	0.000e+00	-	✓
34	4.875e-14	2.00	1.684e-13	1.87	0.000e+00	-	✓
35	1.670e-13	1.87	1.820e-13	1.84	0.000e+00	-	✓
38	1.656e-13	1.88	2.236e-13	1.75	0.000e+00	-	✓
39	1.656e-13	1.88	2.236e-13	1.75	0.000e+00	-	✓
41	1.545e-13	1.91	2.236e-13	1.75	0.000e+00	-	✓
46	3.861e-13	1.51	2.236e-13	1.75	0.000e+00	-	✓
50	1.972e-13	1.80	1.803e-13	1.84	0.000e+00	-	✓
52	1.656e-13	1.88	2.236e-13	1.75	0.000e+00	-	✓
54	1.545e-13	1.91	2.236e-13	1.75	0.000e+00	-	✓
71	1.545e-13	1.91	2.236e-13	1.75	0.000e+00	-	✓
74	1.972e-13	1.80	2.236e-13	1.75	0.000e+00	-	✓

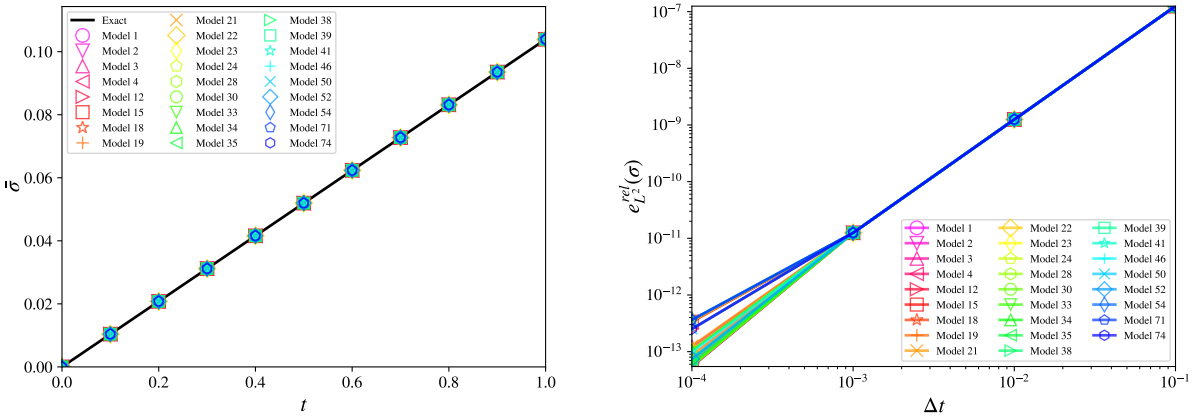

(a) Time-history plot of $\bar{\sigma}$ vs. t using $\Delta t = 0.1$.

(b) Convergence plot for $e_{L^2}^{\text{rel}}(\boldsymbol{\sigma})$ errors vs. Δt.

Figure 4: Isotropic elasticity test 2.

Table 8: Computed errors for isotropic elasticity test 2.

Model	$e_{L^2}^{\text{rel}}(\boldsymbol{\sigma})$	r	$e_{L^2}^{\text{abs}}(\varepsilon_{33})$	r	$e_{L^2}^{\text{abs}}(\bar{\varepsilon}^p)$	r	Status
1	6.380e-14	2.00	6.274e-18	-	0.000e+00	-	✓
2	5.466e-14	2.00	3.568e-17	-	0.000e+00	-	✓
3	1.216e-13	2.00	4.231e-17	-	0.000e+00	-	✓
4	5.485e-14	2.00	8.266e-18	-	0.000e+00	-	✓
12	2.513e-13	1.70	7.427e-17	-	0.000e+00	-	✓
15	3.380e-13	1.57	1.557e-16	-	0.000e+00	-	✓
18	3.380e-13	1.57	1.557e-16	-	0.000e+00	-	✓
19	8.622e-14	2.00	1.557e-16	-	0.000e+00	-	✓
21	1.259e-13	2.00	6.811e-18	-	0.000e+00	-	✓
22	1.044e-13	2.00	1.541e-16	-	0.000e+00	-	✓
23	3.499e-13	1.55	1.541e-16	-	0.000e+00	-	✓
24	1.044e-13	2.00	1.541e-16	-	0.000e+00	-	✓
28	5.681e-14	2.00	4.623e-16	-	0.000e+00	-	✓
30	5.681e-14	2.00	2.452e-17	-	0.000e+00	-	✓
33	5.680e-14	2.00	1.541e-16	-	0.000e+00	-	✓
34	1.044e-13	2.00	1.541e-16	-	0.000e+00	-	✓
35	6.372e-14	2.00	5.246e-17	-	0.000e+00	-	✓
38	7.419e-14	2.00	2.517e-16	-	0.000e+00	-	✓
39	7.419e-14	2.00	2.517e-16	-	0.000e+00	-	✓
41	3.639e-13	1.54	2.517e-16	-	0.000e+00	-	✓
46	9.795e-14	2.00	2.517e-16	-	0.000e+00	-	✓
50	2.509e-13	1.70	4.416e-16	-	0.000e+00	-	✓
52	7.419e-14	2.00	2.517e-16	-	0.000e+00	-	✓
54	3.639e-13	1.54	2.517e-16	-	0.000e+00	-	✓
71	3.639e-13	1.54	2.517e-16	-	0.000e+00	-	✓
74	2.509e-13	1.70	2.517e-16	-	0.000e+00	-	✓

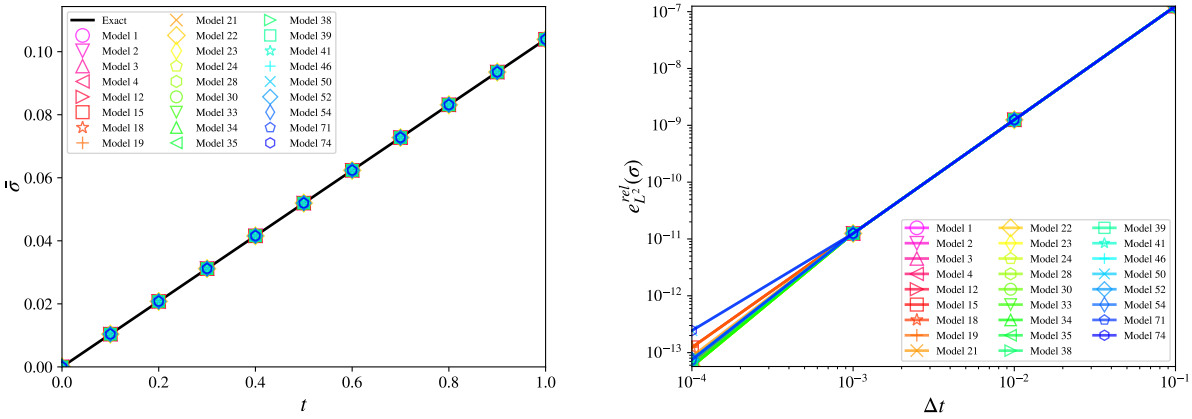

(a) Time-history plot of $\bar{\sigma}$ vs. t using $\Delta t = 0.1$.

(b) Convergence plot for $e_{L^2}^{\text{rel}}(\boldsymbol{\sigma})$ errors vs. Δt.

Figure 5: Isotropic elasticity test 3.

Table 9: Computed errors for isotropic elasticity test 3.

Model	$e_{L^2}^{\text{rel}}(\boldsymbol{\sigma})$	r	$e_{L^2}^{\text{abs}}(\varepsilon_{33})$	r	$e_{L^2}^{\text{abs}}(\bar{\varepsilon}^p)$	r	Status
1	6.392e-14	2.00	6.217e-18	-	0.000e+00	-	✓
2	6.460e-14	2.00	1.558e-17	-	0.000e+00	-	✓
3	7.307e-14	2.00	5.139e-17	-	0.000e+00	-	✓
4	7.856e-14	2.00	6.525e-17	-	0.000e+00	-	✓
12	7.059e-14	2.00	4.080e-17	-	0.000e+00	-	✓
15	1.236e-13	2.00	1.468e-16	-	0.000e+00	-	✓
18	1.236e-13	2.00	1.468e-16	-	0.000e+00	-	✓
19	1.236e-13	2.00	1.468e-16	-	0.000e+00	-	✓
21	8.547e-14	2.00	8.895e-17	-	0.000e+00	-	✓
22	5.695e-14	2.00	3.436e-17	-	0.000e+00	-	✓
23	5.695e-14	2.00	3.436e-17	-	0.000e+00	-	✓
24	5.695e-14	2.00	3.436e-17	-	0.000e+00	-	✓
28	5.695e-14	2.00	1.031e-16	-	0.000e+00	-	✓
30	5.695e-14	2.00	3.436e-17	-	0.000e+00	-	✓
33	5.695e-14	2.00	3.436e-17	-	0.000e+00	-	✓
34	5.695e-14	2.00	3.436e-17	-	0.000e+00	-	✓
35	6.695e-14	2.00	3.822e-17	-	0.000e+00	-	✓
38	7.494e-14	2.00	5.521e-17	-	0.000e+00	-	✓
39	7.494e-14	2.00	5.521e-17	-	0.000e+00	-	✓
41	7.494e-14	2.00	5.521e-17	-	0.000e+00	-	✓
46	7.494e-14	2.00	5.521e-17	-	0.000e+00	-	✓
50	2.439e-13	1.71	5.521e-17	-	0.000e+00	-	✓
52	7.494e-14	2.00	5.521e-17	-	0.000e+00	-	✓
54	7.494e-14	2.00	5.521e-17	-	0.000e+00	-	✓
71	7.494e-14	2.00	5.521e-17	-	0.000e+00	-	✓
74	2.439e-13	1.71	5.521e-17	-	0.000e+00	-	✓

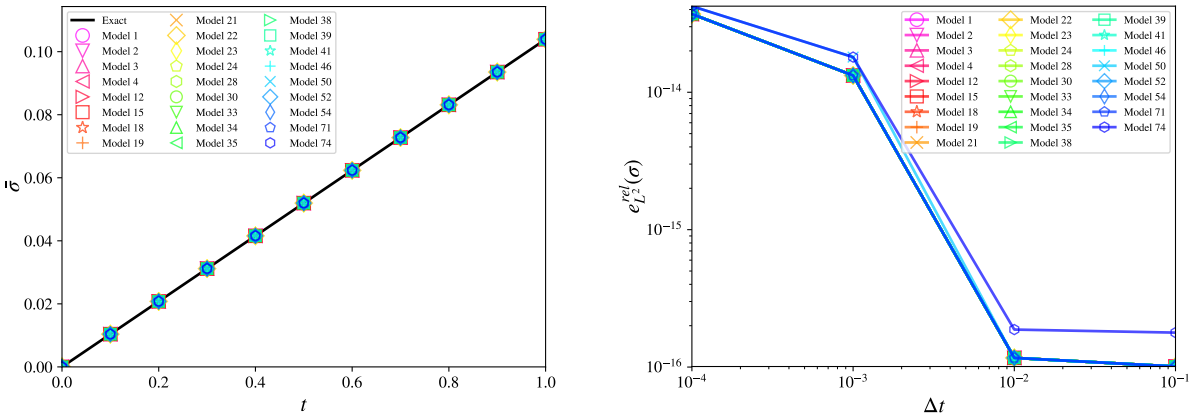

(a) Time-history plot of $\bar{\sigma}$ vs. t using $\Delta t = 0.1$.

(b) Convergence plot for $e_{L^2}^{\text{rel}}(\boldsymbol{\sigma})$ errors vs. Δt.

Figure 6: Isotropic elasticity test 4.

Table 10: Computed errors for isotropic elasticity test 4.

Model	$e_{L^2}^{\text{rel}}(\boldsymbol{\sigma})$	r	$e_{L^2}^{\text{abs}}(\varepsilon_{33})$	r	$e_{L^2}^{\text{abs}}(\bar{\varepsilon}^p)$	r	Status
1	3.710e-14	-	0.000e+00	-	0.000e+00	-	✓
2	3.710e-14	-	0.000e+00	-	0.000e+00	-	✓
3	3.710e-14	-	0.000e+00	-	0.000e+00	-	✓
4	3.710e-14	-	0.000e+00	-	0.000e+00	-	✓
12	3.710e-14	-	0.000e+00	-	0.000e+00	-	✓
15	3.710e-14	-	0.000e+00	-	0.000e+00	-	✓
18	3.710e-14	-	0.000e+00	-	0.000e+00	-	✓
19	3.710e-14	-	0.000e+00	-	0.000e+00	-	✓
21	3.710e-14	-	0.000e+00	-	0.000e+00	-	✓
22	3.710e-14	-	0.000e+00	-	0.000e+00	-	✓
23	3.710e-14	-	0.000e+00	-	0.000e+00	-	✓
24	3.710e-14	-	0.000e+00	-	0.000e+00	-	✓
28	3.710e-14	-	0.000e+00	-	0.000e+00	-	✓
30	3.710e-14	-	0.000e+00	-	0.000e+00	-	✓
33	3.710e-14	-	0.000e+00	-	0.000e+00	-	✓
34	3.710e-14	-	0.000e+00	-	0.000e+00	-	✓
35	3.710e-14	-	0.000e+00	-	0.000e+00	-	✓
38	3.710e-14	-	0.000e+00	-	0.000e+00	-	✓
39	3.710e-14	-	0.000e+00	-	0.000e+00	-	✓
41	3.710e-14	-	0.000e+00	-	0.000e+00	-	✓
46	3.710e-14	-	0.000e+00	-	0.000e+00	-	✓
50	4.233e-14	-	0.000e+00	-	0.000e+00	-	✓
52	3.710e-14	-	0.000e+00	-	0.000e+00	-	✓
54	3.710e-14	-	0.000e+00	-	0.000e+00	-	✓
71	3.710e-14	-	0.000e+00	-	0.000e+00	-	✓
74	4.233e-14	-	0.000e+00	-	0.000e+00	-	✓

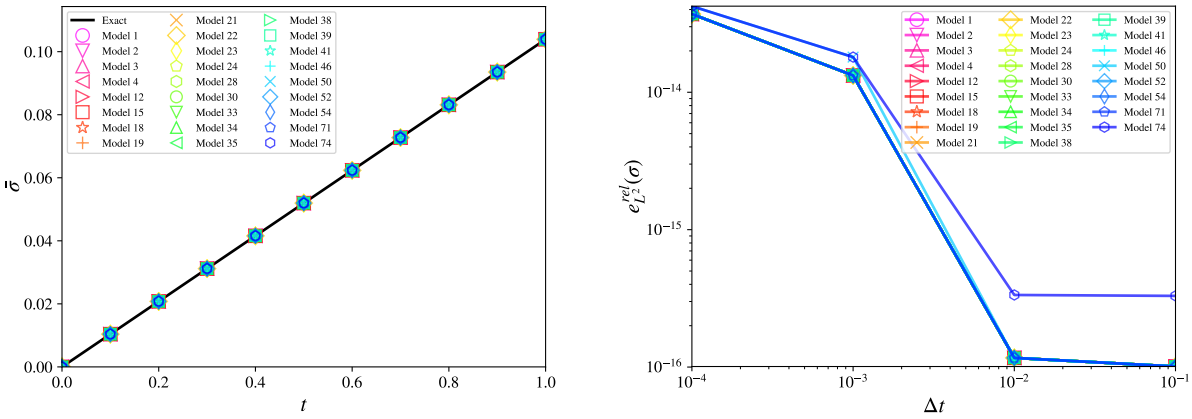

(a) Time-history plot of $\bar{\sigma}$ vs. t using $\Delta t = 0.1$.

(b) Convergence plot for $e_{L^2}^{\text{rel}}(\boldsymbol{\sigma})$ errors vs. Δt.

Figure 7: Isotropic elasticity test 5.

Table 11: Computed errors for isotropic elasticity test 5.

Model	$e_{L^2}^{\text{rel}}(\boldsymbol{\sigma})$	r	$e_{L^2}^{\text{abs}}(\varepsilon_{33})$	r	$e_{L^2}^{\text{abs}}(\bar{\varepsilon}^p)$	r	Status
1	3.710e-14	-	0.000e+00	-	0.000e+00	-	✓
2	3.710e-14	-	0.000e+00	-	0.000e+00	-	✓
3	3.710e-14	-	0.000e+00	-	0.000e+00	-	✓
4	3.710e-14	-	0.000e+00	-	0.000e+00	-	✓
12	3.710e-14	-	0.000e+00	-	0.000e+00	-	✓
15	3.710e-14	-	0.000e+00	-	0.000e+00	-	✓
18	3.710e-14	-	0.000e+00	-	0.000e+00	-	✓
19	3.710e-14	-	0.000e+00	-	0.000e+00	-	✓
21	3.710e-14	-	0.000e+00	-	0.000e+00	-	✓
22	3.710e-14	-	0.000e+00	-	0.000e+00	-	✓
23	3.710e-14	-	0.000e+00	-	0.000e+00	-	✓
24	3.710e-14	-	0.000e+00	-	0.000e+00	-	✓
28	3.710e-14	-	0.000e+00	-	0.000e+00	-	✓
30	3.710e-14	-	0.000e+00	-	0.000e+00	-	✓
33	3.710e-14	-	0.000e+00	-	0.000e+00	-	✓
34	3.710e-14	-	0.000e+00	-	0.000e+00	-	✓
35	3.710e-14	-	0.000e+00	-	0.000e+00	-	✓
38	3.710e-14	-	0.000e+00	-	0.000e+00	-	✓
39	3.710e-14	-	0.000e+00	-	0.000e+00	-	✓
41	3.710e-14	-	0.000e+00	-	0.000e+00	-	✓
46	3.710e-14	-	0.000e+00	-	0.000e+00	-	✓
50	4.233e-14	-	0.000e+00	-	0.000e+00	-	✓
52	3.710e-14	-	0.000e+00	-	0.000e+00	-	✓
54	3.710e-14	-	0.000e+00	-	0.000e+00	-	✓
71	3.710e-14	-	0.000e+00	-	0.000e+00	-	✓
74	4.233e-14	-	0.000e+00	-	0.000e+00	-	✓

5.1.2 Orthotropic Elasticity

For models with orthotropic elastic properties, the inverse constitutive relationship may be written as:

$$\begin{Bmatrix} \varepsilon_{11} \\ \varepsilon_{22} \\ \varepsilon_{33} \\ \varepsilon_{23} \\ \varepsilon_{13} \\ \varepsilon_{12} \end{Bmatrix} = \begin{bmatrix} \frac{1}{E_1} & -\frac{\nu_{21}}{E_2} & -\frac{\nu_{31}}{E_3} & 0 & 0 & 0 \\ -\frac{\nu_{12}}{E_1} & \frac{1}{E_2} & -\frac{\nu_{32}}{E_3} & 0 & 0 & 0 \\ -\frac{\nu_{13}}{E_1} & -\frac{\nu_{23}}{E_2} & \frac{1}{E_3} & 0 & 0 & 0 \\ 0 & 0 & 0 & \frac{1}{2\mu_{23}} & 0 & 0 \\ 0 & 0 & 0 & 0 & \frac{1}{2\mu_{31}} & 0 \\ 0 & 0 & 0 & 0 & 0 & \frac{1}{2\mu_{12}} \end{bmatrix} \begin{Bmatrix} \sigma_{11} \\ \sigma_{22} \\ \sigma_{33} \\ \sigma_{23} \\ \sigma_{13} \\ \sigma_{12} \end{Bmatrix}, \tag{44}$$

subject to the symmetry constraints:

$$\frac{\nu_{21}}{E_2} = \frac{\nu_{12}}{E_1}, \quad \frac{\nu_{31}}{E_3} = \frac{\nu_{13}}{E_1}, \quad \frac{\nu_{32}}{E_3} = \frac{\nu_{23}}{E_2}. \tag{45}$$

The inverse of the compliance matrix yields the (symmetric) 6×6 stiffness tensor:

$$\begin{Bmatrix} \sigma_{11} \\ \sigma_{22} \\ \sigma_{33} \\ \sigma_{23} \\ \sigma_{13} \\ \sigma_{12} \end{Bmatrix} = \begin{bmatrix} C_{11} & C_{12} & C_{13} & 0 & 0 & 0 \\ C_{21} & C_{22} & C_{23} & 0 & 0 & 0 \\ C_{31} & C_{32} & C_{33} & 0 & 0 & 0 \\ 0 & 0 & 0 & 2\mu_{23} & 0 & 0 \\ 0 & 0 & 0 & 0 & 2\mu_{31} & 0 \\ 0 & 0 & 0 & 0 & 0 & 2\mu_{12} \end{bmatrix} \begin{Bmatrix} \varepsilon_{11} \\ \varepsilon_{22} \\ \varepsilon_{33} \\ \varepsilon_{23} \\ \varepsilon_{13} \\ \varepsilon_{12} \end{Bmatrix}. \tag{46}$$

The normal strain is obtained via, $\varepsilon_{33}(t) = -\frac{C_{13}\varepsilon_{11}(t)+C_{23}\varepsilon_{22}(t)}{C_{33}}$, and the corresponding exact solutions for the stress and thickness strain components as functions of time are provided in table 12 for a handful for specific load cases. Independent material parameterizations are defined in tables 13-29 for orthotropic elasticity tests 1-9, whose results are presented in tables 14-30, and figures 8-16.

Table 12: Exact solutions for generic orthotropic elasticity tests

Load Case	$\varepsilon_{33}(t)$	Non-zero stress components (all other $\sigma_{ij}(t) = 0\,\forall t$)
1	$-\frac{C_{13}+C_{23}}{C_{33}}\bar{\gamma}t$	$\sigma_{11}(t) = (C_{11}+C_{12})\bar{\gamma}t + C_{13}\varepsilon_{33}(t)$, $\sigma_{22}(t) = (C_{12}+C_{22})\bar{\gamma}t + C_{23}\varepsilon_{33}(t)$
2	$-\frac{C_{13}-C_{23}}{C_{33}}\bar{\gamma}t$	$\sigma_{11}(t) = (C_{11}-C_{12})\bar{\gamma}t + C_{13}\varepsilon_{33}(t)$, $\sigma_{22}(t) = (C_{12}-C_{22})\bar{\gamma}t + C_{23}\varepsilon_{33}(t)$
3	0	$\sigma_{12}(t) = 2\mu_{12}\bar{\gamma}\,t$
4	0	$\sigma_{23}(t) = 2\mu_{23}\bar{\gamma}\,t$
5	0	$\sigma_{13}(t) = 2\mu_{13}\bar{\gamma}\,t$

Orthotropic elasticity test 1 uses load case 1 ($\bar{\gamma} = 0.01$), and the material parameterization defined in table 13. The results are presented in table 14, and figure 8. All models yield sufficiently small errors in all metrics, and the measured convergence rates are consistent with the theoretical rate of $r = 2$.

Table 13: Material parameterization for orthotropic elasticity test 1

Parameter	Value
Elastic modulus, E_a	8.0
Elastic modulus, $E_b = E_c$	1.0
Poisson's ratio, ν_{ca}	0.25
Poisson's ratio, $\nu_{ba} = \nu_{cb}$	0.0
Shear modulus, $\mu_{ab} = \mu_{bc} = \mu_{ca}$	1.0

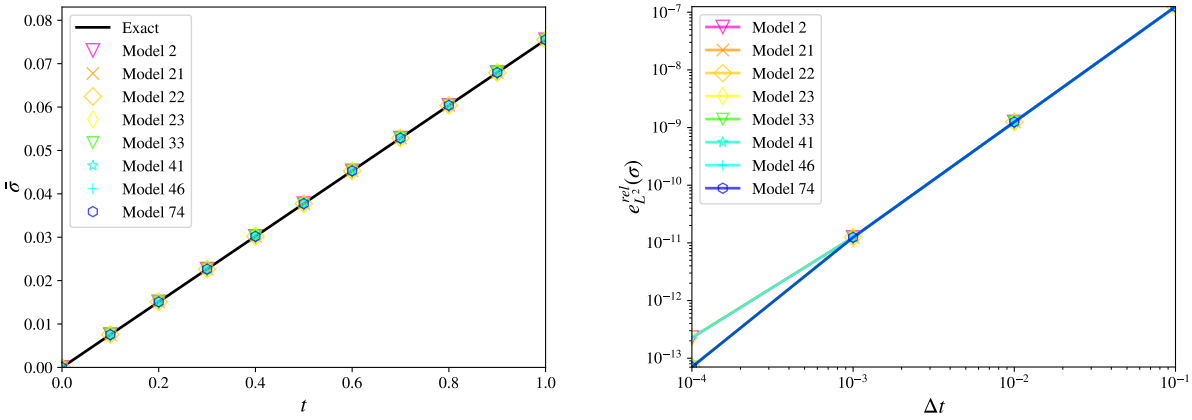

(a) Time-history plot of $\bar{\sigma}$ vs. t using $\Delta t = 0.1$.

(b) Convergence plot for $e^{\text{rel}}_{L^2}(\boldsymbol{\sigma})$ errors vs. Δt.

Figure 8: Orthotropic elasticity test 1.

Table 14: Computed errors for orthotropic elasticity test 1.

Model	$e^{\text{rel}}_{L^2}(\boldsymbol{\sigma})$	r	$e^{\text{rel}}_{L^2}(\varepsilon_{33})$	r	$e^{\text{abs}}_{L^2}(\bar{\varepsilon}^p)$	r	Status
2	2.271e-13	1.74	7.330e-14	2.00	0.000e+00	-	✓
21	7.062e-14	2.00	7.330e-14	2.00	0.000e+00	-	✓
22	7.066e-14	2.00	7.330e-14	2.00	0.000e+00	-	✓
23	2.310e-13	1.73	7.330e-14	2.00	0.000e+00	-	✓
33	7.061e-14	2.00	7.330e-14	2.00	0.000e+00	-	✓
41	7.041e-14	2.00	7.330e-14	2.00	0.000e+00	-	✓
46	2.269e-13	1.74	7.330e-14	2.00	0.000e+00	-	✓
74	7.041e-14	2.00	7.330e-14	2.00	0.000e+00	-	✓

Orthotropic elasticity test 2 uses load case 1 ($\bar{\gamma} = 0.01$), and the material parameterization defined in table 15. The results are presented in table 16, and figure 9. All models yield sufficiently small errors in all metrics, and the measured convergence rates are consistent with the theoretical rate of $r = 2$.

Table 15: Material parameterization for orthotropic elasticity test 2

Parameter	Value
Elastic modulus, E_b	8.0
Elastic modulus, $E_a = E_c$	1.0
Poisson's ratio, ν_{cb}	0.25
Poisson's ratio, $\nu_{ba} = \nu_{ca}$	0.0
Shear modulus, $\mu_{ab} = \mu_{bc} = \mu_{ca}$	1.0

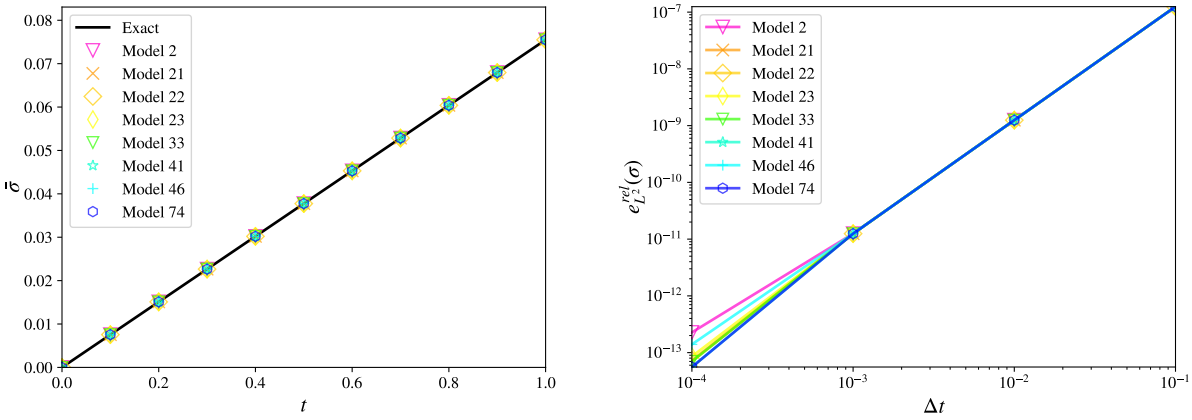

(a) Time-history plot of $\bar{\sigma}$ vs. t using $\Delta t = 0.1$.

(b) Convergence plot for $e^{\text{rel}}_{L^2}(\boldsymbol{\sigma})$ errors vs. Δt.

Figure 9: Orthotropic elasticity test 2.

Table 16: Computed errors for orthotropic elasticity test 2.

Model	$e^{\text{rel}}_{L^2}(\boldsymbol{\sigma})$	r	$e^{\text{rel}}_{L^2}(\varepsilon_{33})$	r	$e^{\text{abs}}_{L^2}(\bar{\varepsilon}^p)$	r	Status
2	2.271e-13	1.74	7.330e-14	2.00	0.000e+00	-	✓
21	7.061e-14	2.00	7.330e-14	2.00	0.000e+00	-	✓
22	7.344e-14	2.00	7.596e-14	2.00	0.000e+00	-	✓
23	8.580e-14	2.00	3.548e-13	1.55	0.000e+00	-	✓
33	7.008e-14	2.00	7.287e-14	2.00	0.000e+00	-	✓
41	5.577e-14	2.00	5.827e-14	2.00	0.000e+00	-	✓
46	1.397e-13	1.95	5.827e-14	2.00	0.000e+00	-	✓
74	5.577e-14	2.00	5.827e-14	2.00	0.000e+00	-	✓

Orthotropic elasticity test 3 uses load case 1 ($\bar{\gamma} = 0.01$), and the material parameterization defined in table 17. The results are presented in table 18, and depicted in figure 10. All models yield sufficiently small errors in all metrics, and the measured convergence rates are consistent with the theoretical rate of $r = 2$.

Table 17: Material parameterization for orthotropic elasticity test 3

Parameter	Value
Elastic modulus, E_c	8.0
Elastic modulus, $E_a = E_b$	2.25
Poisson's ratio, ν_{ba}	0.25
Poisson's ratio, $\nu_{ca} = \nu_{cb}$	0.0
Shear modulus, $\mu_{ab} = \mu_{bc} = \mu_{ca}$	1.0

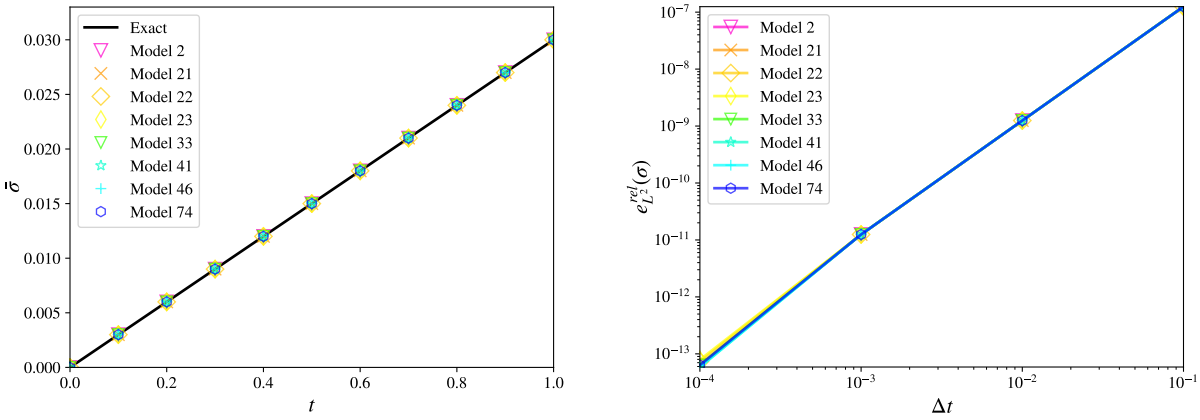

(a) Time-history plot of $\bar{\sigma}$ vs. t using $\Delta t = 0.1$.

(b) Convergence plot for $e^{\text{rel}}_{L^2}(\boldsymbol{\sigma})$ errors vs. Δt.

Figure 10: Orthotropic elasticity test 3.

Table 18: Computed errors for orthotropic elasticity test 3.

Model	$e^{\text{rel}}_{L^2}(\boldsymbol{\sigma})$	r	$e^{\text{abs}}_{L^2}(\varepsilon_{33})$	r	$e^{\text{abs}}_{L^2}(\bar{\varepsilon}^p)$	r	Status
2	6.279e-14	2.00	0.000e+00	-	0.000e+00	-	✓
21	6.279e-14	2.00	0.000e+00	-	0.000e+00	-	✓
22	7.321e-14	2.00	0.000e+00	-	0.000e+00	-	✓
23	7.889e-14	2.00	0.000e+00	-	0.000e+00	-	✓
33	6.362e-14	2.00	0.000e+00	-	0.000e+00	-	✓
41	5.874e-14	2.00	0.000e+00	-	0.000e+00	-	✓
46	5.874e-14	2.00	0.000e+00	-	0.000e+00	-	✓
74	6.359e-14	2.00	0.000e+00	-	0.000e+00	-	✓

Orthotropic elasticity test 4 uses load case 3 ($\bar{\gamma} = 0.01$), and the material parameterization defined in table 19. The results are presented in table 20, and depicted in figure 11. All models yield sufficiently small errors in all metrics, and the measured convergence rates are consistent with the theoretical rate of $r = 2$.

Table 19: Material parameterization for orthotropic elasticity test 4

Parameter	Value
Elastic modulus, $E_a = E_b = E_c$	1.0
Poisson's ratio, $\nu_{ba} = \nu_{ca} = \nu_{cb}$	0.0
Shear modulus, μ_{ab}	2.0
Shear modulus, $\mu_{bc} = \mu_{ca}$	1.0

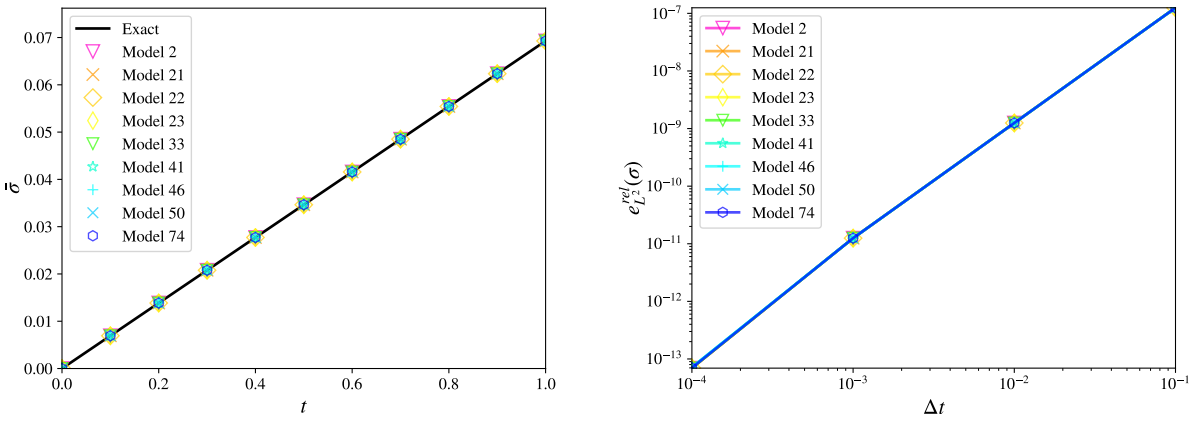

(a) Time-history plot of $\bar{\sigma}$ vs. t using $\Delta t = 0.1$.

(b) Convergence plot for $e^{\text{rel}}_{L^2}(\boldsymbol{\sigma})$ errors vs. Δt.

Figure 11: Orthotropic elasticity test 4.

Table 20: Computed errors for orthotropic elasticity test 4.

Model	$e^{\text{rel}}_{L^2}(\boldsymbol{\sigma})$	r	$e^{\text{abs}}_{L^2}(\varepsilon_{33})$	r	$e^{\text{abs}}_{L^2}(\bar{\varepsilon}^p)$	r	Status
2	6.937e-14	2.00	0.000e+00	-	0.000e+00	-	✓
21	6.932e-14	2.00	0.000e+00	-	0.000e+00	-	✓
22	6.978e-14	2.00	0.000e+00	-	0.000e+00	-	✓
23	6.999e-14	2.00	0.000e+00	-	0.000e+00	-	✓
33	6.955e-14	2.00	0.000e+00	-	0.000e+00	-	✓
41	7.160e-14	2.00	0.000e+00	-	0.000e+00	-	✓
46	7.160e-14	2.00	0.000e+00	-	0.000e+00	-	✓
50	7.160e-14	2.00	0.000e+00	-	0.000e+00	-	✓
74	6.993e-14	2.00	0.000e+00	-	0.000e+00	-	✓

Orthotropic elasticity test 5 uses load case 4 ($\bar{\gamma} = 0.01$), and the material parameterization defined in table 21. The results are presented in table 22, and depicted in figure 12. All models yield sufficiently small errors on the order of machine precision across all time discretizations.

Table 21: Material parameterization for orthotropic elasticity test 5

Parameter	Value
Elastic modulus, $E_a = E_b = E_c$	1.0
Poisson's ratio, $\nu_{ba} = \nu_{ca} = \nu_{cb}$	0.0
Shear modulus, μ_{bc}	2.0
Shear modulus, $\mu_{ab} = \mu_{ca}$	1.0

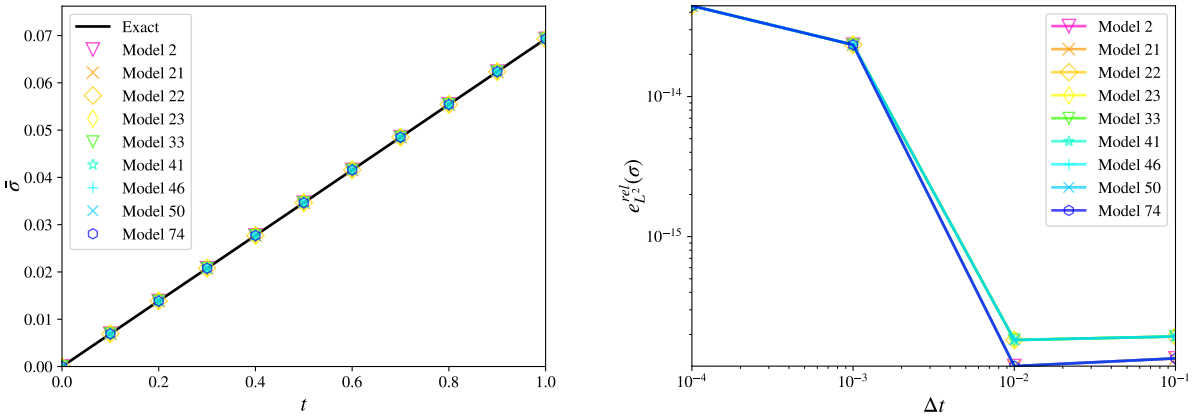

(a) Time-history plot of $\bar{\sigma}$ vs. t using $\Delta t = 0.1$.

(b) Convergence plot for $e^{\text{rel}}_{L^2}(\boldsymbol{\sigma})$ errors vs. Δt.

Figure 12: Orthotropic elasticity test 5.

Table 22: Computed errors for orthotropic elasticity test 5.

Model	$e^{\text{rel}}_{L^2}(\boldsymbol{\sigma})$	r	$e^{\text{abs}}_{L^2}(\varepsilon_{33})$	r	$e^{\text{abs}}_{L^2}(\bar{\varepsilon}^p)$	r	Status
2	4.448e-14	-	0.000e+00	-	0.000e+00	-	✓
21	4.448e-14	-	0.000e+00	-	0.000e+00	-	✓
22	4.448e-14	-	0.000e+00	-	0.000e+00	-	✓
23	4.448e-14	-	0.000e+00	-	0.000e+00	-	✓
33	4.448e-14	-	0.000e+00	-	0.000e+00	-	✓
41	4.448e-14	-	0.000e+00	-	0.000e+00	-	✓
46	4.448e-14	-	0.000e+00	-	0.000e+00	-	✓
50	4.448e-14	-	0.000e+00	-	0.000e+00	-	✓
74	4.448e-14	-	0.000e+00	-	0.000e+00	-	✓

Orthotropic elasticity test 6 uses load case 5 ($\bar{\gamma} = 0.01$), and the material parameterization defined in table 23. The results are presented in table 24, and depicted in figure 13. All models yield sufficiently small errors on the order of machine precision across all time discretizations.

Table 23: Material parameterization for orthotropic elasticity test 6

Parameter	Value
Elastic modulus, $E_a = E_b = E_c$	1.0
Poisson's ratio, $\nu_{ba} = \nu_{ca} = \nu_{cb}$	0.0
Shear modulus, μ_{ca}	2.0
Shear modulus, $\mu_{ab} = \mu_{bc}$	1.0

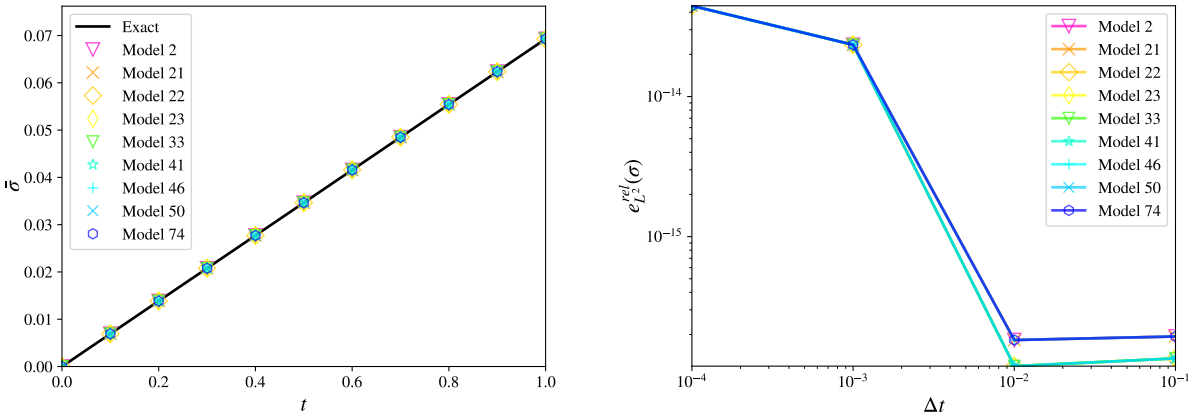

(a) Time-history plot of $\bar{\sigma}$ vs. t using $\Delta t = 0.1$.

(b) Convergence plot for $e^{\text{rel}}_{L^2}(\boldsymbol{\sigma})$ errors vs. Δt.

Figure 13: Orthotropic elasticity test 6.

Table 24: Computed errors for orthotropic elasticity test 6.

Model	$e^{\text{rel}}_{L^2}(\boldsymbol{\sigma})$	r	$e^{\text{abs}}_{L^2}(\varepsilon_{33})$	r	$e^{\text{abs}}_{L^2}(\bar{\varepsilon}^p)$	r	Status
2	4.448e-14	-	0.000e+00	-	0.000e+00	-	✓
21	4.448e-14	-	0.000e+00	-	0.000e+00	-	✓
22	4.448e-14	-	0.000e+00	-	0.000e+00	-	✓
23	4.448e-14	-	0.000e+00	-	0.000e+00	-	✓
33	4.448e-14	-	0.000e+00	-	0.000e+00	-	✓
41	4.448e-14	-	0.000e+00	-	0.000e+00	-	✓
46	4.448e-14	-	0.000e+00	-	0.000e+00	-	✓
50	4.448e-14	-	0.000e+00	-	0.000e+00	-	✓
74	4.448e-14	-	0.000e+00	-	0.000e+00	-	✓

Orthotropic elasticity test 7 uses load case 1 ($\bar{\gamma} = 0.01$), and the material parameterization defined in table 25. The results are presented in table 26, and depicted in figure 14. All models yield sufficiently small errors in all metrics, and the measured convergence rates are consistent with the theoretical rate of $r = 2$.

Table 25: Material parameterization for orthotropic elasticity test 7

Parameter	Value
Elastic modulus, E_a	2.0
Elastic modulus, $E_b = E_c$	1.0
Poisson's ratio, $\nu_{ba} = \nu_{ca} = \nu_{cb}$	0.0
Shear modulus, $\mu_{ab} = \mu_{bc} = \mu_{ca}$	1.0

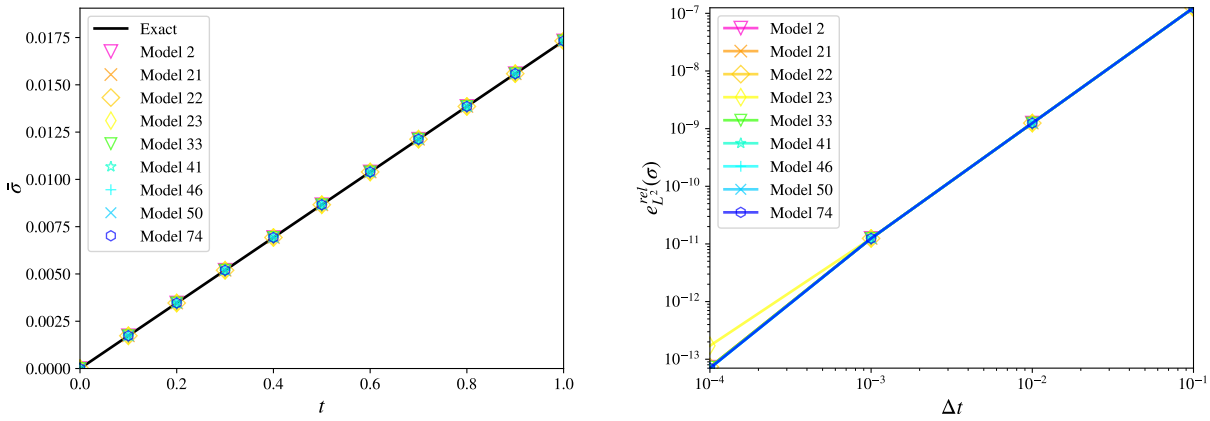

(a) Time-history plot of $\bar{\sigma}$ vs. t using $\Delta t = 0.1$.

(b) Convergence plot for $e^{\text{rel}}_{L^2}(\boldsymbol{\sigma})$ errors vs. Δt.

Figure 14: Orthotropic elasticity test 7.

Table 26: Computed errors for orthotropic elasticity test 7.

Model	$e^{\text{rel}}_{L^2}(\boldsymbol{\sigma})$	r	$e^{\text{abs}}_{L^2}(\varepsilon_{33})$	r	$e^{\text{abs}}_{L^2}(\bar{\varepsilon}^p)$	r	Status
2	7.274e-14	2.00	0.000e+00	-	0.000e+00	-	✓
21	7.274e-14	2.00	0.000e+00	-	0.000e+00	-	✓
22	7.326e-14	2.00	0.000e+00	-	0.000e+00	-	✓
23	1.714e-13	1.86	0.000e+00	-	0.000e+00	-	✓
33	7.265e-14	2.00	0.000e+00	-	0.000e+00	-	✓
41	7.008e-14	2.00	0.000e+00	-	0.000e+00	-	✓
46	7.008e-14	2.00	0.000e+00	-	0.000e+00	-	✓
50	7.008e-14	2.00	0.000e+00	-	0.000e+00	-	✓
74	7.011e-14	2.00	0.000e+00	-	0.000e+00	-	✓

Orthotropic elasticity test 8 uses load case 1 ($\bar{\gamma} = 0.01$), and the material parameterization defined in table 27. The results are presented in table 28, and depicted in figure 15. All models yield sufficiently small errors in all metrics, and the measured convergence rates are consistent with the theoretical rate of $r = 2$.

Table 27: Material parameterization for orthotropic elasticity test 8

Parameter	Value
Elastic modulus, E_a	1.0
Elastic modulus, $E_b = E_c$	2.0
Poisson's ratio, $\nu_{ba} = \nu_{ca} = \nu_{cb}$	0.0
Shear modulus, $\mu_{ab} = \mu_{bc} = \mu_{ca}$	1.0

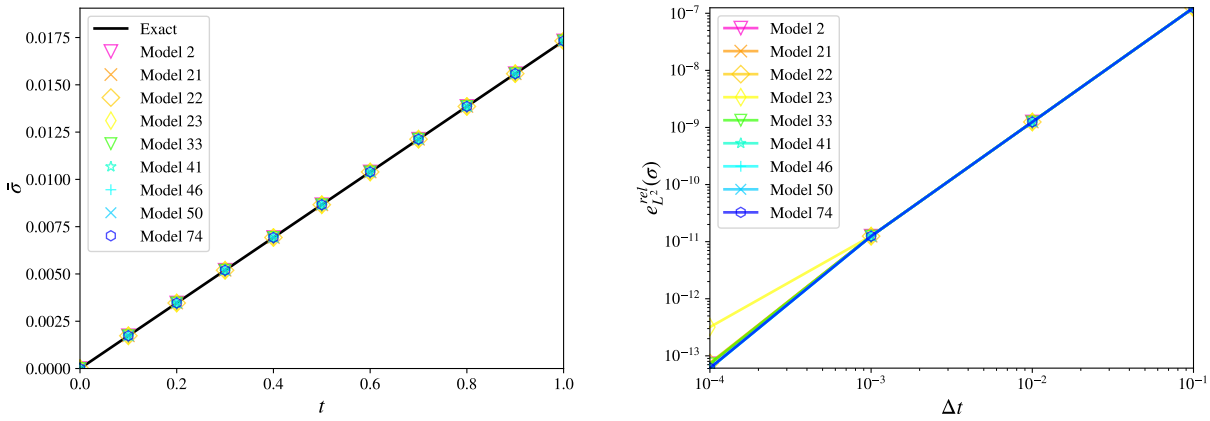

(a) Time-history plot of $\bar{\sigma}$ vs. t using $\Delta t = 0.1$.

(b) Convergence plot for $e^{\text{rel}}_{L^2}(\boldsymbol{\sigma})$ errors vs. Δt.

Figure 15: Orthotropic elasticity test 8.

Table 28: Computed errors for orthotropic elasticity test 8.

Model	$e^{\text{rel}}_{L^2}(\boldsymbol{\sigma})$	r	$e^{\text{abs}}_{L^2}(\varepsilon_{33})$	r	$e^{\text{abs}}_{L^2}(\bar{\varepsilon}^p)$	r	Status
2	7.274e-14	2.00	0.000e+00	-	0.000e+00	-	✓
21	7.274e-14	2.00	0.000e+00	-	0.000e+00	-	✓
22	7.490e-14	2.00	0.000e+00	-	0.000e+00	-	✓
23	3.189e-13	1.59	0.000e+00	-	0.000e+00	-	✓
33	7.240e-14	2.00	0.000e+00	-	0.000e+00	-	✓
41	6.091e-14	2.00	0.000e+00	-	0.000e+00	-	✓
46	6.091e-14	2.00	0.000e+00	-	0.000e+00	-	✓
50	6.091e-14	2.00	0.000e+00	-	0.000e+00	-	✓
74	6.103e-14	2.00	0.000e+00	-	0.000e+00	-	✓

Orthotropic elasticity test 9 uses load case 1 ($\bar{\gamma} = 0.01$), and the material parameterization defined in table 29. The results are presented in table 30, and depicted in figure 16. All models yield sufficiently small errors in all metrics, and the measured convergence rates are consistent with the theoretical rate of $r = 2$.

Table 29: Material parameterization for orthotropic elasticity test 9

Parameter	Value
Elastic modulus, E_c	0.5
Elastic modulus, $E_a = E_b$	1.0
Poisson's ratio, $\nu_{ba} = \nu_{ca} = \nu_{cb}$	0.25
Shear modulus, $\mu_{ab} = \mu_{bc} = \mu_{ca}$	1.0

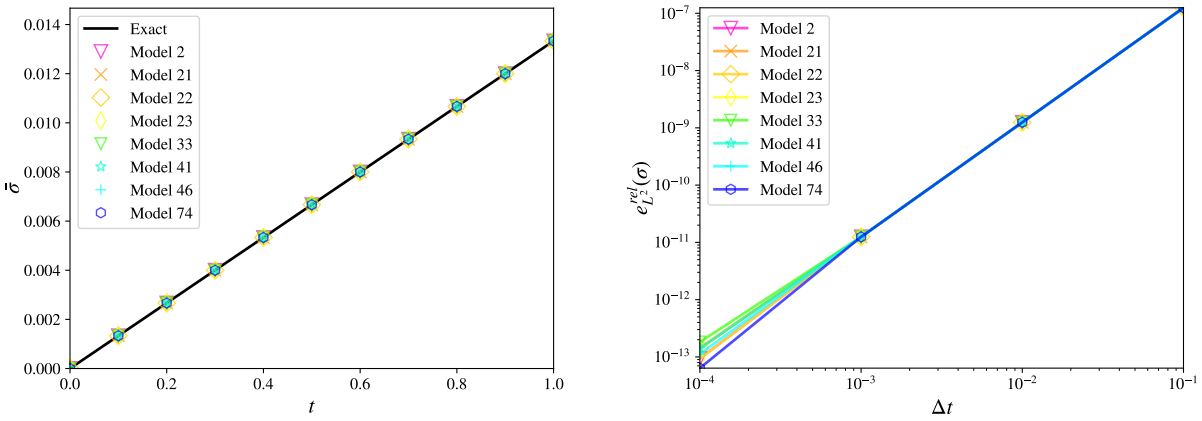

(a) Time-history plot of $\bar{\sigma}$ vs. t using $\Delta t = 0.1$.

(b) Convergence plot for $e^{\text{rel}}_{L^2}(\boldsymbol{\sigma})$ errors vs. Δt.

Figure 16: Orthotropic elasticity test 9.

Table 30: Computed errors for orthotropic elasticity test 9.

Model	$e^{\text{rel}}_{L^2}(\boldsymbol{\sigma})$	r	$e^{\text{rel}}_{L^2}(\varepsilon_{33})$	r	$e^{\text{abs}}_{L^2}(\bar{\varepsilon}^p)$	r	Status
2	9.391e-14	2.00	1.826e-13	1.83	0.000e+00	-	✓
21	1.396e-13	1.95	1.826e-13	1.83	0.000e+00	-	✓
22	1.445e-13	1.94	2.091e-13	1.78	0.000e+00	-	✓
23	9.321e-14	2.00	2.204e-13	1.75	0.000e+00	-	✓
33	1.825e-13	1.84	1.826e-13	1.84	0.000e+00	-	✓
41	1.411e-13	1.95	1.691e-13	1.87	0.000e+00	-	✓
46	1.125e-13	2.00	1.690e-13	1.87	0.000e+00	-	✓
74	6.371e-14	2.00	1.690e-13	1.87	0.000e+00	-	✓

5.2 Thermal Expansion

Thermal strains (denoted $\boldsymbol{\varepsilon}^T$) are included in models 4, 21, 23, 71, and take the general form:

$$\boldsymbol{\varepsilon}^T = (T - T_{\text{ref}})\,\bar{\boldsymbol{\alpha}}(T) \quad \Rightarrow \quad \dot{\boldsymbol{\varepsilon}}^T = \left[(T - T_{\text{ref}})\,\left.\frac{\partial \bar{\boldsymbol{\alpha}}}{\partial T}\right|_T + \bar{\boldsymbol{\alpha}}(T)\right]\dot{T}. \tag{47}$$

For models 4 and 71 which employ isotropic thermal strains in addition to plastic strains:

$$\boldsymbol{\sigma} = \mathbb{C} : (\boldsymbol{\varepsilon} - \boldsymbol{\varepsilon}^p - \boldsymbol{\varepsilon}^T), \qquad \bar{\boldsymbol{\alpha}}(T) = \bar{\alpha}(T)\mathbf{1}. \tag{48}$$

For models 21 and 23 which employ anisotropic thermal strains:

$$\boldsymbol{\sigma} = \mathbb{C} : (\boldsymbol{\varepsilon} - \boldsymbol{\varepsilon}^T), \qquad \bar{\boldsymbol{\alpha}}(T) = \mathbf{Q}^T \begin{bmatrix} \bar{\alpha}_a(T) & 0 & 0 \\ 0 & \bar{\alpha}_b(T) & 0 \\ 0 & 0 & \bar{\alpha}_c(T) \end{bmatrix} \mathbf{Q}, \tag{49}$$

where $\mathbf{Q}$ denotes the 3×3 transformation between the local material coordinate system and the global coordinate system. For models 4, 23, 71, the elastic modulus tensor $\mathbb{C}$ may also depend implicitly upon the current temperature T.

A simple test to verify the correct behavior of thermal strains for the aforementioned material models is given by load case 8 ($T_0 = 0.0$, $\bar{T} = 1.0$), where all in-plane and transverse shear strains are identically zero. In the most general case, let the orthotropic elastic stress-strain relation be written in matrix-vector format as follows:

$$\begin{bmatrix} \mathbf{C}_{ss} & \mathbf{C}_{s3} \\ \mathbf{C}_{3s} & C_{33} \end{bmatrix} \begin{Bmatrix} -\boldsymbol{\varepsilon}_s^T \\ \varepsilon_{33} - \varepsilon_{33}^T \end{Bmatrix} = \begin{Bmatrix} \boldsymbol{\sigma}_s \\ \sigma_{33} \end{Bmatrix}. \tag{50}$$

Given the plane stress constraint $\sigma_{33} = 0$, it follows that

$$\varepsilon_{33} = \varepsilon_{33}^T + \frac{1}{C_{33}}\mathbf{C}_{3s} \cdot \boldsymbol{\varepsilon}_s^T \tag{51}$$

and

$$\boldsymbol{\sigma}_s = \left[\frac{1}{C_{33}}\mathbf{C}_{s3} \otimes \mathbf{C}_{3s} - \mathbf{C}_{ss}\right] \cdot \boldsymbol{\varepsilon}_s^T. \tag{52}$$

For materials with isotropic elastic properties (but potentially orthotropic thermal properties):

$$\varepsilon_{33}(t) = \left[\bar{\alpha}_{33} + \frac{\lambda}{\lambda + 2\mu}(\bar{\alpha}_{11} + \bar{\alpha}_{22})\right]\bar{T}t, \tag{53}$$

$$\sigma_{11}(t) = -2\mu\left[(\bar{\alpha}_{11} - \bar{\alpha}_{33})\bar{T}t + \varepsilon_{33}(t)\right], \qquad \sigma_{22}(t) = -2\mu\left[(\bar{\alpha}_{22} - \bar{\alpha}_{33})\bar{T}t + \varepsilon_{33}(t)\right], \tag{54}$$

$$\sigma_{12}(t) = -2\mu\,\bar{\alpha}_{12}\,\bar{T}t, \qquad \sigma_{23}(t) = -2\mu\,\bar{\alpha}_{23}\,\bar{T}t, \qquad \sigma_{13}(t) = -2\mu\,\bar{\alpha}_{13}\,\bar{T}t. \tag{55}$$

For materials with isotropic thermal properties, the above reduces further to:

$$\varepsilon_{33}(t) = \frac{1+\nu}{1-\nu}\,\bar{\alpha}\,\bar{T}t, \qquad \sigma_{11}(t) = \sigma_{22}(t) = -\frac{E}{1-\nu}\,\bar{\alpha}\,\bar{T}t \qquad \sigma_{12}(t) = \sigma_{23}(t) = \sigma_{13}(t) = 0. \tag{56}$$

A total of four tests are proposed, all of which use load case 8 ($T_0 = 0.0$, $\bar{T} = 1.0$): an isotropic thermal expansion test, and three tests for orthotropic thermal expansion, described in the following sub-sections.

5.2.1 Isotropic Thermal Expansion

The isotropic thermal expansion test uses the material parameterization defined in table 31. The results are presented in table 32, and depicted in figure 17. All models yield sufficiently small errors on the order of machine precision across all time discretizations.

Table 31: Material parameterization for the isotropic thermal expansion test

Parameter	Value
Elastic modulus, E	7.5
Poisson's ratio, ν	0.25
Coefficient of thermal expansion, α	0.01

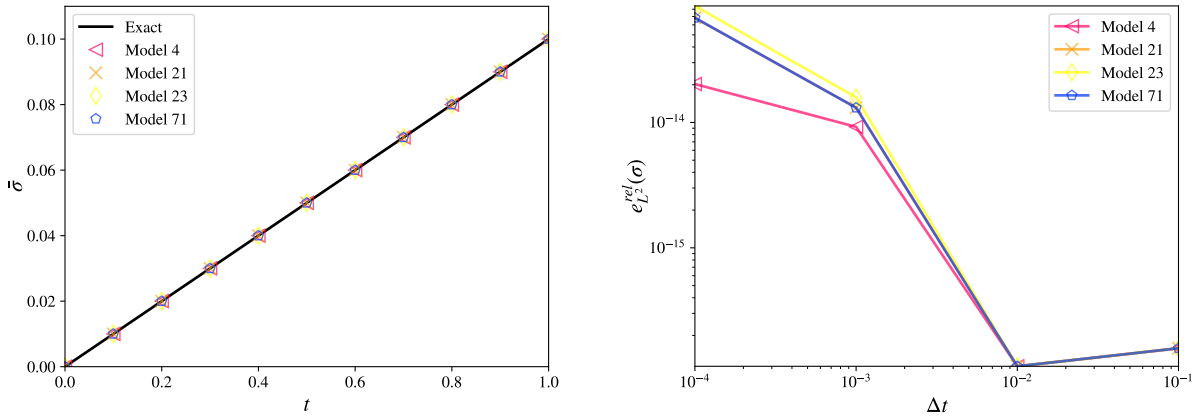

(a) Time-history plot of $\bar{\sigma}$ vs. t using $\Delta t = 0.1$.

(b) Convergence plot for $e^{\text{rel}}_{L^2}(\boldsymbol{\sigma})$ errors vs. Δt.

Figure 17: Isotropic thermal expansion test.

Table 32: Computed errors for the isotropic thermal expansion test.

Model	$e^{\text{rel}}_{L^2}(\boldsymbol{\sigma})$	r	$e^{\text{rel}}_{L^2}(\varepsilon_{33})$	r	$e^{\text{abs}}_{L^2}(\bar{\varepsilon}^p)$	r	Status
4	2.026e-14	-	8.358e-14	-	0.000e+00	-	✓
21	6.831e-14	-	1.202e-13	-	0.000e+00	-	✓
23	8.502e-14	-	1.202e-13	-	0.000e+00	-	✓
71	6.831e-14	-	1.202e-13	-	0.000e+00	-	✓

5.2.2 Orthotropic Thermal Expansion

The orthotropic thermal expansion tests 1-3 use the material parameterizations defined in tables 33, 35, and 37. The results are presented in tables 34, 34, 34, and depicted in figures 18, 19, 20, respectively. For all tests, all models yield sufficiently small errors on the order of machine precision across all time discretizations.

Table 33: Material parameterization for orthotropic thermal expansion test 1

Parameter	Value
Elastic modulus, E	7.5
Poisson's ratio, ν	0.25
Coefficient of thermal expansion, α_a	0.01
Coefficient of thermal expansion, $\alpha_b = \alpha_c$	0.0

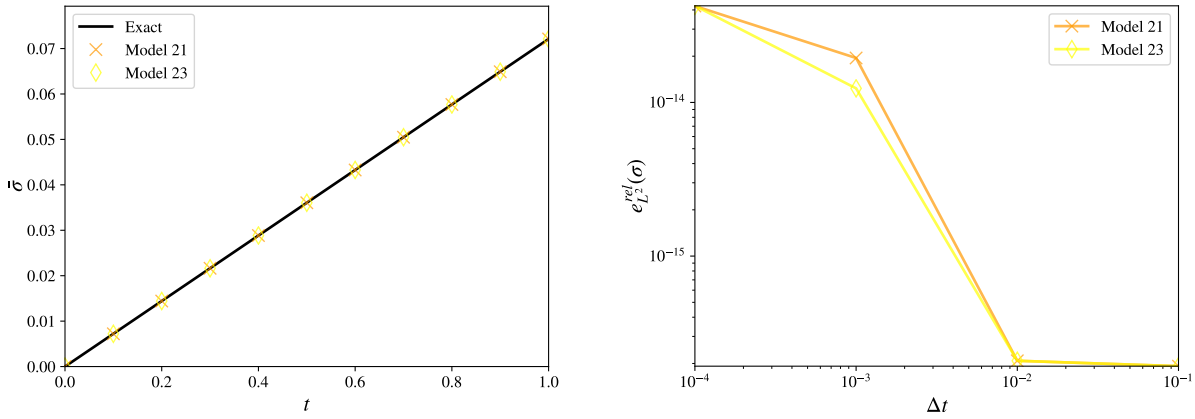

(a) Time-history plot of $\bar{\sigma}$ vs. t using $\Delta t = 0.1$.

(b) Convergence plot for $e^{\text{rel}}_{L^2}(\boldsymbol{\sigma})$ errors vs. Δt.

Figure 18: Orthotropic thermal expansion test 1.

Table 34: Computed errors for orthotropic thermal expansion test 1.

Model	$e^{\text{rel}}_{L^2}(\boldsymbol{\sigma})$	r	$e^{\text{rel}}_{L^2}(\varepsilon_{33})$	r	$e^{\text{abs}}_{L^2}(\bar{\varepsilon}^p)$	r	Status
21	4.243e-14	-	1.409e-13	-	0.000e+00	-	✓
23	4.255e-14	-	1.409e-13	-	0.000e+00	-	✓

Table 35: Material parameterization for orthotropic thermal expansion test 2

Parameter	Value
Elastic modulus, E	7.5
Poisson's ratio, ν	0.25
Coefficient of thermal expansion, α_b	0.01
Coefficient of thermal expansion, $\alpha_a = \alpha_c$	0.0

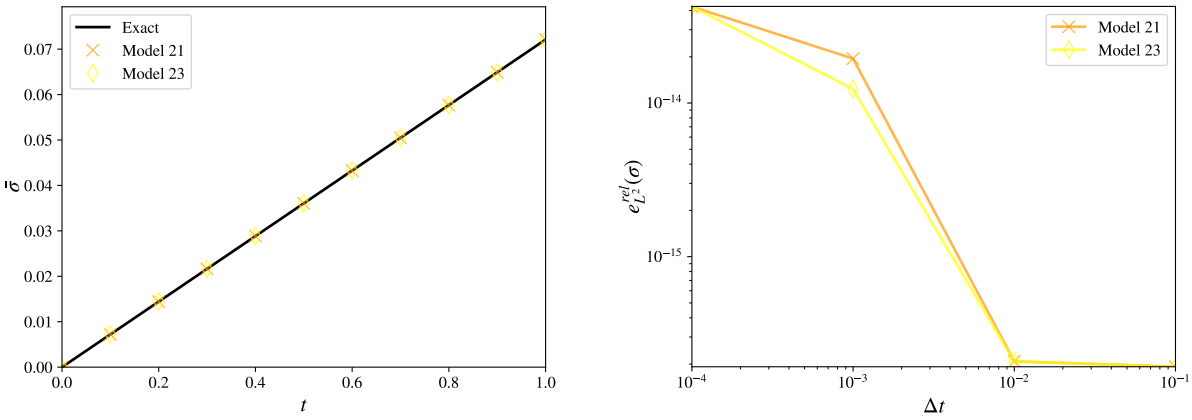

(a) Time-history plot of $\bar{\sigma}$ vs. t using $\Delta t = 0.1$.

(b) Convergence plot for $e^{\text{rel}}_{L^2}(\boldsymbol{\sigma})$ errors vs. Δt.

Figure 19: Orthotropic thermal expansion test 2.

Table 36: Computed errors for orthotropic thermal expansion test 2.

Model	$e^{\text{rel}}_{L^2}(\boldsymbol{\sigma})$	r	$e^{\text{rel}}_{L^2}(\varepsilon_{33})$	r	$e^{\text{abs}}_{L^2}(\bar{\varepsilon}^p)$	r	Status
21	4.243e-14	-	1.409e-13	-	0.000e+00	-	✓
23	4.255e-14	-	1.409e-13	-	0.000e+00	-	✓

Table 37: Material parameterization for orthotropic thermal expansion test 3

Parameter	Value
Elastic modulus, E	7.5
Poisson's ratio, ν	0.25
Coefficient of thermal expansion, α_c	0.01
Coefficient of thermal expansion, $\alpha_a = \alpha_b$	0.0

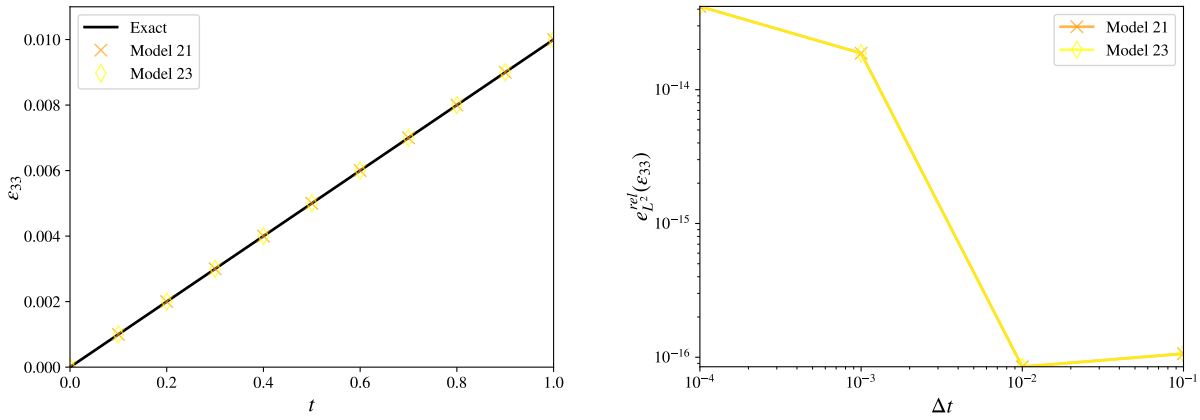

(a) Time-history plot of ε_{33} vs. t using $\Delta t = 0.1$.

(b) Convergence plot for $e_{L^2}^{\text{rel}}(\varepsilon_{33})$ errors vs. Δt.

Figure 20: Orthotropic thermal expansion test 3.

Table 38: Computed errors for orthotropic thermal expansion test 3.

Model	$e_{L^2}^{\text{abs}}(\boldsymbol{\sigma})$	r	$e_{L^2}^{\text{rel}}(\varepsilon_{33})$	r	$e_{L^2}^{\text{abs}}(\bar{\varepsilon}^p)$	r	Status
21	0.000e+00	-	4.194e-14	-	0.000e+00	-	✓
23	0.000e+00	-	4.194e-14	-	0.000e+00	-	✓

5.3 Isotropic Plasticity

The yield surface for a general plasticity model is described by

$$f(\boldsymbol{\sigma}, \mathbf{q}) = 0, \tag{57}$$

where $\boldsymbol{\sigma}$ denotes the Cauchy stress tensor, and $\mathbf{q}$ comprise a set of internal state variables of variable tensorial character. The consistency condition necessitates that $\dot{f} = 0$ during plastic loading, i.e.

$$\frac{\partial f}{\partial \boldsymbol{\sigma}} : \dot{\boldsymbol{\sigma}} + \frac{\partial f}{\partial \mathbf{q}} \cdot \dot{\mathbf{q}} = 0. \tag{58}$$

For rate-, temperature-, and pressure-independent plasticity, the internal state variables are assumed to depend only upon the equivalent plastic strain $\bar{\varepsilon}^p$, such that

$$\dot{\mathbf{q}} = \frac{\partial \mathbf{q}}{\partial \bar{\varepsilon}^p}\, \dot{\bar{\varepsilon}}^p, \qquad \bar{\varepsilon}^p = \int_0^t \dot{\bar{\varepsilon}}^p \, dt, \qquad \dot{\bar{\varepsilon}}^p \geq 0 \quad \forall t. \tag{59}$$

For an isotropic material employing a von Mises yield criterion:

$$\dot{\bar{\varepsilon}}^p = \sqrt{\frac{2}{3} \dot{\boldsymbol{\varepsilon}}^p : \dot{\boldsymbol{\varepsilon}}^p}, \qquad \mathrm{tr}(\dot{\boldsymbol{\varepsilon}}^p) = 0 \quad \forall t, \tag{60}$$

where $\dot{\boldsymbol{\varepsilon}}^p$ denotes the plastic strain rate. Assuming an additive decomposition of the total strain rate into elastic and plastic parts:

$$\dot{\boldsymbol{\varepsilon}} = \dot{\boldsymbol{\varepsilon}}^e + \dot{\boldsymbol{\varepsilon}}^p, \qquad \dot{\boldsymbol{\sigma}} = \mathbb{C} : \dot{\boldsymbol{\varepsilon}}^e. \tag{61}$$

The general flow rule takes the form $\dot{\boldsymbol{\varepsilon}}^p = \mathbf{n}\, \dot{\bar{\varepsilon}}^p$, with $\mathbf{n} = \frac{\partial f}{\partial \boldsymbol{\sigma}}$ for associated flow. It follows that

$$\dot{\bar{\varepsilon}}^p = \frac{\frac{\partial f}{\partial \boldsymbol{\sigma}} : \mathbb{C} : \dot{\boldsymbol{\varepsilon}}}{k + \frac{\partial f}{\partial \boldsymbol{\sigma}} : \mathbb{C} : \mathbf{n}}, \qquad k(\bar{\varepsilon}^p) \equiv -\frac{\partial f}{\partial \bar{\varepsilon}^p} = -\frac{\partial f}{\partial \mathbf{q}} \cdot \frac{\partial \mathbf{q}}{\partial \bar{\varepsilon}^p}, \tag{62}$$

$$\dot{\boldsymbol{\sigma}} = \mathbb{C}^p : \dot{\boldsymbol{\varepsilon}}, \qquad \mathbb{C}^p = \mathbb{C} - \frac{(\mathbb{C} : \frac{\partial f}{\partial \boldsymbol{\sigma}}) \otimes (\mathbf{n} : \mathbb{C})}{k + \frac{\partial f}{\partial \boldsymbol{\sigma}} : \mathbb{C} : \mathbf{n}}. \tag{63}$$

For a general von Mises plasticity model incorporating both kinematic and isotropic hardening, the yield surface is defined as:

$$f(\boldsymbol{\sigma}, \boldsymbol{\alpha}, \bar{\varepsilon}^p) = \bar{\sigma}(\boldsymbol{\sigma}, \boldsymbol{\alpha}) - \sigma_y(\bar{\varepsilon}^p) = 0, \tag{64}$$

$$\bar{\sigma}(\boldsymbol{\sigma}, \boldsymbol{\alpha}) = \sqrt{\frac{3}{2} \boldsymbol{\eta} : \boldsymbol{\eta}}, \qquad \boldsymbol{\eta} = \mathbf{s} - \boldsymbol{\alpha}, \qquad \mathbf{s} = \boldsymbol{\sigma} - \frac{1}{3}\mathrm{tr}(\boldsymbol{\sigma})\mathbf{1}, \qquad \frac{\partial f}{\partial \boldsymbol{\sigma}} = \frac{3}{2\bar{\sigma}} \boldsymbol{\eta}, \tag{65}$$

The hardening modulus k is therefore

$$k = \frac{\partial \sigma_y}{\partial \bar{\varepsilon}^p} - \frac{\partial \bar{\sigma}}{\partial \boldsymbol{\alpha}} : \frac{\partial \boldsymbol{\alpha}}{\partial \bar{\varepsilon}^p} = \frac{\partial \sigma_y}{\partial \bar{\varepsilon}^p} + \frac{\partial f}{\partial \boldsymbol{\sigma}} : \frac{\partial \boldsymbol{\alpha}}{\partial \boldsymbol{\varepsilon}^p} : \mathbf{n}. \tag{66}$$

Consider the special case of proportional loading of a general elastoplastic material employing an associated flow rule, such that:

$$\boldsymbol{\varepsilon}(t) = \mathbf{n}\, \bar{\varepsilon}(t), \tag{67}$$

where $\mathbf{n}$ remains constant $\forall t$, and $\bar{\varepsilon}(t)$ denotes the total (i.e. deviatoric) effective strain. Thus, during plastic loading:

$$\dot{\bar{\sigma}} = k\, \dot{\bar{\varepsilon}}^p, \qquad \dot{\bar{\varepsilon}}^p = h\, \dot{\bar{\varepsilon}}, \qquad h(\bar{\varepsilon}^p) \equiv \frac{\partial \bar{\varepsilon}^p}{\partial \bar{\varepsilon}} = \frac{\mathbf{n} : \mathbb{C} : \mathbf{n}}{k + \mathbf{n} : \mathbb{C} : \mathbf{n}}. \tag{68}$$

For an isotropic material with shear modulus μ, it can easily be shown that $\mathbf{n} : \mathbb{C} : \mathbf{n} = 3\mu$.

For isotropic plasticity models, load cases 2, 3, 4, 5, and 6 all satisfy $\boldsymbol{\varepsilon}(t) = \mathbf{n}\, \bar{\varepsilon}(t)$, with $\bar{\varepsilon}(t) = \dot{\bar{\varepsilon}}\, t$ for some constant total strain rate $\dot{\bar{\varepsilon}}$. Moreover, $\varepsilon_{33}(t) = 0\, \forall t$ during both elastic and plastic loading. For all of

the aforementioned tests, one obtains the following separable differential equation in terms of the equivalent plastic strain:

$$\dot{\bar{\varepsilon}}^p = \dot{\bar{\varepsilon}}\, h(\bar{\varepsilon}^p), \qquad \bar{\varepsilon}^p(t_0) = 0, \tag{69}$$

where $t_0 = \frac{\bar{\varepsilon}_0}{\dot{\bar{\varepsilon}}}$ denotes the time of initial yielding, $\bar{\varepsilon}_0 = \frac{\sigma_0}{3\mu}$ is the corresponding total effective strain at time t_0, and σ_0 denotes the initial yield stress of the material. The corresponding exact solutions for the stress and thickness strain components as functions of time may be computed as shown in table 39, assuming strain-hardening behavior:

Table 39: Exact solutions for generic isotropic plasticity tests

Load Case	$\bar{\varepsilon}(t)$	$\bar{\sigma}(t)$	$\sigma_{11}(t)$	$\sigma_{22}(t)$	$\sigma_{12}(t)$	$\sigma_{23}(t)$	$\sigma_{13}(t)$
2	$\frac{1}{\sqrt{3}}2\bar{\gamma}t$	$\min\{3\mu\,\bar{\varepsilon}(t),\, \sigma_y(\bar{\varepsilon}^p)\}$	$\frac{1}{\sqrt{3}}\bar{\sigma}(t)$	$-\frac{1}{\sqrt{3}}\bar{\sigma}(t)$	0	0	0
3	$\frac{1}{\sqrt{3}}2\bar{\gamma}t$	$\min\{3\mu\,\bar{\varepsilon}(t),\, \sigma_y(\bar{\varepsilon}^p)\}$	0	0	$\frac{1}{\sqrt{3}}\bar{\sigma}(t)$	0	0
4	$\frac{1}{\sqrt{3}}2\bar{\gamma}t$	$\min\{3\mu\,\bar{\varepsilon}(t),\, \sigma_y(\bar{\varepsilon}^p)\}$	0	0	0	$\frac{1}{\sqrt{3}}\bar{\sigma}(t)$	0
5	$\frac{1}{\sqrt{3}}2\bar{\gamma}t$	$\min\{3\mu\,\bar{\varepsilon}(t),\, \sigma_y(\bar{\varepsilon}^p)\}$	0	0	0	0	$\frac{1}{\sqrt{3}}\bar{\sigma}(t)$
6	$2\bar{\gamma}t$	$\min\{3\mu\,\bar{\varepsilon}(t),\, \sigma_y(\bar{\varepsilon}^p)\}$	$\frac{1}{3}\bar{\sigma}(t)$	$-\frac{1}{3}\bar{\sigma}(t)$	0	$\frac{1}{3}\bar{\sigma}(t)$	$\frac{1}{3}\bar{\sigma}(t)$

The solutions provided in table 39 remain valid across a wide variety of hardening rules for $\sigma_y(\bar{\varepsilon}^p)$. For a given hardening law, it therefore remains to determine the particular solution $\bar{\varepsilon}^p(t)$ to the differential equation in (69). Several specific hardening rules are examined in the following sub-sections.

5.3.1 Linear Hardening

For models 3, 4, 12, 15, 19, 24, 28, 30, 33, 34, 35, 38, 39, 50, 52, 54, and 71 employing a linear hardening law of the form:

$$\sigma_y(\bar{\varepsilon}^p) = \sigma_0 + E_p\bar{\varepsilon}^p, \tag{70}$$

as well as for the combined linear isotropic and Prager kinematic hardening law of the form:

$$\sigma_y(\bar{\varepsilon}^p) = \sigma_0 + \beta E_p\,\bar{\varepsilon}^p, \qquad \mathring{\boldsymbol{\alpha}}(\bar{\varepsilon}^p) = (1-\beta)\frac{2}{3}E_p\,\dot{\boldsymbol{\varepsilon}}^p, \tag{71}$$

the hardening modulus remains constant under proportional loading, such that $k = E_p\,\forall\beta$, and thus

$$\bar{\varepsilon}^p(t) = 2\bar{\gamma}\frac{3\mu}{E_p + 3\mu}\langle t - t_0\rangle, \qquad \langle x\rangle = \begin{cases} x & x > 0 \\ 0 & x \le 0 \end{cases}, \tag{72}$$

where $\langle\cdot\rangle$ denotes the Macaulay bracket (ramp) function.

A single test using load case 6 ($\bar{\gamma} = 0.1$) and the material parameterization in table 40 is investigated, with the results presented in table 41, and depicted in figure 21. All models yield sufficient accuracy and convergence under temporal refinement.

Table 40: Material parameterization for the linear hardening isotropic plasticity test

Parameter	Value
Elastic modulus, E	2.25
Poisson's ratio, ν	0.125
Yield stress, σ_0	0.3
Tangent modulus, E_p	1.8
Hardening parameter, β	1.0 (isotropic hardening)

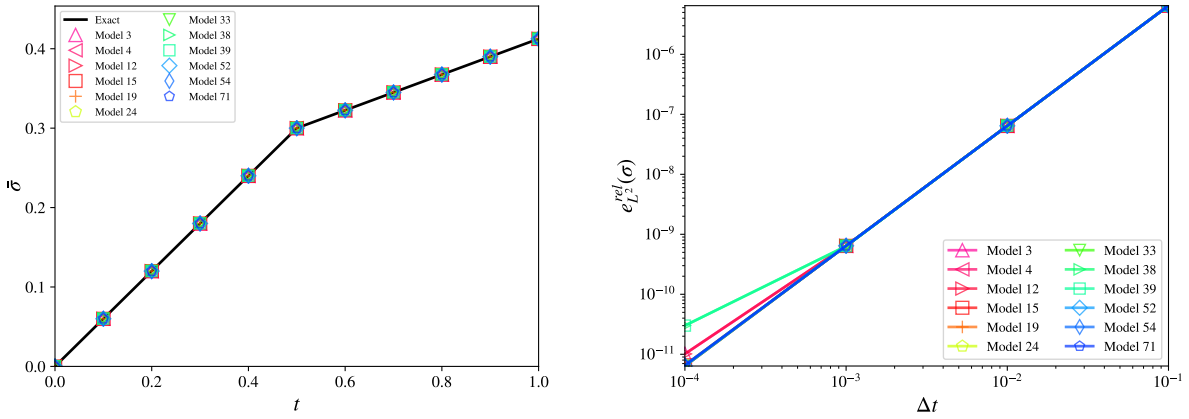

(a) Time-history plot of $\bar{\sigma}$ vs. t using $\Delta t = 0.1$.

(b) Convergence plot for $e^{\text{rel}}_{L^2}(\boldsymbol{\sigma})$ errors vs. Δt.

Figure 21: Isotropic plasticity test.

Table 41: Computed errors for the linear hardening plasticity test.

Model	$e^{\text{rel}}_{L^2}(\boldsymbol{\sigma})$	r	$e^{\text{abs}}_{L^2}(\varepsilon_{33})$	r	$e^{\text{rel}}_{L^2}(\bar{\varepsilon}^p)$	r	Status
3	1.013e-11	1.80	3.385e-15	2.00	4.702e-11	1.37	✓
4	6.384e-12	2.00	1.282e-14	1.70	1.126e-11	1.98	✓
12	1.014e-11	1.80	3.421e-15	2.00	4.702e-11	1.37	✓
15	6.559e-12	1.99	1.909e-15	2.00	1.164e-11	1.98	✓
19	6.380e-12	2.00	1.266e-14	1.72	1.138e-11	1.98	✓
24	6.556e-12	1.99	1.625e-15	2.00	1.162e-11	1.98	✓
33	6.389e-12	2.00	1.242e-14	1.52	1.154e-11	1.98	✓
38	3.006e-11	1.32	7.545e-15	1.74	1.258e-10	0.99	✓
39	3.006e-11	1.32	7.103e-15	1.77	1.258e-10	0.99	✓
52	6.370e-12	2.00	9.041e-15	1.76	1.136e-11	1.98	✓
54	6.567e-12	1.99	1.192e-15	2.00	1.165e-11	1.98	✓
71	6.567e-12	1.99	1.192e-15	2.00	1.165e-11	1.98	✓

5.3.1.1 Plane Stress Plasticity Because models 28, 30, 34, and 35 employ the assumption of plane stress plasticity (they ignore the contributions of the transverse shear stresses within the computations for the effective stress), a secondary test using load case 2 ($\bar{\gamma} = 0.1$) and the same material parameterization as in table 40 is also examined, with the results presented in table 42, and depicted in figure 22. With the exception of model 28, all models yield sufficient accuracy and convergence under temporal refinement.

The main discrepancy in model 28 regards its implementation of the radial return algorithm. For ordinary plasticity models (those other than model 28), the return-mapping trajectory is co-linear with the deviatoric stress. In the case of model 28, additional terms appear in the expression for the effective stress to account for the influence of the bending stress resultants. Consequently, the classical radial return algorithm cannot be directly applied in this context. Moreover, the implementation of model 28 is such that the return trajectory proportionally scales back *all* of the stress resultants – not just the stress deviator. This assumption is evidently necessary for the sake of establishing an equivalent return-mapping algorithm in the context of resultant plasticity, but it precludes consistency with conventional J_2 plasticity theory. Prospective users are therefore cautioned against the present use of model 28.

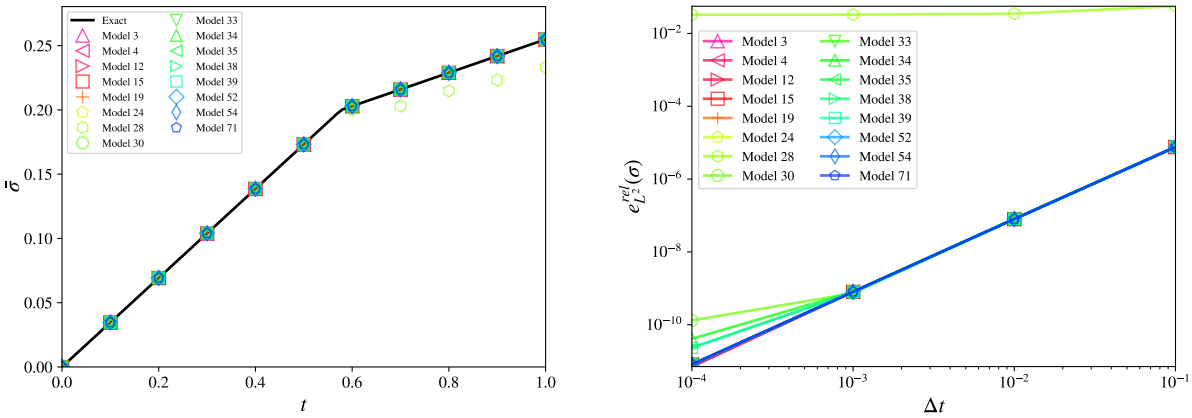

(a) Time-history plot of $\bar{\sigma}$ vs. t using $\Delta t = 0.1$.

(b) Convergence plot for $e^{\text{rel}}_{L^2}(\boldsymbol{\sigma})$ errors vs. Δt.

Figure 22: Plane stress linear hardening isotropic plasticity test.

Table 42: Computed errors for the plane stress plasticity test.

Model	$e^{\text{rel}}_{L^2}(\boldsymbol{\sigma})$	r	$e^{\text{abs}}_{L^2}(\varepsilon_{33})$	r	$e^{\text{rel}}_{L^2}(\bar{\varepsilon}^p)$	r	Status
3	7.090e-12	1.98	2.681e-15	2.00	7.903e-11	1.71	✓
4	8.031e-12	1.98	1.103e-14	1.76	4.096e-11	2.00	✓
12	7.091e-12	1.98	2.729e-15	2.00	7.902e-11	1.71	✓
15	8.146e-12	1.98	2.185e-15	2.00	4.218e-11	1.99	✓
19	8.024e-12	1.98	1.088e-14	1.74	4.085e-11	2.00	✓
24	8.153e-12	1.98	1.907e-15	2.00	4.217e-11	1.99	✓
28	3.265e-02	0.00	1.818e-14	2.00	2.727e-01	-0.12	✗
30	1.315e-10	0.75	4.053e-15	1.98	7.224e-10	0.82	✓
33	7.997e-12	1.98	9.346e-15	1.55	4.064e-11	2.00	✓
34	4.101e-11	1.29	2.512e-15	2.00	1.404e-10	1.46	✓
35	8.012e-12	1.98	1.828e-15	2.01	4.081e-11	2.00	✓
38	2.325e-11	1.53	5.773e-15	1.82	1.767e-10	1.38	✓
39	2.325e-11	1.53	5.773e-15	1.82	1.767e-10	1.38	✓
52	8.012e-12	1.98	7.988e-15	1.71	4.081e-11	2.00	✓
54	8.158e-12	1.98	1.423e-15	2.00	4.218e-11	1.99	✓
71	8.158e-12	1.98	1.423e-15	2.00	4.218e-11	1.99	✓

5.3.2 Piecewise Hardening

Models 24, 35, and 52 allow for the yield stress to be specified by a piecewise linear hardening curve. In such cases, the solution to equation (69) is given by a piecewise linear solution for $\bar{\varepsilon}^p(t)$, the representation of which may be tabulated for ease of presentation.

A single test using load case 6 ($\bar{\gamma} = 0.1$) and the material parameterization in table 43 is investigated, with the results presented in table 44, and depicted in figure 23. The corresponding exact solution for the plastic strain as a piecewise linear function of time is tabulated in discrete $(t, \bar{\varepsilon}^p(t))$ pairs as:

$$\{(t_i, \bar{\varepsilon}^p(t_i))\}_{i=1}^{6} = \{(0.0, 0.0), (0.2, 0.0), (0.4, 0.008), (0.6, 0.024), (0.8, 0.048), (1.0, 0.08)\}\,. \tag{73}$$

Despite the anomalous overshooting behavior exhibited by models 35 and 52 (refer to figure 23a), all models yield sufficient accuracy and convergence of order $r \geq 1$ under temporal refinement.

Table 43: Material parameterization for the piecewise hardening isotropic plasticity test

Parameter	Value
Elastic modulus, E	2.0
Poisson's ratio, ν	0.2
Tabulated plastic strain values, $\bar{\varepsilon}^p$	{0.0, 0.008, 0.024, 0.048, 0.08}
Tabulated yield stress values, σ_y	{0.1, 0.18, 0.24, 0.28, 0.3}

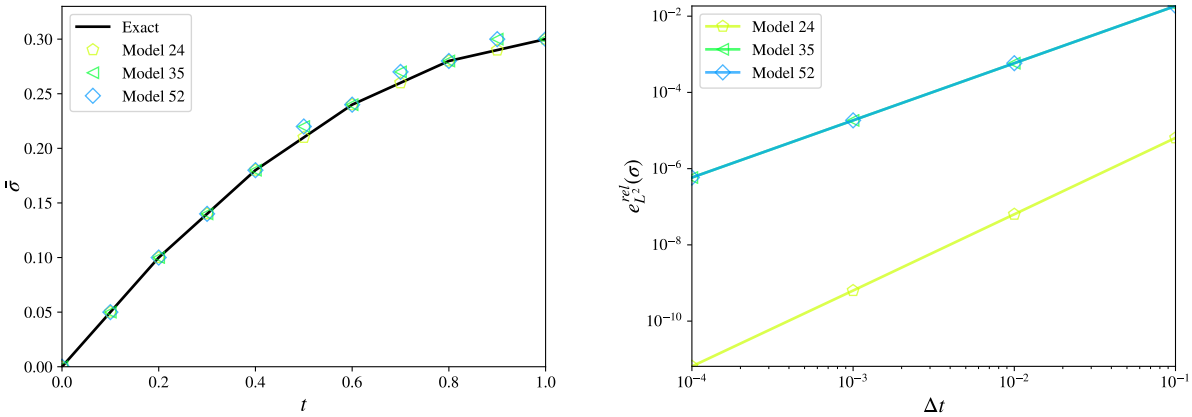

(a) Time-history plot of $\bar{\sigma}$ vs. t using $\Delta t = 0.1$.

(b) Convergence plot for $e^{\text{rel}}_{L^2}(\boldsymbol{\sigma})$ errors vs. Δt.

Figure 23: Piecewise hardening plasticity test.

Table 44: Computed errors for the piecewise hardening plasticity test.

Model	$e^{\text{rel}}_{L^2}(\boldsymbol{\sigma})$	r	$e^{\text{abs}}_{L^2}(\varepsilon_{33})$	r	$e^{\text{rel}}_{L^2}(\bar{\varepsilon}^p)$	r	Status
24	6.505e-12	1.99	6.658e-15	1.99	9.691e-12	1.98	✓
35	5.842e-07	1.50	4.753e-15	1.99	1.435e-06	1.50	✓
52	5.842e-07	1.50	1.825e-14	1.76	1.435e-06	1.50	✓

5.3.3 Power-Law Hardening

For models 15, 18, 24, 50, 54, and 71 employing a power hardening law with a fractional exponent of 1/2 of the form:

$$\sigma_y(\bar{\varepsilon}^p) = \sigma_0 + E_p\sqrt{\bar{\varepsilon}^p}, \tag{74}$$

the solution to equation (69) is given by

$$\bar{\varepsilon}^p(t) = \frac{1}{2}\left(\frac{E_p}{3\mu}\right)^2 + 2\bar{\gamma}\langle t - t_0\rangle - \frac{E_p}{3\mu}\sqrt{\frac{1}{4}\left(\frac{E_p}{3\mu}\right)^2 + 2\bar{\gamma}\langle t - t_0\rangle}. \tag{75}$$

A single test using load case 6 ($\bar{\gamma} = 0.1$) and the material parameterization in table 45 is investigated, with the results presented in table 46, and depicted in figure 24. All models yield sufficient accuracy and convergence under temporal refinement.

Table 45: Material parameterization for the power-law hardening isotropic plasticity test

Parameter	Value
Elastic modulus, E	2.25
Poisson's ratio, ν	0.125
Yield stress, σ_0	0.0
Hardening modulus, E_p	1.8

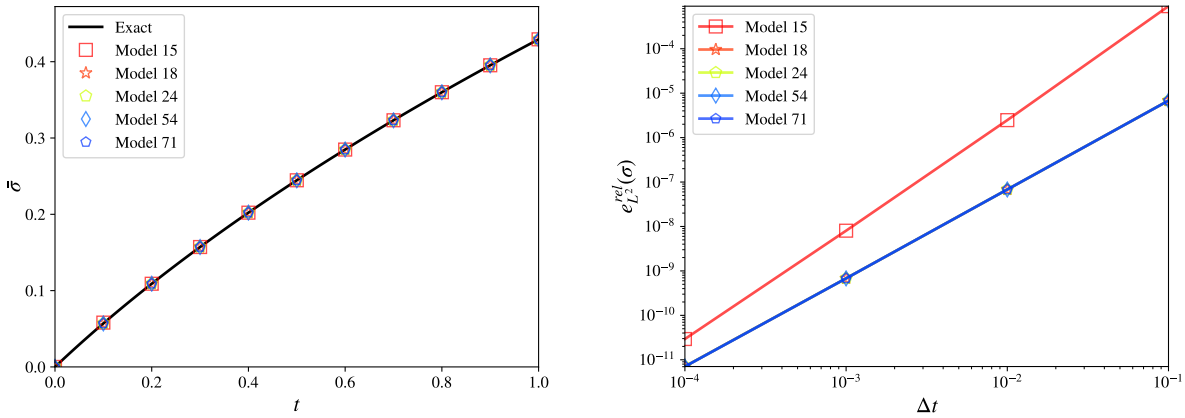

(a) Time-history plot of $\bar{\sigma}$ vs. t using $\Delta t = 0.1$.

(b) Convergence plot for $e^{\text{rel}}_{L^2}(\boldsymbol{\sigma})$ errors vs. Δt.

Figure 24: Power-law hardening plasticity test.

Table 46: Computed errors for the power-law hardening plasticity test.

Model	$e^{\text{rel}}_{L^2}(\boldsymbol{\sigma})$	r	$e^{\text{abs}}_{L^2}(\varepsilon_{33})$	r	$e^{\text{rel}}_{L^2}(\bar{\varepsilon}^p)$	r	Status
15	2.934e-11	2.44	2.362e-15	2.00	9.087e-11	2.45	✓
18	7.091e-12	1.98	2.339e-15	2.00	7.120e-12	1.97	✓
24	7.097e-12	1.98	2.334e-15	2.00	7.125e-12	1.97	✓
54	7.054e-12	1.98	2.433e-15	2.00	7.377e-12	1.96	✓
71	7.051e-12	1.98	2.203e-15	2.00	7.363e-12	1.96	✓

5.3.4 Exponential Hardening

For model 71 employing an exponential hardening law of the form:

$$\sigma_y(\bar{\varepsilon}^p) = \sigma_0 e^{E_p \bar{\varepsilon}^p}, \tag{76}$$

the solution to equation (69) is given by

$$\bar{\varepsilon}^p(t) = \bar{\varepsilon}_0 + 2\bar{\gamma}\langle t - t_0 \rangle - \frac{1}{E_p} W\left(E_p \bar{\varepsilon}_0 e^{E_p(\bar{\varepsilon}_0 + 2\bar{\gamma}\langle t - t_0\rangle)}\right), \tag{77}$$

where $W(x)$ denotes the Lambert W function.

A single test using load case 6 ($\bar{\gamma} = 0.1$) and the material parameterization in table 47 is investigated, with the results presented in table 48, and depicted in figure 25. All models yield sufficient accuracy and convergence under temporal refinement.

Table 47: Material parameterization for the exponential hardening isotropic plasticity test

Parameter	Value
Elastic modulus, E	2.25
Poisson's ratio, ν	0.125
Yield stress, σ_0	0.3
Hardening modulus, E_p	-5.0

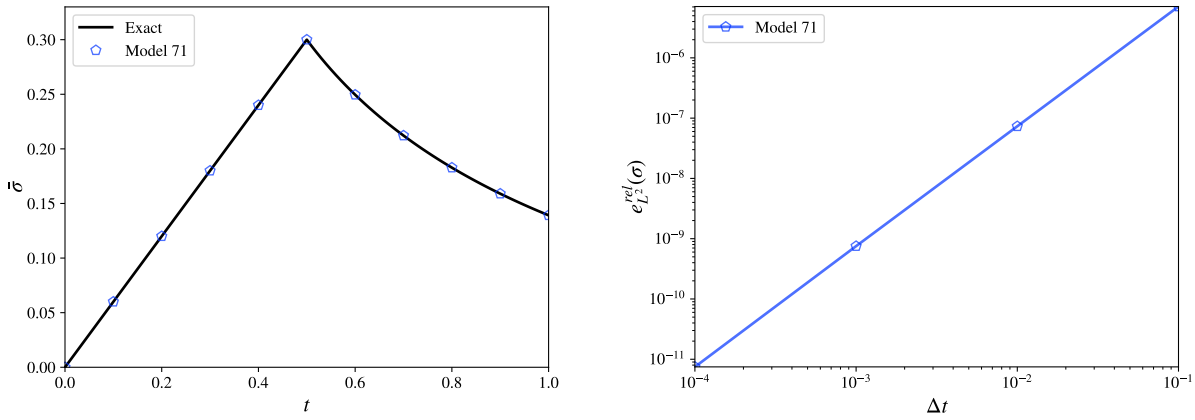

(a) Time-history plot of $\bar{\sigma}$ vs. t using $\Delta t = 0.1$.

(b) Convergence plot for $e^{\text{rel}}_{L^2}(\boldsymbol{\sigma})$ errors vs. Δt.

Figure 25: Exponential hardening plasticity test.

Table 48: Computed errors for the exponential hardening plasticity test.

Model	$e^{\text{rel}}_{L^2}(\boldsymbol{\sigma})$	r	$e^{\text{abs}}_{L^2}(\varepsilon_{33})$	r	$e^{\text{rel}}_{L^2}(\bar{\varepsilon}^p)$	r	Status
71	7.473e-12	1.99	5.335e-15	2.00	1.055e-11	1.98	✓

5.4 Anisotropic Plasticity

Models 33 and 34 incorporate anisotropic yield conditions consistent with the Hill yield criterion set forth in [5]. Model 33 possesses a more complete set of parameters to specify the anisotropy in different material directions, whereas model 34 incorporates only a single (normal) anisotropy parameter, R. Both models exhibit linear strain hardening behavior.

For all tests presented herein, the material is presumed to have isotropic elastic properties, but a potentially anisotropic yield criterion. The generic (default) parameterization for all anisotropic plasticity tests is presented in table 49.

Table 49: Default parameterization for all anisotropic plasticity tests

Parameter	Value
Elastic modulus, E	2.25
Poisson's ratio, ν	0.125
Yield stress, σ_0	0.2
Tangent modulus, E_T	1.0
Strain rate, $\bar{\gamma}$	0.1
Anisotropy coefficient, R	1.0
Anisotropy coefficient, P	1.0
Anisotropy coefficient, Q_{ab}	1.0
Anisotropy coefficient, Q_{bc}	1.0
Anisotropy coefficient, Q_{ca}	1.0

The specific parameterizations for each test are summarized in table 50, and are characterized by the anisotropy parameter value that they override. All unspecified parameters assume their default values as prescribed in table 49. The intent behind this approach is to isolate, test, and verify the behavior each anisotropy parameter, individually.

Table 50: Overriding parameterizations for anisotropic plasticity tests 1-5

Test	Overriding Parameters
1	$R = P = 2.0$
2	$P = 2.0$
3	$Q_{ab} = 2.0$
4	$Q_{bc} = 2.0$
5	$Q_{ca} = 2.0$

Table 51: Assigned load cases and corresponding exact stress solutions for anisotropic plasticity tests 1-5

Test	Load Case	Non-zero stress components (all other $\sigma_{ij}(t) = 0\,\forall t$)
1	2	$\sigma_{11}(t) = -\sigma_{22}(t) = \min\left\{2\mu\bar{\gamma}\,t, \sqrt{0.3}\,\sigma_y(t)\right\}$
2	7	$\sigma_{11}(t) = 2\sigma_{22}(t) = \min\left\{2\mu\bar{\gamma}\,t, \sqrt{16/15}\,\sigma_y(t)\right\}$
3	3	$\sigma_{12}(t) = \min\left\{2\mu\bar{\gamma}\,t, \sqrt{0.2}\,\sigma_y(t)\right\}$
4	4	$\sigma_{23}(t) = \min\left\{2\mu\bar{\gamma}\,t, \sqrt{0.2}\,\sigma_y(t)\right\}$
5	5	$\sigma_{13}(t) = \min\left\{2\mu\bar{\gamma}\,t, \sqrt{0.2}\,\sigma_y(t)\right\}$

The assigned load cases and exact solutions for the individual stress components as functions of time are provided in table 51. Test 1 (documented in sub-section 5.4.1) seeks to verify normal anisotropic behavior, while the remaining tests (documented in sub-section 5.4.2) are intended to verify the more general implementation of anisotropic plasticity in model 33. The results are in close agreement to the reference solutions for each test, with the observed errors converging under temporal refinement at a rate of $r = 2.0$ for tests 1 and 3, and a rate of $r = 1.0$ for test 2. Tests 4 and 5 achieve accuracy on the order of machine precision across all temporal discretizations.

5.4.1 Normal Anisotropic Plasticity

Figure 26 depicts the numerical results for anisotropic plasticity test 1 using model 33 compared against the exact reference solution, while table 52 presents the computed error measures and convergence rates.

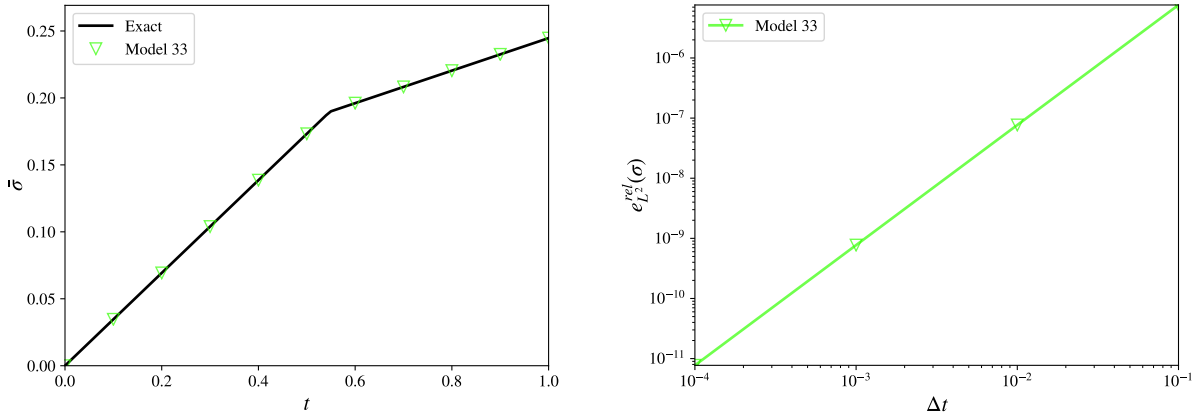

(a) Time-history plot of $\bar{\sigma}$ vs. t using $\Delta t = 0.1$.

(b) Convergence plot for $e^{\text{rel}}_{L^2}(\boldsymbol{\sigma})$ errors vs. Δt.

Figure 26: Anisotropic plasticity test 1 for model 33.

Table 52: Computed errors for anisotropic plasticity test 1 using model 34.

Model	$e^{\text{rel}}_{L^2}(\boldsymbol{\sigma})$	r	$e^{\text{abs}}_{L^2}(\varepsilon_{33})$	r	$e^{\text{rel}}_{L^2}(\bar{\varepsilon}^p)$	r	Status
33	7.728e-12	1.99	1.156e-14	1.48	3.763e-11	1.99	✓

It should be noted that the solutions obtained for anisotropic plasticity test 1 using models 33 and 34 are not consistent with one another. As described by the original authors of the model in [10], the definition for the rate of equivalent plastic strain in model 34 is given by

$$\dot{\bar{\varepsilon}}^p = \sqrt{\frac{2}{3}\dot{\boldsymbol{\varepsilon}}^p : \dot{\boldsymbol{\varepsilon}}^p} = \sqrt{\{\dot{\boldsymbol{\varepsilon}}^p\} \cdot \mathbf{P} \cdot \{\dot{\boldsymbol{\varepsilon}}^p\}}, \qquad \mathbf{P} \equiv \frac{4}{3}\begin{bmatrix} 1 & \frac{1}{2} & 0 \\ \frac{1}{2} & 1 & 0 \\ 0 & 0 & \frac{1}{4} \end{bmatrix}, \qquad \{\dot{\boldsymbol{\varepsilon}}^p\} \equiv \begin{Bmatrix} \dot{\varepsilon}^p_{11} \\ \dot{\varepsilon}^p_{22} \\ 2\dot{\varepsilon}^p_{12} \end{Bmatrix}, \tag{78}$$

corresponding to the usual definition for $\dot{\bar{\varepsilon}}^p$ employed by isotropic plasticity models. This stands in contrast with the traditional definition for the rate of equivalent plastic strain as set forth by Hill in [5], employed by most anisotropic plasticity models (i.e. model 33). When specialized to the case of normal anisotropy under plane stress conditions:

$$\dot{\bar{\varepsilon}}^p = \sqrt{\dot{\boldsymbol{\varepsilon}}^p : \mathbb{B}^{-1} : \dot{\boldsymbol{\varepsilon}}^p} = \sqrt{\{\dot{\boldsymbol{\varepsilon}}^p\} \cdot \mathbf{B}^{-1} \cdot \{\dot{\boldsymbol{\varepsilon}}^p\}}, \tag{79}$$

$$\mathbf{B} \equiv \begin{bmatrix} 1 & -\frac{R}{R+1} & 0 \\ -\frac{R}{R+1} & 1 & 0 \\ 0 & 0 & 2\frac{2R+1}{R+1} \end{bmatrix}, \qquad \mathbf{B}^{-1} = \frac{R+1}{2R+1}\begin{bmatrix} R+1 & R & 0 \\ R & R+1 & 0 \\ 0 & 0 & \frac{1}{2} \end{bmatrix}, \tag{80}$$

wherein $\dot{\bar{\varepsilon}}^p$ is synonymous with the plastic consistency parameter λ appearing in the associated flow rule:

$$\dot{\boldsymbol{\varepsilon}}^p = \lambda\,\mathbf{n}, \qquad \mathbf{n} \equiv \frac{\partial f}{\partial \boldsymbol{\sigma}}. \tag{81}$$

For model 34, this equivalence between $\dot{\bar{\varepsilon}}^p$ and λ does not hold. Rather, for the associated flow rule given by equation (81), it can be shown that

$$\lambda = \frac{\partial \lambda}{\partial \dot{\bar{\varepsilon}}^p}\dot{\bar{\varepsilon}}^p, \qquad \frac{\partial \lambda}{\partial \dot{\bar{\varepsilon}}^p} = \left(\frac{2}{3}\mathbf{n} : \mathbf{n}\right)^{-\frac{1}{2}}. \tag{82}$$

Consequently, the behavior of model 34 differs from that of model 33. Specifically, for linear isotropic hardening, the equivalent plastic strain rate is obtained via

$$\dot{\bar{\varepsilon}}^p = \frac{\mathbf{n} : \mathbb{C} : \dot{\boldsymbol{\varepsilon}}}{E_p + \mathbf{n} : \mathbb{C} : \mathbf{n}\,\frac{\partial \lambda}{\partial \dot{\bar{\varepsilon}}^p}}. \tag{83}$$

It is only for the special case of isotropy (i.e. when $R = 1$) that one recovers the equivalence $\lambda = \dot{\bar{\varepsilon}}^p$, and the behavior of models 33 and 34 coincide.

For this reason, an altogether separate reference solution was created specifically for model 34, although the loading and material parameters remain identical to those of the preceding test for model 33. Nonetheless, while the implementation of the model is consistent with what is described in [10], it is recommended that the model be revised such that it produces consistent results with model 33.

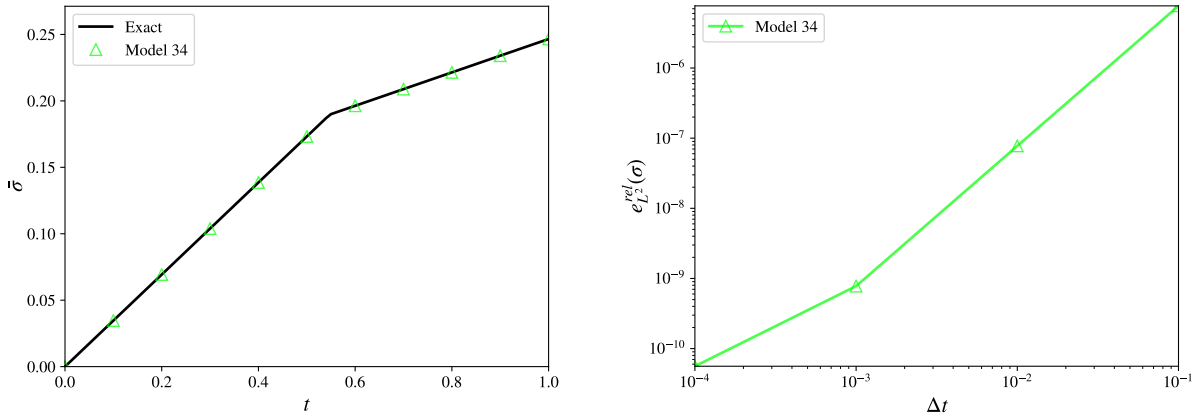

(a) Time-history plot of $\bar{\sigma}$ vs. t using $\Delta t = 0.1$.

(b) Convergence plot for $e^{\text{rel}}_{L^2}(\boldsymbol{\sigma})$ errors vs. Δt.

Figure 27: Anisotropic plasticity test 1 for model 34.

Table 53: Computed errors for anisotropic plasticity test 1 using model 33.

Model	$e^{\text{rel}}_{L^2}(\boldsymbol{\sigma})$	r	$e^{\text{abs}}_{L^2}(\varepsilon_{33})$	r	$e^{\text{rel}}_{L^2}(\bar{\varepsilon}^p)$	r	Status
34	5.607e-11	1.14	3.265e-15	2.00	1.855e-10	1.31	⚠

5.4.2 General Anisotropic Plasticity

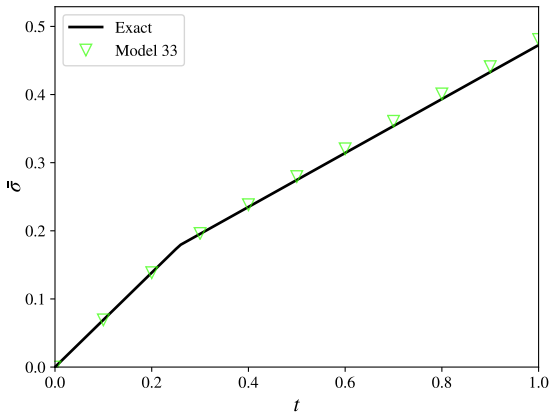

(a) Time-history plot of $\bar{\sigma}$ vs. t using $\Delta t = 0.1$.

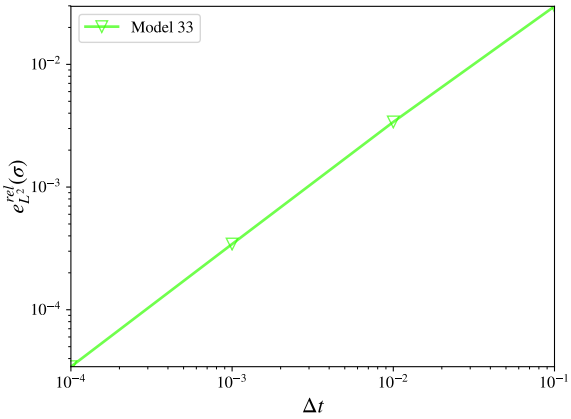

(b) Convergence plot for $e^{\text{rel}}_{L^2}(\boldsymbol{\sigma})$ errors vs. Δt.

Figure 28: Anisotropic plasticity test 2.

Table 54: Computed errors for anisotropic plasticity test 2.

Model	$e^{\text{rel}}_{L^2}(\boldsymbol{\sigma})$	r	$e^{\text{rel}}_{L^2}(\varepsilon_{33})$	r	$e^{\text{rel}}_{L^2}(\bar{\varepsilon}^p)$	r	Status
33	3.435e-05	0.94	3.078e-05	0.85	7.206e-09	1.85	✓

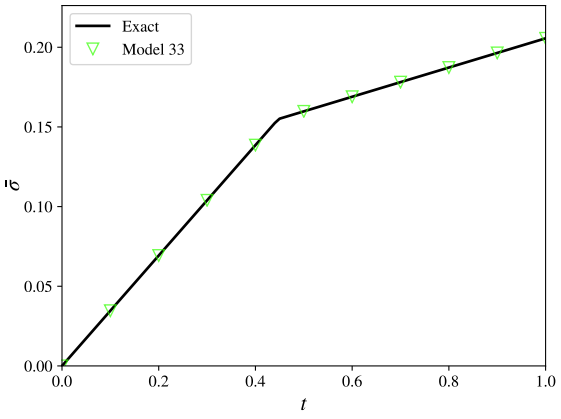

(a) Time-history plot of $\bar{\sigma}$ vs. t using $\Delta t = 0.1$.

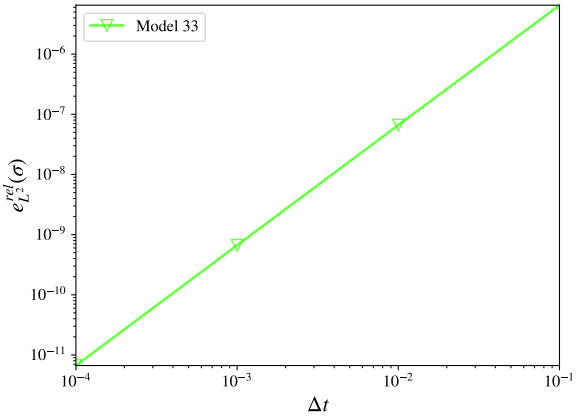

(b) Convergence plot for $e^{\text{rel}}_{L^2}(\boldsymbol{\sigma})$ errors vs. Δt.

Figure 29: Anisotropic plasticity test 3.

Table 55: Computed errors for anisotropic plasticity test 3.

Model	$e^{\text{rel}}_{L^2}(\boldsymbol{\sigma})$	r	$e^{\text{abs}}_{L^2}(\varepsilon_{33})$	r	$e^{\text{rel}}_{L^2}(\bar{\varepsilon}^p)$	r	Status
33	6.666e-12	1.99	1.377e-14	1.46	2.914e-11	2.00	✓

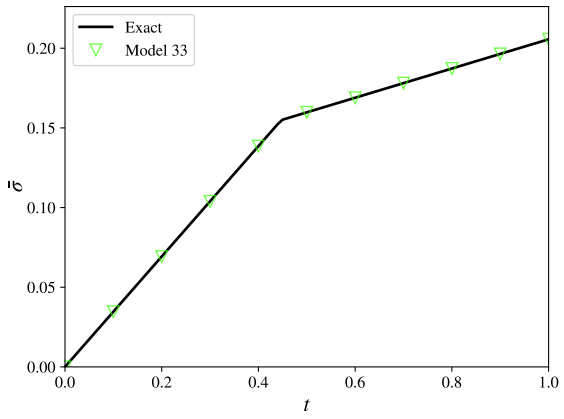

(a) Time-history plot of $\bar{\sigma}$ vs. t using $\Delta t = 0.1$.

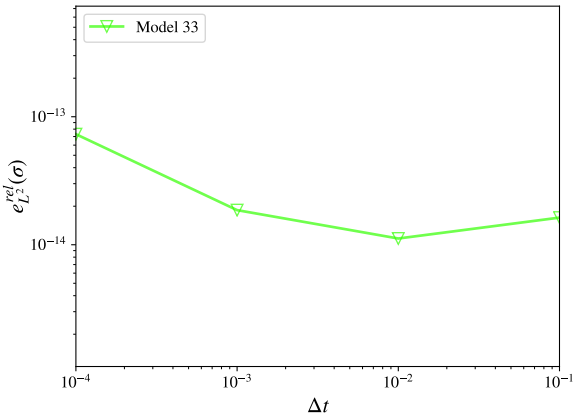

(b) Convergence plot for $e^{\text{rel}}_{L^2}(\boldsymbol{\sigma})$ errors vs. Δt.

Figure 30: Anisotropic plasticity test 4.

Table 56: Computed errors for anisotropic plasticity test 4.

Model	$e^{\text{rel}}_{L^2}(\boldsymbol{\sigma})$	r	$e^{\text{abs}}_{L^2}(\varepsilon_{33})$	r	$e^{\text{rel}}_{L^2}(\bar{\varepsilon}^p)$	r	Status
33	7.308e-14	-	0.000e+00	-	4.796e-13	-	✓

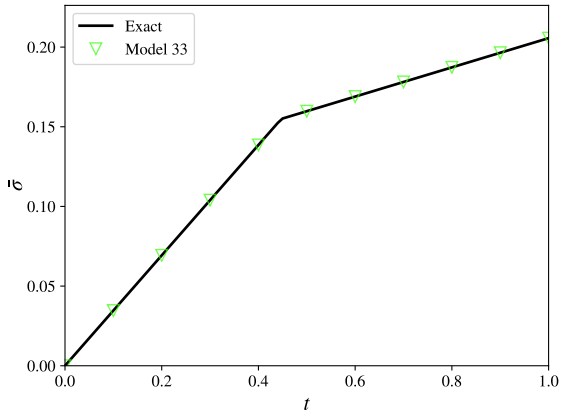

(a) Time-history plot of $\bar{\sigma}$ vs. t using $\Delta t = 0.1$.

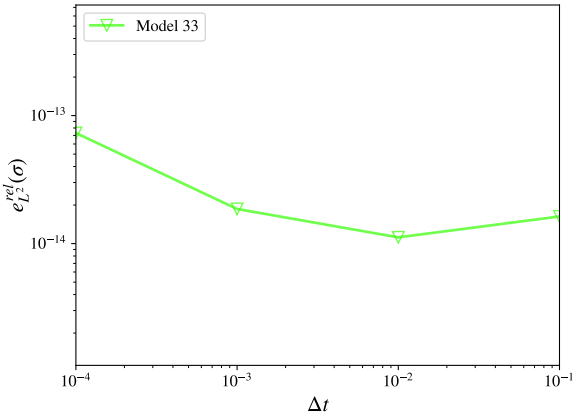

(b) Convergence plot for $e^{\text{rel}}_{L^2}(\boldsymbol{\sigma})$ errors vs. Δt.

Figure 31: Anisotropic plasticity test 5.

Table 57: Computed errors for anisotropic plasticity test 5.

Model	$e^{\text{rel}}_{L^2}(\boldsymbol{\sigma})$	r	$e^{\text{abs}}_{L^2}(\varepsilon_{33})$	r	$e^{\text{rel}}_{L^2}(\bar{\varepsilon}^p)$	r	Status
33	7.308e-14	-	0.000e+00	-	4.796e-13	-	✓

5.5 Rate-Dependent Plasticity

Models 15, 19, 24, 35, 52, 54, and 71 all incorporate rate-dependent material properties. However, the form of the rate-dependence included within each of these models is somewhat unique, yet can be grouped into two primary categories: dependence upon the total effective strain rate $\dot{\bar{\varepsilon}}$, and dependence upon the effective plastic strain rate $\dot{\bar{\varepsilon}}^p$. While the former modeling assumption (employed by models 15, 19, 35, and 52) is sufficiently accurate if one assumes that $\dot{\bar{\varepsilon}} \approx \dot{\bar{\varepsilon}}^p$, the latter approach (employed by models 24, 54, and 71) can be justified more rigorously in terms of thermodynamic arguments. The attention of the following sub-sections is dedicated to the latter category of models, in part because their corresponding reference solutions exhibit greater mathematical complexity.

Moreover, for load cases 2-6 which apply a constant effective strain rate, reference solutions for the former category can easily be obtained which otherwise closely resemble the solutions derived in previous sub-sections (albeit modulated by the strain rate parameter). Such tests are not presented within this report, but are reserved for the sequel.

5.5.1 Linear Rate-Hardening

The von Mises yield surface for a simple linear rate-hardening perfect plasticity model (encompassed as a special case by models 24, 54, and 71) is characterized by

$$f(\boldsymbol{\sigma}, \dot{\bar{\varepsilon}}^p) = \bar{\sigma}(\boldsymbol{\sigma}) - \sigma_y(\dot{\bar{\varepsilon}}^p) = 0, \qquad \sigma_y(\dot{\bar{\varepsilon}}^p) = \sigma_0 + k_{\dot{\bar{\varepsilon}}^p}\, \dot{\bar{\varepsilon}}^p. \tag{84}$$

The consistency condition necessitates that $\dot{f} = 0$ during plastic loading, i.e.

$$\frac{\partial f}{\partial \boldsymbol{\sigma}} : \dot{\boldsymbol{\sigma}} + \frac{\partial f}{\partial \dot{\bar{\varepsilon}}^p} \ddot{\bar{\varepsilon}}^p = 0. \tag{85}$$

For the special case of proportional loading of an isotropic material employing an associated flow rule, it follows that during plastic loading:

$$3\mu\, (\dot{\bar{\varepsilon}} - \dot{\bar{\varepsilon}}^p) = k_{\dot{\bar{\varepsilon}}^p}\, \ddot{\bar{\varepsilon}}^p. \tag{86}$$

The above characterizes a second order ordinary differential equations in terms of the equivalent plastic strain $\bar{\varepsilon}^p$.

For load case 6 ($\bar{\gamma} = 0.1$), the total effective strain rate $\dot{\bar{\varepsilon}}(t) = 2\bar{\gamma}$ remains constant $\forall t$, and the general solution to the above differential equation is

$$\bar{\varepsilon}^p(t) = \begin{cases} \bar{\varepsilon}(t) + A - Be^{-3\mu t / k_{\dot{\bar{\varepsilon}}^p}} & t \geq t_0 \\ 0 & t < t_0 \end{cases}. \tag{87}$$

In the limiting case as $t \to \infty$, the following conditions are obtained:

$$\lim_{t\to\infty} \dot{\bar{\varepsilon}}^p = \dot{\bar{\varepsilon}} \quad \Rightarrow \quad \lim_{t\to\infty} \sigma_y = \sigma_0 + k_{\dot{\bar{\varepsilon}}^p}\, \dot{\bar{\varepsilon}} \quad \Rightarrow \quad \lim_{t\to\infty} \bar{\varepsilon}^e = \frac{\sigma_0 + k_{\dot{\bar{\varepsilon}}^p}\, \dot{\bar{\varepsilon}}}{3\mu} = -A. \tag{88}$$

Further, imposing the initial conditions $\bar{\varepsilon}^p(t_0) = 0$ and $\dot{\bar{\varepsilon}}^p(t_0) = 0$ at the time of initial yielding t_0:

$$B = -\frac{k_{\dot{\bar{\varepsilon}}^p}\, \dot{\bar{\varepsilon}}}{3\mu} e^{3\mu t_0 / k_{\dot{\bar{\varepsilon}}^p}}, \qquad t_0 = \frac{\bar{\varepsilon}_0}{\dot{\bar{\varepsilon}}}, \qquad \bar{\varepsilon}_0 = \frac{\sigma_0}{3\mu}, \tag{89}$$

leading to the following exact solution for the time-evolution of the plastic strain:

$$\bar{\varepsilon}^p(t) = \begin{cases} \bar{\varepsilon}(t) - \frac{\sigma_0 + k_{\dot{\bar{\varepsilon}}^p}\, \dot{\bar{\varepsilon}}}{3\mu} + \frac{k_{\dot{\bar{\varepsilon}}^p}\, \dot{\bar{\varepsilon}}}{3\mu} e^{-3\mu(t-t_0)/k_{\dot{\bar{\varepsilon}}^p}} & t \geq t_0 \\ 0 & t < t_0 \end{cases}. \tag{90}$$

The material parameterization for the linear rate-hardening plasticity test using load case 6 ($\bar{\gamma} = 0.1$) is presented in table 58. The exact solutions for the normal strain and stress components are consistent with the solutions presented in table 39 for the generic isotropic plasticity test. Figure 32 depicts a comparison of the numerical results for the linear rate-hardening test using models 24, 54, and 71 against the exact solution, while table 59 presents the computed error measures and convergence rates. Despite the comparatively large errors, it was observed that all errors converge under temporal refinement at the (approximate) minimum rate of $r \approx 1.0$.

Table 58: Material parameterization for the linear rate-hardening test

Parameter	Value
Elastic modulus, E	0.8
Poisson's ratio, ν	0.2
Yield stress, σ_0	0.1
Linear rate-dependence coefficient, $k_{\dot{\bar{\varepsilon}}^p}$	0.1

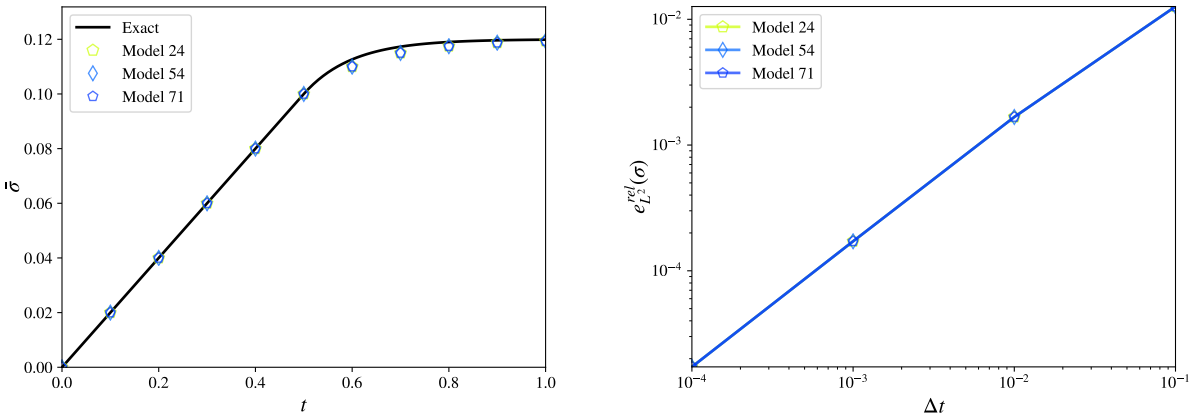

(a) Time-history plot of $\bar{\sigma}$ vs. t using $\Delta t = 0.1$.

(b) Convergence plot for $e_{L^2}^{\text{rel}}(\boldsymbol{\sigma})$ errors vs. Δt.

Figure 32: Linear rate-hardening plasticity test.

Table 59: Computed errors for the linear rate-dependent plasticity test.

Model	$e_{L^2}^{\text{rel}}(\boldsymbol{\sigma})$	r	$e_{L^2}^{\text{abs}}(\varepsilon_{33})$	r	$e_{L^2}^{\text{rel}}(\bar{\varepsilon}^p)$	r	Status
24	1.721e-05	0.88	2.704e-15	2.00	5.309e-05	0.88	✓
54	1.721e-05	0.88	2.718e-15	2.00	5.309e-05	0.88	✓
71	1.721e-05	0.88	2.892e-15	2.00	5.309e-05	0.88	✓

5.5.2 Logarithmic Rate-Hardening

For the logarithmic rate-hardening plasticity model (included as a special case for model 71):

$$\sigma_y(\dot{\bar{\varepsilon}}^p) = \sigma_0 + \log(k_0 + k_1\,\dot{\bar{\varepsilon}}^p), \tag{91}$$

one obtains the Riccati differential equation:

$$\ddot{\bar{\varepsilon}}^p(t) = 3\mu(\dot{\bar{\varepsilon}} - \dot{\bar{\varepsilon}}^p)(\dot{\bar{\varepsilon}}^p + k_0/k_1). \tag{92}$$

For load case 6 ($\bar{\gamma} = 0.1$), $\dot{\bar{\varepsilon}} = 2\bar{\gamma}$ remains constant $\forall t$, and the general solution to equation (92) is

$$\bar{\varepsilon}^p(t) = \begin{cases} A - (k_0/k_1)t + \frac{1}{3\mu}\log(1 - e^{(\dot{\bar{\varepsilon}}+k_0/k_1)(B+3\mu t)}) & t \geq t_0 \\ 0 & t < t_0 \end{cases}. \tag{93}$$

In the limiting case as $t \to \infty$, the following conditions are obtained:

$$\lim_{t\to\infty} \dot{\bar{\varepsilon}}^p = \dot{\bar{\varepsilon}} \quad \Rightarrow \quad \lim_{t\to\infty} \sigma_y = \sigma_0 + \log(k_0 + k_1\,\dot{\bar{\varepsilon}}) \quad \Rightarrow \quad \lim_{t\to\infty} \bar{\varepsilon}^e = \frac{\sigma_0 + \log(k_0 + k_1\,\dot{\bar{\varepsilon}})}{3\mu}. \tag{94}$$

Enforcing the initial conditions $\bar{\varepsilon}^p(t_0) = 0$ and $\dot{\bar{\varepsilon}}^p(t_0) = 0$:

$$A = (k_0/k_1)t_0 - \frac{1}{3\mu}\log(1 - e^{(\dot{\bar{\varepsilon}}+k_0/k_1)(B+3\mu t_0)}), \qquad B = \frac{\log\left(-\frac{k_0/k_1}{\dot{\bar{\varepsilon}}}\right)}{\dot{\bar{\varepsilon}} + k_0/k_1} - 3\mu t_0, \tag{95}$$

leading to the following exact solution for the plastic strain:

$$\bar{\varepsilon}^p(t) = \begin{cases} -(k_0/k_1)(t-t_0) + \frac{1}{3\mu}\log\left(\frac{\dot{\bar{\varepsilon}}+k_0/k_1 e^{3\mu(\dot{\bar{\varepsilon}}+k_0/k_1)(t-t_0)}}{\dot{\bar{\varepsilon}}+k_0/k_1}\right) & t \geq t_0 \\ 0 & t < t_0 \end{cases}. \tag{96}$$

The material parameterization for the logarithmic rate-hardening plasticity test is presented in table 60. The exact solutions for the normal strain and stress components are consistent with the solutions presented

Table 60: Material parameterization for the logarithmic rate-hardening test

Parameter	Value
Elastic modulus, E	0.8
Poisson's ratio, ν	0.2
Yield stress, σ_0	0.1
First log rate-dependence coefficient, k_0	1.0
Second log rate-dependence coefficient, k_1	0.1

in table 39 for the generic isotropic plasticity test. Figure 33 depicts a comparison of the numerical results for the logarithmic rate-hardening test using model 71 against the exact solution, while table 61 presents the computed error measures which converge at the minimum rate of $r \approx 1.0$.

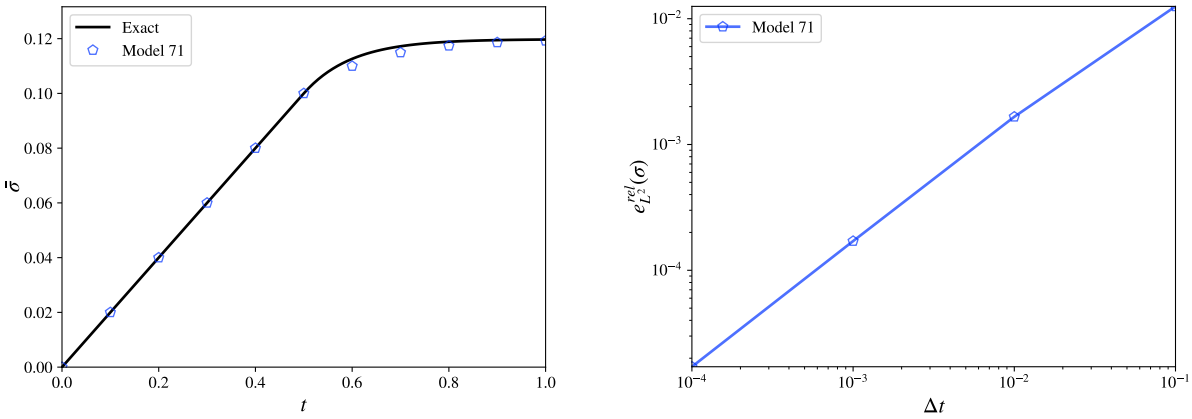

(a) Time-history plot of $\bar{\sigma}$ vs. t using $\Delta t = 0.1$.

(b) Convergence plot for $e^{\text{rel}}_{L^2}(\boldsymbol{\sigma})$ errors vs. Δt.

Figure 33: Logarithmic rate-hardening plasticity test.

Table 61: Computed errors for the logarithmic rate-dependent plasticity test.

Model	$e^{\text{rel}}_{L^2}(\boldsymbol{\sigma})$	r	$e^{\text{abs}}_{L^2}(\varepsilon_{33})$	r	$e^{\text{rel}}_{L^2}(\bar{\varepsilon}^p)$	r	Status
71	1.711e-05	0.88	2.671e-15	2.00	5.258e-05	0.88	✓

5.6 Pressure-Dependent Plasticity

Material models 15, 24, and 71 incorporate a pressure-dependent yield surface, in its simplest form:

$$f(\boldsymbol{\sigma}) = \bar{\sigma}(\boldsymbol{\sigma}) - \sigma_y(\boldsymbol{\sigma}) = 0, \qquad \sigma_y(\boldsymbol{\sigma}) = \sigma_0 + k_p\, p(\boldsymbol{\sigma}), \qquad p(\boldsymbol{\sigma}) = -\mathrm{tr}(\boldsymbol{\sigma}). \tag{97}$$

This is equivalent to the Drucker-Prager yield criterion, corresponding to a conic surface in principal stress space. During plastic loading, the consistency condition necessitates:

$$\dot{f} = \frac{\partial f}{\partial \boldsymbol{\sigma}} : \dot{\boldsymbol{\sigma}} = 0, \qquad \frac{\partial f}{\partial \boldsymbol{\sigma}} = \frac{\partial \bar{\sigma}}{\partial \boldsymbol{\sigma}} - \frac{\partial \sigma_y}{\partial \boldsymbol{\sigma}}. \tag{98}$$

The plane stress constraint additionally requires that $\sigma_{33} = 0\ \forall t$. Consequently,

$$\frac{\partial \sigma_y}{\partial \sigma_{33}} = \frac{\partial \bar{\sigma}}{\partial \sigma_{33}} \quad \Rightarrow \quad k_p = \frac{\sigma_{11} + \sigma_{22}}{2\bar{\sigma}}. \tag{99}$$

For the special case of proportional loading with $\sigma_{11} = \sigma_{22}$ and all other $\sigma_{ij} = 0\,\forall t$, it follows that during plastic loading: $\bar{\sigma} = \sigma_{11} = \frac{\sigma_0}{3}$, $k_p = 1$, and

$$\frac{\partial f}{\partial \boldsymbol{\sigma}} = \frac{3}{2}\begin{bmatrix} 1 & 0 & 0 \\ 0 & 1 & 0 \\ 0 & 0 & 0 \end{bmatrix} \quad \forall t. \tag{100}$$

For isotropic materials, the chosen loading may be induced via the motion described by load case 1 (i.e. $\varepsilon_{11}(t) = \varepsilon_{22}(t) = \bar{\gamma}\, t$), leading to the exact solutions given in table 62.

Table 62: Exact solutions for the Drucker-Prager yield test

Load Case	$\bar{\sigma}(t)$	$\sigma_{11}(t)$	$\sigma_{22}(t)$	$\sigma_{12}(t)$	$\sigma_{23}(t)$	$\sigma_{13}(t)$
1	$\min\left\{2\mu\frac{3\lambda+2\mu}{\lambda+2\mu}\bar{\gamma}\, t, \frac{\sigma_0}{3}\right\}$	$\bar{\sigma}(t)$	$\bar{\sigma}(t)$	0	0	0

For the pressure-dependent plasticity test so described, the onset of yielding occurs at $t_0 = \frac{\varepsilon_0}{\bar{\gamma}}$, where $\varepsilon_0 = \frac{\sigma_0}{6\mu}\frac{\lambda+2\mu}{3\lambda+2\mu}$. Assuming the non-associative flow rule:

$$\dot{\varepsilon}^p = \mathbf{n}\,\dot{\bar{\varepsilon}}^p, \qquad \mathbf{n} = \frac{\partial \bar{\sigma}}{\partial \boldsymbol{\sigma}} = \begin{bmatrix} \frac{1}{2} & 0 & 0 \\ 0 & \frac{1}{2} & 0 \\ 0 & 0 & -1 \end{bmatrix}, \tag{101}$$

it follows that $\dot{\bar{\varepsilon}}^p = 2\bar{\gamma}$ and $\dot{\varepsilon}_{33} = -2\bar{\gamma}$ during plastic loading, and therefore:

$$\bar{\varepsilon}^p(t) = 2\bar{\gamma}\langle t - t_0\rangle, \qquad \varepsilon_{33}(t) = -2\bar{\gamma}\frac{\lambda t + 2\mu\langle t - t_0\rangle}{\lambda + 2\mu}. \tag{102}$$

The material parameterization for the Drucker-Prager yield test using load case 1 ($\bar{\gamma} = 0.05$) is presented in table 63. For the chosen parameterization: $t_0 = 0.5$, and $\bar{\sigma}(t) = \min\left\{\frac{4}{3}t, \frac{2}{3}\right\}$. Figure 34 depicts a comparison of the numerical results for the present test using models 15, 24, and 71 against the exact solution, while table 64 presents the computed error measures and convergence rates. All models yield sufficiently small errors in all metrics, and converge to the exact solution at the optimal rate of $r = 2.0$ (for models 24 and 71), or at least at the (approximate) minimum rate of $r \approx 1.0$ (for model 15).

Table 63: Parameterization for the Drucker-Prager yield test

Parameter	Value
Elastic modulus, E	24.0
Poisson's ratio, ν	0.1
Yield stress, σ_0	2.0
Pressure-dependence coefficient, k_p	1.0

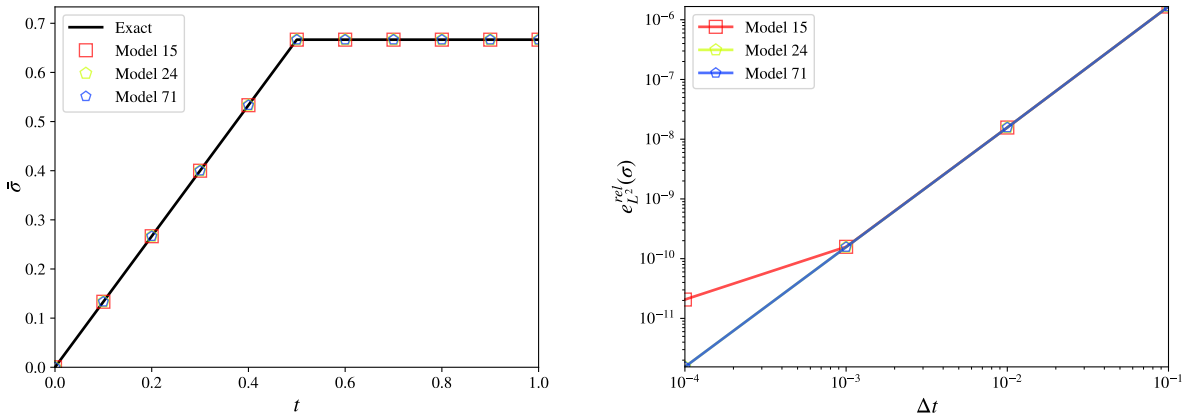

(a) Time-history plot of $\bar{\sigma}$ vs. t using $\Delta t = 0.1$.

(b) Convergence plot for $e_{L^2}^{\text{rel}}(\boldsymbol{\sigma})$ errors vs. Δt.

Figure 34: Drucker-Prager yield test.

Table 64: Computed errors for the pressure-dependent plasticity test.

Model	$e_{L^2}^{\text{rel}}(\boldsymbol{\sigma})$	r	$e_{L^2}^{\text{rel}}(\varepsilon_{33})$	r	$e_{L^2}^{\text{rel}}(\bar{\varepsilon}^p)$	r	Status
15	2.068e-11	0.88	2.336e-11	1.50	3.204e-11	1.43	✓
24	1.542e-12	2.00	7.510e-12	1.98	8.793e-12	1.98	✓
71	1.543e-12	2.00	7.401e-12	1.99	8.733e-12	1.98	✓

6 Conclusions and Future Work

While the verification test suite proposed in this report does not yet comprehensively test all of the currently available features for shell element material models in DYNA3D, the developed set of core tests (and the chosen methodology used to verify each model) establish a high degree of fidelity for the majority of these features.

In addition to creating and documenting the results of the currently proposed suite of verification tests, a substantial effort was also invested in developing an extensible testing infrastructure with the purpose of generating and documenting additional verification tests more easily. It is intended that this framework be used to extend the current suite of tests for shell models to encompass the remaining model-specific features enumerated in table 2, and to establish a similar such suite of comprehensive verification tests for solid elements.

In the interim, table 65 provides prospective users with an indication of a given model's level of fidelity in terms of the scope of currently tested (and untested) features.

6.1 Resolved Issues

In process of creating the proposed verification suite, examination of the results for each test led to the discovery of 18 independent implementation errors/inconsistencies. Each discovered issue was subsequently documented in Jira, and later resolved. For reference, a short description (the Jira ticket name) of each issue is provided below, along with its corresponding Jira ticket number. For specific details regarding each issue, the reader is referred to the corresponding documentation for each ticket in Jira.

PARADYN-109: Incorrect behavior of model 19 using a strain rate-dependent elastic modulus

PARADYN-110: Incorrect strains being computed for shell element material models using thermal effects (models 4, 21, 23)

PARADYN-114: Shell model 34 - implicit typing causes memory access problems/seg faults during plastic loading

PARADYN-129: Incorrect shear resultant output for shell model 28

PARADYN-130: Incorrect computation of internal energy for shell models 4, 22, 30, and 33

PARADYN-132: Shell model 74 does not compute thickness strain

PARADYN-133: In-plane stresses for shell model 41 being computed incorrectly when orthotropic properties are specified

PARADYN-134: POPT variable for shell model 50 does not output the requested variables

PARADYN-135: Shell model 30 computes thickness strain incorrectly

PARADYN-136: Shell model 15 plastic iteration procedure inconsistent with other shell models

PARADYN-137: Shell model 28 computes thickness strain incorrectly

PARADYN-138: Shell model 28 produces inconsistent hsp output for stress resultants in place of stresses

PARADYN-139: Inconsistent variables being output to 7-th slot in hsp element print blocks for orthotropic shell models

PARADYN-141: Shell models 34 and 35 produce incorrect results for problems involving plasticity

PARADYN-142: The DYNA3D manual incorrectly states the Hill effective stress for model 33

PARADYN-143: Shell model 33 produces non-zero normal stresses in output

PARADYN-144: Shell model 35 produces incorrect normal strains

PARADYN-145: Shell model 33 produces minor errors on the order of 1.0e-7

6.2 Final Summary of Verification Test Results

Table 65 provides a complete summary of the determined verification status of all tested (and untested) features for shell element material models in DYNA3D. A "passing" status (✓) for a specific test is reserved only for those models which have been thoroughly verified to be consistent with the exact mathematical solutions for all feature-specific problems, and consistent with the assumptions made by other relevant models in DYNA3D. In this regard, prospective users of a given feature can be assured that the indicated models are functioning correctly.

Table 65: Verification status of tested features for shell element material models in DYNA3D

Model	Isotropic Elasticity	Orthotropic Elasticity	Isotropic Thermal Expansion	Orthotropic Thermal Expansion	Linear Hardening	Piecewise Hardening	Power-Law Hardening	Exponential Hardening	Hill Yield Criterion	Linear Rate-Hardening	Logarithmic Rate-Hardening	Drucker-Prager Yield Criterion	Kinematic Hardening	Temperature-Sensitive Properties	Strain Rate-Sensitive Properties	Variable Properties	Damage and Failure
1	✓	-	-	-	-	-	-	-	-	-	-	-	-	-	-	-	-
2	✓	✓	-	-	-	-	-	-	-	-	-	-	-	-	-	-	-
3	✓	-	-	-	✓	-	-	-	-	-	-	-	?	-	-	-	-
4	✓	-	✓	-	✓	-	-	-	-	-	-	-	-	?	-	-	-
12	✓	-	-	-	✓	-	-	-	-	-	-	-	-	-	-	-	-
15	✓	-	-	-	✓	-	✓	-	-	-	-	✓	-	?	?	?	?
18	✓	-	-	-	-	-	✓	-	-	-	-	-	-	?	-	?	-
19	✓	-	-	-	✓	-	-	-	-	-	-	-	-	-	?	-	-
21	✓	✓	✓	✓	-	-	-	-	-	-	-	-	-	?	-	-	-
22	✓	✓	-	-	-	-	-	-	-	-	-	-	-	-	-	-	?
23	✓	✓	✓	✓	-	-	-	-	-	-	-	-	-	?	-	-	-
24	✓	-	-	-	✓	✓	✓	-	-	✓	-	✓	-	-	?	-	-
28	⚠	-	-	-	✗	-	-	-	-	-	-	-	-	-	-	-	-
30	✓	-	-	-	✓	-	-	-	-	-	-	-	?	-	-	-	-
33	✓	✓	-	-	✓	-	-	-	✓	-	-	-	-	-	-	-	-
34	✓	-	-	-	✓	-	-	-	⚠	-	-	-	-	-	-	-	-
35	✓	-	-	-	✓	✓	-	-	-	-	-	-	-	-	-	-	?
38	✓	-	-	-	✓	-	-	-	-	-	-	-	?	-	-	-	-
39	✓	-	-	-	✓	-	-	-	-	-	-	-	?	-	-	-	-
41	✓	✓	-	-	-	-	-	-	-	-	-	-	-	-	-	-	?
42	-	-	-	-	-	-	-	-	-	-	-	-	-	-	-	-	-
46	✓	✓	-	-	-	-	-	-	-	-	-	-	-	-	-	-	-
50	✓	✓	-	-	-	-	?	-	?	-	-	-	-	-	-	-	?
52	✓	-	-	-	✓	✓	-	-	-	-	-	-	-	-	?	-	?
54	✓	-	-	-	✓	-	✓	-	-	✓	-	-	-	?	?	-	?
71	✓	-	✓	-	✓	-	✓	✓	-	✓	✓	✓	-	?	?	-	?
74	✓	✓	-	-	-	-	-	-	-	-	-	-	-	-	-	-	?

✓: Passed all verification tests.
⚠: Inconsistent model assumption.
✗: Failed one or more verification tests.
?: Model feature currently remains untested.

References

[1] T. Belytschko, J.I. Lin, and C.S. Tsay. Explicit algorithms for the nonlinear dynamics of shells. *Computer Methods in Applied Mechanics and Engineering*, 42(2):225–251, 1984.

[2] T. Belytschko and C.S. Tsay. Explicit algorithms for nonlinear dynamics of shells. 43, 01 1981.

[3] T. Belytschko and C.S. Tsay. A stabilization procedure for the quadrilateral plate element with one-point quadrature. *International Journal for Numerical Methods in Engineering*, 19(3):405–419, 1983.

[4] B.D. Giffin. Verification problems for parameterized load curves in DYNA3D. Technical Report LLNL-TR-765860, Lawrence Livermore National Laboratory, 2019.

[5] R. Hill and E. Orowan. A theory of the yielding and plastic flow of anisotropic metals. *Proceedings of the Royal Society of London. Series A. Mathematical and Physical Sciences*, 193(1033):281–297, 1948.

[6] T.J.R. Hughes. *The Finite Element Method: Linear Static and Dynamic Finite Element Analysis (Dover Civil and Mechanical Engineering)*. Dover Publications, August 2000.

[7] T.J.R. Hughes and J. Winget. Finite rotation effects in numerical integration of rate constitutive equations arising in large-deformation analysis. *International Journal for Numerical Methods in Engineering*, 15(12):1862–1867, 1980.

[8] R. D. Krieg and D. B. Krieg. Accuracies of Numerical Solution Methods for the Elastic-Perfectly Plastic Model. *Journal of Pressure Vessel Technology*, 99(4):510–515, 11 1977.

[9] J.C. Simo and T.J.R. Hughes. *Computational Inelasticity*. Interdisciplinary applied mathematics. Springer, 1998.

[10] R.G. Whirley and B.E. Engelmann. An implementation of Hill's theory of normal anisotropic plasticity for explicit shell analysis. *NASA STI/Recon Technical Report N*, 8 1991.

[11] H. Xiao, O.T. Bruhns, and A. Meyers. Logarithmic strain, logarithmic spin and logarithmic rate. *Acta Mechanica*, 124(1):89–105, Mar 1997.

[12] E. Zywicz and J. I. Lin. *DYNA3D: A Nonlinear, Explicit, Three-Dimensional Finite Element Code for Solid and Structural Mechanics User Manual - Version 18*. Lawrence Livermore National Laboratory, October, 2018.